Dynamical Climatology

Climate simulations for 9000 years before present: Seasonal variations and the effect of the Laurentide ice sheet.

by

J.F.B. Mitchell, N.S. Grahame and
K.J. Needham

DCTN 57

June 1987

Meteorological Office (Met. O. 20)
London Road
Bracknell
Berkshire RG12 2SZ

DYNAMICAL CLIMATOLOGY TECHNICAL NOTE NO. 57

CLIMATE SIMULATIONS FOR 9000 YEARS BEFORE PRESENT: SEASONAL VARIATIONS AND THE EFFECT OF THE LAURENTIDE ICE SHEET

by

J F B Mitchell, N S Grahame and K J Needham

Submitted for publication in J. Geophys. Res.

Met O 20 (Dynamical Climatology Branch)
Meteorological Office
London Road
Bracknell
Berkshire, U.K. RG12 2SZ

Note: This paper has not been published. Permission to quote from it should be obtained from the Assistant Director of the above Meteorological Office Branch.

LF/M020*

Climate simulations for 9000 years before present: Seasonal variations and effect of the Laurentide ice sheet

J F B Mitchell, N S Grahame and K J Needham

Meteorological Office, Bracknell, England

Abstract

A detailed climate model is used to investigate the factors contributing to differences in climate between 9000 years ago and the present. The climate model comprises an atmospheric general circulation model coupled to a mixed layer ocean in which heat convergence due to oceanic advection is prescribed. In the first experiment, only the earth's orbital parameters are changed. As in earlier work, it is found that monsoon circulations are enhanced during northern summer, and weakened during the northern winter, and mid-latitudes become drier throughout the year. Various feedback mechanisms modify the local response to the changes in insolation at the top of the atmosphere. In the northern hemisphere, the warming in high latitudes is greatest in autumn and winter due to changes in sea ice, the mid-latitude oceans are warmer throughout the year due to changes in cloud, and the surface temperature change over land in summer is reduced in low latitudes and enhanced in mid-latitudes due to changes in cloud and soil moisture. Thus the climatic response to a simple change in boundary conditions may be complex, a fact which should be borne in mind when interpreting palaeoclimatic data. In a second experiment, a representation of the Laurentide ice sheet is also included. The warming

in high latitudes is substantially reduced, especially just downstream of the ice sheets. This suggests that there may have been a substantial warming in high latitudes just after the Laurentide ice sheet collapsed.

1. Introduction

Our present understanding of past climates is based largely on the interpretation of palaeoclimatic evidence. Palaeoclimatic data are irregularly distributed in space and time. Many of the quantitative estimates of meteorological variables such as temperature and precipitation are based on proxy data using empirical relationships (transfer functions) derived from the present. These estimates are at best approximate and, since values of a given parameter may be derived from different types of proxy data, are not necessarily uniform from region to region. Although great care is taken in interpreting parameters derived from proxy data, certain ambiguities may remain. For example, it may be uncertain whether 'temperature' represents an annual mean temperature, a mean temperature, a mean temperature during the growing season, or a combination of these and other factors. Nevertheless, palaeoclimatic data are the 'observations' to be accounted for in any theory of past climate.

Data generated by 3-dimensional models of climate are uniform, evenly distributed and unambiguous. With the tacit assumption that simulated (and observed) climate depends uniquely on the specification of certain boundary conditions assumed to be stationary over the period of interest (for example orbital parameters, distribution of continents), one can investigate the effects of specified changes in boundary conditions on climate. If the relevant information is available, numerical simulations can be made with anomalous and present day boundary conditions and compared to determine the geographical distribution of changes in climatic variables. Unfortunately, it is not always evident which boundary

conditions have a significant impact on climate, and in many cases the boundary conditions are derived from palaeoclimatic data. However, the use of numerical models is becoming increasingly important in the understanding of past climates. A more detailed account of palaeoclimatic analysis and modelling is given in Hecht (1985).

One of the main applications of climate models has been to explore the climatic effects of enhanced CO_2 (see for example Manabe, 1983, Schlesinger and Mitchell, 1987). This is more than an academic exercise, since CO_2 concentrations have risen by at least 25% since 1860 (Gammon et al, 1985). Model sensitivity studies indicate that increased CO_2 may produce changes in climate which have potential social and economic impacts, such as a drying of the northern mid-latitude continents in summer (Manabe and Wetherald, 1987). Hence there is an urgent need to establish the ability of climate models to simulate a climate significantly different from that of the present. Assessments have been made of model simulations of the present annual cycle (see for example Schlesinger and Mitchell, 1987). However, an accurate simulation of present day climate does not guarantee an accurate simulation of climate change, nor do deficiencies in the simulation of present day climate necessarily disqualify a model for use in climate change experiments, provided that the deficiencies are properly taken into account (see Mitchell et al, 1987). Hence modelling of past climates may not only help in the interpretation of palaeoclimatic data; palaeoclimatic data may also indicate aspects of simulated climate change which are unrealistic (Manabe and Brocolli, 1985).

In order to validate a model in the above manner, a large change in boundary conditions is required to produce significant change in the model. The changed boundary conditions and the concurrent climate must be well established from palaeoclimatic data. Early experiments centred on the last glacial maximum (Manabe and Hahn, 1977; Williams et al, 1974 and Gates, 1976). However, there are known to be several relevant changes in forcing for that period - in the distribution of ice sheets, CO_2 concentrations and sea surface temperatures, as well as probable changes in land albedo and atmospheric aerosol loadings. Furthermore, experiments using an idealized dynamical ocean-atmosphere model indicate that the oceanic circulation may have changed substantially during periods colder than present (Manabe and Bryan, 1985).

We have chosen to investigate a more recent period around 9000 years before present (9 Kbp) when the changes in the ice sheets were smaller, CO_2 concentrations and sea surface temperatures were much closer to their present day values, and the most important change in boundary conditions is thought to have been the change in orbital parameters (Kutzbach and Street-Perrott, 1985). Then, the earth passed closest to the sun during the boreal summer, as opposed to winter, and the obliquity of the earth's axis and the eccentricity of its orbit were slightly larger than at present (Berger, 1979). As a result insolation at the top of the atmosphere was greatest during the boreal summer, particularly in high northern latitudes, and smaller during the boreal winter. The global annual mean insolation received by the planet was effectively unchanged.

Mitchell (1976, 1977) investigated the effect of these changes in two 60 day experiments using, respectively, model generated and prescribed present day sea surface temperatures in an atmospheric general circulation model, and found a warming of several degrees in high northern latitudes in summer. Kutzbach and Otto-Bliesner (1982) found that the simulated African-Asian monsoon intensified in a very low resolution atmospheric general circulation model when the orbital parameters for 9 Kbp rather than present were used. This finding was confirmed using a more sophisticated model with higher horizontal (and vertical) resolution (Kutzbach and Street-Perrott, 1985). Both precipitation and precipitation minus evaporation (averaged over land from 0 to 30°N) increased in July simulations with orbital parameters for 9 Kbp; over the northern mid-latitude continents there was a smaller increase in precipitation, but precipitation minus evaporation (P-E) decreased (Kutzbach and Guetter, 1986).

We have extended the work of Kutzbach and his co-workers by coupling an atmospheric model to a 50 metre mixed layer ocean with prescribed heat convergence and a thermodynamic model of sea ice in order to investigate the effects of allowing sea surface temperature and sea ice extents to change. Both the annual and diurnal cycle of insolation are included, and the evolution of soil moisture and snow cover are determined by the model. Kutzbach and Guetter (1986) allude briefly to short experiments with a model including a seasonal cycle and interactive soil moisture, whereas we describe detailed results from more extensive simulations. In this paper, the emphasis is on the simulated changes in temperature and circulation. The model and the experimental design are described in Section 2.

Three aspects of the results are presented in Section 3: the changes over the annual cycle and associated feedbacks (3.1), seasonally averaged changes (3.2) and the influence of the Laurentide ice sheet (3.3). A second paper (in preparation) will describe in more detail the simulated changes in the hydrological cycle, the dependence of those changes on the surface parametrization, and a comparison of the simulated results against palaeoclimatic data.

2. The model, model climatology and experimental design

2.1 The model

The global climate model used in this study comprises the 11-layer atmospheric general circulation model of the UK Meteorological Office (Slingo, 1985a) coupled to a static mixed layer ocean and a simple energy balance sea-ice model (Gordon and Bottomley, 1984) and is the same as that used by Wilson and Mitchell (1987) in a study of the effect of increasing atmospheric CO_2.

Earlier versions of the atmospheric model have been used by Slingo (1985b), Cunnington and Rowntree (1986), Palmer and Mansfield (1986) and Mitchell et al (1987), and were based on the 5-layer model described by Corby et al (1977). The version used here solves the primitive equations using σ (= pressure/surface pressure) as a vertical co-ordinate and a regular latitude longitude grid of 5° x 7.5° resolution.

The seasonal and diurnal variation of solar radiation are represented as is the effect of the eccentricity of the orbit on the orbital radius and angular velocity round the sun. Radiative fluxes are a function of temperature, water vapour, cloud and the prescribed concentrations of carbon dioxide and ozone. Clouds are assigned a reflectivity of 0.5, except for high cloud which has a reflectivity of 0.2. Over snow free land the value of surface albedo is specified based on land cover and soil data compiled by Wilson and Henderson-Sellers (1985). Over snow covered land, albedo increases with snow depth to a maximum of 0.6, and values of 0.06 and 0.7 are used over open sea and land ice respectively. The albedo of sea-ice increases linearly from 0.4 at 271.2K to 0.7 at or below 261.2K. The long wave fluxes are calculated using an emissivity approximation (Slingo and Wilderspin, 1986).

The fluxes of heat, moisture and momentum from the surface are based on Monin-Obukhov similarity theory with evaporation limited where appropriate by soil moisture following Manabe (1969). The boundary layer is represented using a diffusive mixing scheme (Richards 1980a, b) which is an extension of the ideas of Clarke (1970). Mixing extends through the lowest three model layers, or to the lowest inversion forming in those three layers. Convection is modelled by a penetrative scheme (Lyne and Rowntree, 1976; Rowntree 1984) which allows entrainment of environmental air and detrainment from the parcel at each level. Excess moisture due to condensation following convection or large scale ascent is removed as precipitation.

The cloud scheme allows up to three layer clouds (low, medium and high) and a convective tower simultaneously in each grid box. Layer cloud is assumed to be one sigma layer thick, and fractional amounts are calculated as a function of relative humidity. Convective cloud is diagnosed from the maximum parcel size involved in moist convection, with the base and top determined from the levels between which moist convection occurs.

The ocean is represented by a 50 m well mixed layer with a prescribed seasonally varying heat flux C. Thus, the rate of change $\frac{\partial T}{\partial t}$ in surface temperature T is given by

$$\rho C_p h \frac{\partial T}{\partial t} = C + S \qquad (1)$$

where ρ and C_p are respectively the density and heat capacity of sea water, h is the depth of the mixed layer, and S is the net downward surface heat flux from the atmosphere. The heat convergence C is derived from (1) by diagnosing S as a function of month and location in an atmospheric integration with prescribed sea surface temperatures, and using climatological sea surface temperatures to estimate $\frac{\partial T}{\partial t}$. These values of C are prescribed and used along with the surface fluxes S produced in the coupled integration to update the surface temperatures using (1).

Sea-ice forms when the ocean temperature falls below 271.2K, and the temperature of the mixed layer under the ice is kept at this value. A thermodynamic model of sea-ice similar to the zero-dimensional model of Semtner (1976) is used to determine the evolution of ice thickness, and

both the effect of snowfall on top of the ice and the diffusive heat flux through the ice are included. Surface temperature is updated every atmospheric model time step but ice and snow depths and changes in classification are updated along with sea surface temperatures every 5 days using the accumulated budgets of heat and snow (Gordon and Bottomley, 1984).

2.2 Model climatology

An assessment of the simulation of present climate by the model is given by Wilson and Mitchell (1987), and is summarized here. The model reproduces the main features of the general circulation; the sub-tropical anticyclones form predominantly over the oceans in summer and the continents in winter; heat lows form over the continents in summer, particularly over North Africa and Southern Asia, and the mid-latitude depression belts are most pronounced in winter. The Antarctic circumpolar surface pressure trough is over 12 mbs too shallow and displaced to the north of the observed position (Schutz and Gates, 1971) and, as is common with other low resolution models, the Azores ridge extends further north than observed during summer producing north easterly as opposed to westerly flow over western Europe. The Asian monsoon trough extends further east than observed.

The main bands of precipitation (Figure 1) are associated with the main regions of low level atmospheric convergence - along the mid-latitude depression tracks and the intertropical convergence zone and in summer, equatorward and eastward of the continental heat lows. In northern summer,

the precipitation rates associated with the Asian and west African monsoons are less than the climatological values given by Jaeger (1976), and over Africa the rain band extends further north than observed so that simulated rates over the central Sahara are too high. Precipitation over the Bay of Bengal and the West Pacific ocean, and along the eastern coasts of North America and Asia is also heavier than observed. Errors of this magnitude are typical of low resolution climate models (see Schlesinger and Mitchell, 1987). The simulation of precipitation is improved, particularly in the tropics, if the horizontal resolution is improved (Manabe et al, 1979), but the extra cost in computing (a factor of 8 in halving the grid length) is such that long coupled ocean atmosphere simulations are impractical at present.

The simulated sea surface temperatures (not shown) are generally within 2 K of those observed, the model being slightly cooler in the tropics and warmer in high latitudes. The simulated fractional sea-ice cover in both hemispheres is within a few per cent of climatological values used in the prescribed sea surface temperature integration, and the simulated depths of perennial ice in the Arctic are around 2 m, consistent with the observations (Maykut and Untersteiner, 1971). The Antarctic ice cover tends to be more extensive than observed in autumn and winter.

In summary, the simulated control climate is typical of that produced by a low resolution atmospheric model. By specifying the oceanic heat convergence, we have avoided the over-extensive sea-ice and excessively warm tropical sea surface temperatures reported by Meehl and Washington (1985). Although the monsoon circulations are rather weak, there is no

excessive winter precipitation over India and southeast Asia as found in the lower resolution model used by Hansen et al (1984). We believe that the model is sufficiently realistic to simulate the large scale response to orbital perturbations, provided the known model errors are taken into account.

2.3 Experimental design

The orbital parameters used for present day and 9 Kbp (Table 1) may be derived from Berger (1979). These changes produce increased insolation during northern summer, due to the orbit being close to aphelion as opposed to perihelion, and reduced insolation at most latitudes during northern winter (Figure 2a). Annual mean insolation is enhanced at high latitudes at the expense of low latitudes (Figure 2b).

Further details of the changes in orbital parameters are given in Appendix 1. The results presented in section 4 are computed using data from the last 13 years of a 17 year simulation for 9 Kbp and the last 15 years of a 20 year control simulation (Wilson and Mitchell, 1987). Some tests of statistical significance are given in Appendix 2.

3. Results

First, the evolution of the changes in zonally averaged surface temperature through the year are described, and some feedback mechanisms are discussed. Secondly, the detailed geographical distributions of the changes at 9 Kbp during the solsticial seasons are presented and compared

with the findings of Kutzbach and Guetter (1986, henceforth referred to as KG) who used a model with prescribed present day sea surface temperatures and a fixed solar declination. Finally, the effect of including a representation of the Laurentide ice sheet is discussed.

3.1 Zonally averaged changes over the annual cycle and associated feedbacks

It is not surprising, given the seasonal variation of the changes in forcing (Figure 2a), that the anomaly patterns at 9 Kbp undergo substantial variation, even within the four main seasons. The changes in insolation at the top of the atmosphere are reduced before reaching the surface by reflection from cloud, and by atmospheric absorption and scattering (Figure 3). The changes in insolation in the northern hemisphere correspond to an enhancement of the seasonal cycle. This is manifested by generally higher temperatures over land in the summer, and lower temperatures in the tropics and sub-tropics in winter (Figure 4a). The changes in sea surface temperature are considerably smaller than those over land, and lag the changes over land by 1 to 2 months (Figure 4b). This is due to the larger thermal inertia of the ocean (50 m water equivalent compared to 3 m water equivalent for the land surface and atmosphere combined). There are three major exceptions to this simple picture of a lagged response to periodic forcing.

a. In high northern latitudes over the oceans, where the warming is a maximum in winter and a minimum in summer even though the changes in insolation (Figure 2a) are a maximum in summer.

b. Over land near 20°N, where the surface temperature changes in summer are much smaller than at neighbouring latitudes.

c. The northern mid-latitude oceans, where there is a warming throughout the year.

These anomalies are now considered in detail.

a. Northern high latitudes

Why is the warming over the Arctic a minimum in summer when the increases in insolation are largest? Consider the zonally averaged changes over the ocean at 77.5°N. The surface temperature averaged over sea and sea-ice in both the control and anomaly simulations rises to 271.2K in summer (Figure 5a), and cannot rise any further until sea-ice is melted. Even when sea-ice has melted, the large thermal inertia of the mixed layer is such that any further warming over the short ice-free season is very small.

On the other hand, the mixed layer absorbs a large amount of heat through the summer months (Figure 5b), and this delays the regrowth of the ice in autumn. Once the sea-ice does start to extend, the surface temperature falls rapidly. The delay in the onset of ice-formation at 9 Kbp gives rise to the large apparent warming (Figure 5a). After December, there is little difference in sea-ice extents, but the ice thickness is substantially less at 9 Kbp (Figure 5c). As a result, the heat flux through the ice is increased, maintaining higher surface temperatures (and a larger upward net flux of heat from the surface, as can be seen in Figure 5b). The differences in thickness and temperature decrease until May, when increased insolation at 9 Kbp once more starts to reduce sea-ice thickness more quickly. The pronounced winter warming is similar to that found by Manabe and Stouffer (1980) and other studies with increased atmospheric CO_2, except that here there is no increase in radiative heating during the winter months.

The distribution of sea-ice is identical at 9 Kbp and present during May (Figure 6a), but by July, the ice is retreating much more rapidly at 9 Kbp. The areal extent is a minimum in both simulations in September (Figure 6c), and increases less rapidly during early winter at 9 Kbp (Figure 6d).

b. Land, low and middle latitudes of the northern hemisphere

The summer warming near 20°N is smaller than in surrounding latitudes. The increased land-sea contrast and consequent strengthening of the monsoon circulation (discussed in more detail later) lead to an increase in cloud cover, and hence in the fraction of downward insolation reflected back to space (planetary albedo) (Figure 7c). Although the insolation at the top of the atmosphere is increased substantially in summer, the change at the surface is reduced by the increase in cloud cover, and from August onwards, is actually lower than in the control simulation (Figure 7b). The net radiative heating at the surface remains greater due to increased downward longwave radiation from the warmer, moister atmosphere (this is not shown but is evident from the sum of sensible and latent heat fluxes (Figs 7e, f)). A further mechanism restricts the rise in surface temperature. Throughout much of this zone in the control simulation, the soil moisture levels are so low that evaporation is well below potential evaporation, and so most of the radiation absorbed at the surface is used to raise the surface temperature, rather than for evaporation. During August and September, soil moisture is much larger in the 9 Kbp simulation, so relatively more radiant energy is used for evaporation and less is partitioned to sensible heat (Figure 7e, f, solid lines).

The mechanisms operating over land at 17.5°N in summer are reversed at 42.5°N. Here cloud and planetary albedo are reduced, the surface dries out, and during August and September, evaporation is reduced at the expense of sensible heat flux (Figure 7, dashed lines). Similar changes in cloud and soil moisture are found at these latitudes in simulations with enhanced CO_2 (see for example Manabe and Wetherald, 1987).

c. Northern mid-latitude oceans

Although the net annual mean change in downward insolation at 42.5°N is negligible (see Figure 2b), there is a substantial warming over the oceans throughout the year (Figure 8a). The net solar heating at the surface reaches a maximum in June (Figure 8b), but then reaches a further maximum in August. This secondary maximum is due to a marked reduction in cloud cover (Figure 8b) which in August is sufficient to lower the planetary albedo from 26.5% to 23.3%. Cloud cover decreases at 9 Kbp because of stronger atmospheric subsidence over the oceans compensating the enhanced ascent over land associated with more vigorous monsoon circulations.

3.2 Seasonally averaged changes; vertical and geographical distributions

The time latitude diagrams provide a useful summary of the seasonal variations. In this section, the vertical distribution of the simulated response for the solsticial seasons is presented. However, zonal averages may be misleading, particularly where there are large variations at a particular latitude. Furthermore, palaeoclimatic data is usually collected at a few specific sites which are sparsely distributed, so that it is not possible to produce meaningful zonal averages. Hence, the geographical distributions of the changes in selected parameters are also presented.

a. June to August (JJA)

During JJA, there is a warming in the northern hemisphere which generally increases towards the poles (Figure 9a) with temperature rises exceeding 4 K in the middle troposphere north of 45°N. This latitudinal variation in warming is qualitatively consistent with the variation in incoming radiation at this time. In general the warming of the troposphere increases with height due to the release of latent heat accompanying enhanced convective precipitation. Moist convection tends to adjust the vertical temperature gradient towards the moist adiabatic lapse rate which decreases as temperature is increased. Over the Arctic, however, the lesser warming near the surface is due rather to the large thermal inertia of sea-ice, as discussed

earlier. In the southern hemisphere, the extratropics are cooler at 9 Kbp, even though insolation was similar or even greater than at present. This may be attributed to the reduction in incoming solar radiation earlier in the year (Figure 2b) producing a cooling which persists due to the large thermal inertia of the mixed layer.

The reduced meridional temperature gradient produces a marked reduction in the westerly component of the wind at upper levels near 30°N (Figure 9b), consistent with the thermal wind relationship. This corresponds to a poleward extension of the equatorial easterly flow found at upper levels in the present day simulation (not shown). Apart from a slight strengthening of the mid-latitude westerly flow in the southern hemisphere, which is consistent with the high latitude cooling, other changes in zonally averaged flow are negligible.

The warming of the northern hemisphere in summer is also accompanied by a reduction in middle and upper tropospheric cloud and increased cloud cover near the tropopause (Figure 9c). Similar changes in cloud are found in simulations in which the troposphere is warmed due to increased concentrations of atmospheric CO_2 (Wetherald and Manabe, 1986; Wilson and Mitchell, 1987) and are consistent with a raising of the height of the tropopause. There is a marked increase in low cloud over the Arctic associated with the increased static stability (see Figure 9a).

The surface warming exceeds 4 K over much of the interior of the northern continents (Figure 10a), with a maximum of 6 K in central Asia. The largest increases coincide with regions of reduced soil moisture (shown later) which may explain why the increases here are larger than in earlier studies which neglect changes in surface properties (KG, see also Schneider et al, 1987). In some regions, the surface temperature is lower at 9 Kbp, due to increases in soil moisture (Arabia) and cloud (India). The warming is also less pronounced over the southern hemisphere continents where the changes in insolation are smaller. The northern oceans are generally 1 to 2 K warmer, the largest changes occurring in regions where cloud cover is reduced. Over the northeast Pacific, cloud cover increases at 9 Kbp, and there is a local cooling. Over perennial sea-ice in the northern hemisphere the changes in temperature are negligible for the reasons discussed in the previous section.

The increased land-sea temperature contrast in the northern hemisphere produces a reduction in surface pressure over the continents and increases in pressure over the neighbouring oceans (Figure 10b). In general, this enhances low level convergence and ascent over the northern continents in low latitudes and leads to stronger subsidence and divergence over the surrounding oceans (Figure 10c). A band of increased convergence stretches from North Africa across Arabia into Mongolia, corresponding to a strengthening of the southwest monsoon. The low-level westerly

flow over southern Asia is shifted polewards, giving rise to easterly anomalies at 850 mb south of the Himalayas, and stronger westerly flow to the north. These changes are in qualitative agreement with those found by KG. There is also stronger convergence at 850 mb over the northern part of South America associated with enhanced onshore flow. At 250 mb, there is anomalous easterly flow between 15°S and 30°N with maximum changes greater than 10 m/s extending from northern India to the northern equatorial Atlantic (Figure 10d). Stronger outflow from the monsoon with greater divergence aloft is compensated by increased convergence aloft and subsidence over the equatorial Atlantic and Caribbean (not shown).

The stronger monsoonal flow intensifies precipitation over southern Asia and eastern North America and North Africa (Figure 10e). This is particularly noticeable in regions where onshore flow is enhanced, as for example over the southeastern United States. Note that there are also increases over much of northern South America. On the western side of Eurasia and Africa, there is a general decrease in precipitation associated with anomalous northerly and easterly flow which inhibits the progress of warm moist air from the south. However over Morocco and the western United States where there is an increase in the onshore component of the wind, rainfall increases. KG found a substantial increase in precipitation over Africa near 15°N extending from west to east, contrasting with the region of reduced rainfall extending from Libya to the Gulf of Guinea in

Figure 10e. In the model used here, soil moisture is determined by the model and where appropriate, used to limit evaporation. During early summer, the enhanced northerly flow over western North Africa at 9 Kbp reduces precipitation over western North Africa, reducing soil moisture (Figure 10f). This reduces evaporation which may further contribute to the reduction in precipitation (Walker and Rowntree, 1977; Rowntree and Bolton, 1983; Yeh et al, 1984). In the companion paper, we examine the changes in the hydrological cycle over North Africa in more detail, and the reason for the discrepancy with the results of KG in this region.

In low latitudes, the increases in soil moisture generally are associated with the changes in precipitation (Figure 10e). Over the remainder of the northern continents, there is a general reduction in soil moisture, even though there is an increase in precipitation in high latitudes. Here the increases in evaporation more than offset the increased precipitation.

b. December to February (DJF)

At 9 Kbp, insolation was reduced at all latitudes during northern winter (Figure 2a). Temperature reductions of over 0.5 K are found in low latitudes of the southern hemisphere (Figure 11) where the reduction in insolation is greatest. In the northern extratropics there is a warming throughout the troposphere. The largest increases occur near 80°N (discussed in

section 3.1) and are restricted to lower levels due to the strong surface inversion found at high latitudes in winter. The reduction in the meridional temperature gradient reduces the zonally averaged westerly component of wind (not shown) near 40°N.

The high latitude warming extends southwards over much of North America and Eurasia poleward of 45°N (Figure 12a). (The warming over the mid-latitude oceans was discussed in section 3.1). In low latitudes, it is generally cooler at 9 Kbp, especially in the continental interiors. The oceans cool more slowly than the continents because of their much larger thermal inertia. Hence, over land where the maritime influence is large, as at mid-latitudes in the southern hemisphere, the cooling is substantially reduced. In southern low latitudes, there is a reduction in cloud over the continents (not shown) which also ameliorates the cooling.

Surface pressure is raised over the continents in low latitudes, especially southern Asia, South America and southern Africa (Figure 12b), in response to the reduced insolation. Surface pressure is reduced over most of the oceans in middle and low latitudes where the surface temperature is generally higher at 9 Kbp. There are also reductions in surface pressure over northeastern Canada, the Arctic and near Kamchatka associated with a pronounced surface warming and the thinning or removal of sea-ice. Although these changes are not statistically

significant, Wilson and Mitchell (1987) did find significant reductions in surface pressure where winter sea-ice was removed in a simulation with enhanced CO_2.

In the southern hemisphere, the reduction in the sea-to-land pressure gradient indicates the weakening of the summer monsoonal circulation which is a direct result of the reduction in insolation. Thus there is less low level convergence and high level divergence in these regions (not shown), and a substantial decrease in precipitation (Figure 12c) which is also evident over southern Asia. The reduction in precipitation over the continents is compensated by enhanced rainfall over the oceans, for example, over the Arabian Sea and to the north and east of South America. These increases occur despite the general cooling of the low latitude oceans, indicating that it is the change in land-sea temperature contrast and the subsequent changes in circulation rather than local changes in sea surface temperature which dominate the changes in oceanic precipitation. Note however that the largest increases in precipitation occur where there is least cooling, or even slight warming (Figure 12a).

There is a widespread increase in precipitation poleward of 45°N which may be due to the general increase in temperature which enables northward moving air masses to transport more moisture into high latitudes, as discussed by Manabe and

Wetherald (1987). Furthermore, the higher surface temperatures and less extensive sea-ice will tend to increase the moisture in the atmosphere available for precipitation.

There is a widespread reduction in soil moisture during DJF at 9 Kbp (Figure 12d). The main exceptions are the mostly small increases in arid regions in the northern subtropics including the southern United States and the region extending from the Sahara northeast through the Arabian peninsula and east towards the Gobi desert. These areas were also wetter in JJA.

c. Comparisons with Kutzbach and Guetter, 1986 (KG)

The mean changes in simulated climate are similar in most respects to those found by KG in 'constant' July and January simulations. In both studies, the monsoon circulations are stronger in July and weaker in January. The changes in selected variables meaned over the northern hemisphere and 0° to 30°N are displayed in Tables 2 and 3 respectively. In July, the larger increase in surface temperature in the present work, due mainly to a greater warming in mid-latitudes, may be attributed to the warming of the surrounding ocean (recall KG prescribed present day sea surface temperatures), a positive feedback between soil moisture and temperature (KG effectively prescribe soil moisture) and probably a stronger positive cloud-temperature feedback. KG also included a small ice sheet over eastern Canada at 9 Kbp which would also tend to reduce the warming found in their

simulations. In low latitudes, the changes in surface temperature are smaller than found by KG (Table 3) due to larger increases in cloud and increases in soil moisture. There is a much smaller increase in land-sea temperature contrast, but the enhancement in the sea to land pressure gradient and the fractional increase in precipitation are similar.

In January, the cooling of the northern hemisphere continents is marginally less pronounced in the present experiment (Table 2), due both to the lack of an ice sheet over North America and the warming over the surrounding areas of ocean and sea-ice in middle and high latitudes. In low latitudes, the magnitude of the cooling is similar (Table 3), but the change in land-sea contrast is less marked due to the reduction in sea temperatures. In KG, there is no change in precipitation whereas here there is a reduction.

3.3 Simulation for 9 Kbp with a Laurentide ice sheet

Glaciological evidence indicates that a substantial portion of the Laurentide ice sheet remained at 9 Kbp (Paterson, 1972; Denton and Hughes, 1981). There is considerable uncertainty concerning the volume and distribution of the ice sheet, so KG arbitrarily prescribed a single dome with a maximum height of 800 m. Recently, Boulton et al (1985) have questioned the validity of geological models which produce a single dome since they do not account for the observed dispersal of erratics. They suggest an alternative basal boundary condition which

is more appropriate for water soaked sediments than the bedrock which is more typical of current high latitude ice sheets. This leads to a two-centred dome and a higher volume/area ratio for the Laurentide ice sheet than found in previous work.

We have compared the initial 9 Kbp simulation with a second simulation which includes a two-centred dome representing the Laurentide ice sheet (Figure 13). The topography of the ice sheet is based loosely on Boulton et al (1985). Given the arbitrariness with which Boulton et al (1985) had to prescribe their lower boundary condition, and the 'ad hoc' manner in which we have interpreted their results, the ice sheet experiment is probably best regarded as a sensitivity study. Note that the maximum height of the ice sheet (2000 m) is much larger than that used by KG. The analysis of this experiment will concentrate on comparison of the surface temperature in the ice sheet simulation (9I) with that in the present day simulation and that at 9 Kbp without an ice sheet (9C).

The major impact of including the Laurentide ice sheet is to reduce the warming over North America and downstream over the north Atlantic and much of northern Eurasia. During JJA, temperatures on the ice sheet are up to 15K colder than present, although the warming over southern Canada and the United States is similar to that found in experiment 9C (Figure 14, compare Figure 10a). In 9C, the north Atlantic is up to 2 K warmer than present, whereas in the 9I simulation, it is colder to the east of the ice sheet, particularly in both the Davis Strait and the Greenland Sea where sea-ice is thicker

rather than thinner at 9 Kbp. The warming over Europe and northern Asia is 1 to 2 K less than in the 9C experiment (see also Table 4). The temperature changes are similar equatorward of 30°N, and there is no consistent pattern in the southern hemisphere, although the warming over South America and southern Africa is less extensive in the ice sheet experiment.

The fall in surface pressure over the northern continents (Table 4) is smaller than in the 9C experiment though the patterns (not shown) are generally similar. Surface pressure is increased to the south and east of the ice sheet due to enhanced subsidence of air. Rind et al (1986) find similar results in the vicinity of the higher ice sheets in their 11 Kbp experiments. The changes in precipitation, moisture supply and cloud are also smaller in 9I than in 9C (Table 4). There is an increase in the supply of moisture (precipitation minus evaporation) over the ice sheet, but this is more than offset by snowmelt, giving a mean annual ablation of 0.7 m.

During DJF, the north American continent is substantially colder with the ice sheet than in 9C or in the control simulation (Figure 15). However, there is an isolated area of warming in northern Canada associated with anomalous south westerly flow round the western flank of the ice sheet (KG noted a similar effect in their 9 Kbp experiment). The general cooling extends across the north Atlantic into Europe and parts of Asia. As in JJA, the cooling is particularly marked in the Davis Strait and the Greenland Sea due to sea-ice becoming thicker and more extensive, in contrast to the

changes in the 'no ice sheet' experiment. In both 9 Kbp integrations, there is a substantial warming elsewhere in high latitudes associated with thinner and less extensive sea ice. Once again, there is no systematic difference between the anomaly simulations in the tropics and southern hemisphere. The changes in surface pressure (not shown) are generally similar, the main difference occurring near the ice sheet where anomalous anticyclonic flow is generated through the depth of the troposphere.

4. Summary and Concluding Remarks

The effect on climate of changing the earth's orbital parameters from their present value to those valid 9000 years ago has been investigated using an atmospheric model coupled to a mixed layer ocean. At 9Kbp, the summer monsoon circulations are more vigorous in the northern hemisphere and weaker in the southern hemisphere. These findings are in broad agreement with those of KG who used an atmospheric model with prescribed sea surface temperature and soil moisture. Here, sea-ice, sea surface temperature and soil moisture are all determined within the model, and modify the simulated response. In high latitudes, the increase in summer insolation produces thinner less extensive sea-ice which leads to a pronounced warming in autumn and winter. Over the northern mid-latitude oceans there is a marked reduction in cloud in late summer which enhances the warming of the mixed layer to such an extent that the sea surface temperatures are higher than present throughout the year. The northern mid-latitude land surface is drier throughout the year. At lower

latitudes, the summer warming is limited by increases in soil moisture and cloud whereas the reverse is true in mid-latitudes. Changes in soil moisture modify the changes in the southwest monsoon over Africa.

The 9 Kbp simulation was repeated with a Laurentide ice sheet. The changes in sea-ice are substantially reduced downstream, and the warming over land and ocean in mid-latitudes is reduced. The timing of the collapse of the Laurentide ice sheet is uncertain, so the 'ice sheet' and 'no ice sheet' experiments are appropriate respectively to just before and just after this event.

By comparing the changes in insolation (Figure 2a) with the changes in surface temperature (Figure 4a, b), it can be seen that the response of the simulated climate to changes in orbital forcing has been modified substantially by various feedbacks, lags and changes in circulation. It is evident that the changes in climate between 9 Kbp and present are likely to have been far from uniform. Furthermore the relationship between the changes in 'forcing' (in this case, changes in insolation) and the climatic response may be complex, as found here with the winter changes in temperature in northern high latitudes. These facts must be borne in mind when interpreting palaeoclimatic data.

The experiments described above are very much sensitivity experiments to determine those factors most likely to have been important in determining climate at 9 Kbp. The broad agreement between the results presented here and those reported by KG and others suggests that the large scale changes (for example in the monsoon circulations) are probably

qualitatively realistic. However, the regional details may vary considerably from model to model (see for example, Mitchell et al (1987)) so great care must be exercised when comparing the changes in climate deduced from palaeoclimatic data at a particular site and the simulated changes from the model. Even if the model were 'perfect', the horizontal resolution is too coarse to represent local effects due to topography, variations in vegetation etc..

There are several ways in which the present work may be extended. First, the experiments could be repeated using higher resolution models in order to obtain a better simulation of the present day climate (and hopefully the response to orbital parametrizations). Secondly, the experiments could be repeated using alternative or improved parametrizations of selected sub-grid scale processes (eg cloud, convection etc). Experiments with several different parametrizations of the land surface are to be reported in a forthcoming paper. Third, experiments could be carried out using an atmospheric model coupled to a dynamical model of the ocean and sea-ice, so as to take into account changes in circulation and salinity. Such a model has recently been developed at the Meteorological Office.

The art of simulating past climates using detailed numerical models is only in its infancy. Whereas 10 years ago, lack of computing resources limited the duration of most simulations to a few months, simulations of a century or longer have now been made (Hansen et al 1986, Manabe, personal communication). Thus we have the prospects of modelling providing new insights into mechanisms of climatic change, and guiding the search for new

palaeoclimatic evidence, and of palaeoclimatic data being used to help determine which aspects of the models are unrealistic. This is important not only for the understanding of past climates but also for the prediction of future changes in climate, including that due to increases in atmospheric CO_2 and other trace gases.

5. Acknowledgements

We wish to thank Dr Alayne Street-Perrott for helpful advice and comments during various stages of this work, Prof. Geoff Boulton for providing information concerning the Laurentide ice sheet and Bruce Ingleby for setting up and checking the initial 9 Kbp simulation. Dr Peter Rowntree also contributed useful comments on the manuscript.

APPENDIX 1

Changes in orbital parameters and choice of calendar

The changes in orbital parameters alter the intervals between the solstices and equinoxes (Table 5). This introduces a degree of arbitrariness in how the calendar months for 9 Kbp and present are aligned. We have chosen to fix the calendar by choosing the summer solstice to be the 22nd of June in each experiment. This gives smaller maximum differences in the dates of equinoxes and solstices than using the vernal equinox, and minimizes the differences in the calendar dates during the northern hemisphere summer when insolation changes are largest. The enhanced warming in high latitudes of the southern hemisphere during October and November at 9 Kbp is a result of the autumnal equinox occurring over 5 days earlier at 9 Kbp than present (see Table 5).

Some authors (for example Kutzbach and Otto-Bliesner, 1982) use astronomical or 'celestial' months in which equal weight is given to equal angular distances in the earth's orbit round the sun. In this case, the equinoxes and solstices for 9 Kbp and present coincide. The differences in insolation at the top of the atmosphere for the 'celestial' months are shown in Figure 16, and for a particular month, may be compared with Figure 2a. Note however that each 'celestial' month has a different length at 9 Kbp than at present, so that Figure 16 cannot for example be used to estimate the annual mean change in insolation at a particular latitude.

The model uses a 360 day year with twelve 30 day months (Slingo, 1982). The consequent errors in calendar monthly means of incoming solar radiation are generally less than 1 Wm^{-2} and do not exceed 4 Wm^{-2} for either set of orbital parameters, and the error in the difference in monthly mean incoming solar radiation is everywhere less than 0.5 Wm^{-2}.

Appendix 2

Statistical significance of changes in surface temperature, mean sea level pressure (PMSL), precipitation and soil moisture

A 2-tailed Student's t-test was carried out on the JJA and DJF seasonal means from the last 13 years of the 9Kbp simulation and the last 15 years of the present day (control) simulation for each of the changes in surface temperature, PMSL, precipitation and soil moisture. The limitations of such a test applied to meteorological variables which are correlated in space and which may not be sampled from a normal population (especially true of precipitation) have been noted by Mitchell et al (1987).

1. June, July, August

Charts of the t-statistic show that the increase in surface temperature over much of the extratropical northern hemisphere (both land and ocean) in JJA is significant at the 99% level of confidence although over sea-ice this is not the case for reasons given earlier (Figure 17). The cooling over India and Arabia due to cloud and soil moisture feedbacks is shown also to be significant at the same level of confidence. In the southern hemisphere the increase in surface temperature over the continents in response to the increased insolation shows up generally whilst some areas of the ocean are significantly colder because of excessive heat loss earlier in the year.

The increased land-sea contrast in the northern hemisphere produces significant changes in PMSL (Figure 18). Over India and southeast Asia the significant increases in PMSL are related to a poleward shift of the westerly flow associated with the Asian monsoon. Over the southern oceans the significant pressure rises correspond to the areas of colder sea surface temperature mentioned above.

Precipitation is inherently more variable spatially than temperature (Figure 19). Note the significant increases over southern Asia, the eastern United States and the northern part of South America. In northern mid- and high latitudes, for example central Asia and Canada, precipitation is also significantly greater, but here increased evaporation gives rise to a net decrease in (P-E). This is illustrated to some extent in the t-statistic chart of soil moisture which shows a significant drying at these latitudes (Figure 20). Over the northern oceans there are generally significant decreases in precipitation as one might expect from the enhanced land-sea temperature contrast.

2. December, January, February

The extratropical northern hemisphere warming (see Figure 11a) is, in general, not statistically significant above the 90% level over the continents whereas over the mid-latitude oceans, for instance, the warming is significant at the 99% level of confidence (Figure 21). In low latitudes the cooling of the land surface is significant at the 99% level north of the Equator. Over southern Africa and South America the signal is

smaller but the weakening of the monsoon circulation is still significant (Figure 22). Note that a spatially coherent significant area of warming is found over the southern Pacific Ocean.

At low latitudes over land the statistical significance of increases in PMSL is greatest to the north of the Equator (Figure 22). Over the north Pacific the pressure falls are significant at the 90% level of confidence but the pattern over the north Atlantic is somewhat different with an area between Greenland and Europe exhibiting statistically significant PMSL increases above the 90% level.

The t-statistics of precipitation appear spatially incoherent save for the weakening of the southern hemisphere summer monsoonal circulation, clearly apparent with reductions in rainfall over the low latitude continents, and increases over extensive areas of the oceans, both showing significance above the 90% level of confidence (Figure 23). In the northern hemisphere poleward of 45°N there are substantial areas of significant increases in precipitation as discussed earlier. The corresponding soil moisture chart for DJF shows a significantly wetter land surface over southern and central Asia and parts of North Africa whereas at higher latitudes in the northern hemisphere there is still a significant drying similar to, but less extensive than that seen in JJA (Figure 24). The weakened southern hemisphere monsoon is depicted by areas of significantly reduced soil moisture in South America, southern Africa and Australia.

References

Berger, A L 1979 Long term variations of daily insolation and quartenary climatic changes. J. Atmos. Sci., 35, 2362-2367.

Boulton, G S, Smith, G D, Jones, A S and Newsome, J 1985 Glacial geology and glaciology of the last mid-latitude ice sheets. J. Geol. Soc. London, 142, 447-474.

Clarke, R H 1970 Recommended methods for the treatment of the boundary layer in numerical models. Australian Met. Mag. 18, 51-73.

Corby, G A, Gilchrist, A and Rowntree, P R 1977 United Kingdom Meteorological Office 5 level general circulation model. Methods in computational physics, Vol. 17, Academic Press INc., New York, San Francisco and London, 67-110.

Cunnington, W M and Rowntree, P R 1986 Simulation of the Saharan Atmosphere - Dependence on moisture and albedo. Quart. J.R. Met. Soc. 12, 971-1000.

Denton, G H and Hughes, T J (ed) 1981 The last great ice sheets, Wiley, pp 484.

Gammon, R H, Sundquist, E T and Fraser, P J 1985 History of carbon dioxide in the atmosphere. In 'Atmospheric Carbon Dioxide and the Global Carbon Cycle' (ed J R Trabalka). DOE/ER-0239, p25-62. US Dept. of Energy, Washington DC.

Gates, W L 1976 Modelling the Ice-Age Climate. Science, 191, 1138-1144.

Gordon, C and Bottomley, M 1984 A scheme for incorporating the thermodynamic sea-ice model into a coupled ocean-atmosphere model. Met O 20 DCTN No. 1, Meteorological Office, Bracknell.

Hansen, J, Lacis, A, Rind, D, Russell, G, Stone, P, Fung, I, Ruedy, R and Lerner, J 1984 Climate Sensitivity and Analysis of Feedback Mechanisms. In Climate Sensitivity (ed. J Hansen and T Takahashi) Geophysical Monograph 29, 130-163. American Geophysical Union, Washington DC.

Hansen, J, Lacis, A, Rind, D, Russell, G, Fung, I, Ashcraft, P, Lebedeff, S, Ruedy, R and Stone, P 1986 The greenhouse effect: Projections of global climate change. In 'Effects of changes in stratospheric ozone and global climate'. Volume 1. Overview. p 99-218. US Environmental Protection Agency, Washington DC.

Hecht, A D (ed.) 1985 Palaeoclimatic Analysis and Modelling. John Wiley and Sons (New York, Chichester, Brisbane, Toronto, Singapore) pp 445.

Jaeger, L 1976 Monatskarten des Niederschlags fur die ganze Erde. Ber. Deutch. Wet. 18, no. 139, 38 pp.

Kutzbach, J E and Guetter, P J 1986 The influence of changing orbital parameters and surface boundary conditions on climate simulations for the past 18000 years. J. Atmos. Sci. 43, 1726-1759.

Kutzbach, J E and Otto-Bliesner, B 1982 The sensitivity of the African-Asian monsoonal climate to orbital parameter changes for 9000 years BP in a low resolution general circulation model. J. Atmos. Sci. 39, 1177-1188.

Kutzbach, J E and Street-Perrott, F A 1985 Milankovitch forcing of fluctuations in the level of tropical lakes from 18 to 0 kyr BP. Nature, 317, 130-134.

Lyne, W H and Rowntree, P R 1976 Development of a convective parametrization using GATE data. Met O 20 Tech. Note II/70 Meteorological Office, Bracknell, Berkshire RG12 2SZ.

Manabe, S 1969 Climate and the ocean circulation I. The atmospheric circulation and the hydrology of the earth's surface. Month. Weath. Rev., 97, 739-774.

Manabe, S 1983 Carbon Dioxide and Climatic Change Advances in Geophysics 25, 39-82 Academic Press Inc.

Manabe, S and Broccoli, A J 1985 A comparison of Climate Model Sensitivity with data from the last glacial maximum. J. Atmos. Sci.

Manabe, S and Bryan, K, Jr 1985 CO_2-induced Change in a Coupled Ocean-Atmosphere Model and its Palaeoclimatic Implications. J. Geophys. Res. 90, C6, 11689-11707.

Manabe, S, Hahn, D G and Holloway, J R, Jr 1979 Climate Simulations with GFDL Spectral Models of the Atmosphere: Effect of Spectral Truncation. Report of JOC Study Conference on Climate Models: Performance, intercomparison and sensitivity studies. GARP Publication series No. 22. 41-94.

Manabe, S and Hahn, D G 1977 Simulation of the Tropical Climate of an Ice Age. J. Geophys. Res., 82, 3889-3911.

Manabe, S and Stouffer, R J 1980 Sensitivity of a global climate model to an increase in the CO_2 concentration in the atmosphere. J. Geophys. Res. 85, 5529-5554.

Manabe, S and Wetherald, R T 1987 Large scale changes of soil wetness induced by an increase in atmospheric carbon dioxide. J. Atmos. Sci. (To appear).

Maykut, G A and Untersteiner, N 1971 Some results from a time-dependent thermodynamic model of sea-ice. J. Geophys. Res. 76, 1550.

Meehl, G A and Washington, W M 1985 Sea surface temperatures computed by a simple ocean mixed layer coupled to an atmospheric GCM. J. Phys. Oceanogr. 15, 92-104.

Mitchell, J F B 1976 The effect on climate of changing the parameters of the earth's orbit: two summer integrations incorporating a fully interactive surface. Met O 20 Tech. Note II/72, Meteorological Office, Bracknell, Berkshire RG12 2SZ.

Mitchell, J F B 1977 The effect on climate of changing the earth's orbital parameters: two summer integrations with fixed sea surface temperatures. Met O 20 Tech. Note II/100, Meteorological Office, Bracknell, Berkshire RG12 2SZ.

Mitchell, J F B, Wilson, C A and Cunnington, W M 1987 On CO_2 climate sensitivity and model dependence of results. Quart. J. R. Met. Soc. 113, 293-322.

Palmer, T N and Mansfield, D A 1986 Wintertime Circulation Anomalies during past El Nino Events, using a High Resolution General Circulation Model I. Influence of model climatology. Quart. J. R. Met. Soc., 112, 613-638.

Paterson, W S B 1972 Laurentide Ice Sheet: Estimated Volumes during Late Wisconsin. Reviews of Geophysics and Space Physics, 10, No. 4, 885-917.

Richards, P J R 1980a An objective assessment of specifications of boundary-layer eddy diffusion coefficients. Met O 20 Tech. Note II/140, Meteorological Office, Bracknell.

Richards, P J R 1980b The parametrization of boundary layer processes in general circulation models. Ph. D. Thesis, Department of Meteorology, University of Reading, England.

Rind, D, Peteet, D, Broecker, W, McIntyre, A, and Ruddiman, W 1986 The impact of cold North Atlantic sea surface temperatures on climate: implications for the Younger Dryas cooling (11-10k). Climate Dynamics, 1, 3-33.

Rowntree, P R 1984 Sensitivity of global simulations to the evaporation of convective condensates. Workshop on convection in large scale numerical models, 28 November to 1 December 1983, ECMWF. Also appears as Met O 20 Tech. Note II/226, Meteorological Office, Bracknell.

Rowntree, P R and Bolton, J A 1983 Simulation of the atmospheric response to soil moisture anomalies over Europe. Quart. J. R. Met. Soc. 109, 501-526.

Schlesinger, M E and Mitchell, J F B 1987 Model Projections of Equilibrium Climatic Response to Increased CO_2 Concentrations. Reviews of Geophysics. (To appear).

Schneider, S H, Peteet, D, and North, G R 1987 A climate model intercomparison for the Younger Dryas and its implications for Palaeoclimatic data collection in Abrupt Climatic Change, NATO/NSF Workshop, Bivier (Grenoble), W H Berger and L Labeyrie (eds), D Reidel, Dordrecht. (To appear).

Schutz, C and Gates, W L 1971 Global climatic data for surface, 800 mb, 400 mb: January. Advanced Research Projects Agency. Rept. R-915-ARPA, Rand Corporation, Santa Monica 173 pp.

Semtner, A J Jr 1976 A model for the thermodynamic growth of sea-ice in numerical investigations of climate. J. Phys. Oceanogr., 6, 379-389.

Slingo, A (ed.) 1985a Handbook of the Meteorological Office 11-layer atmospheric general circulation model. Met O 20 DCTN 29. UK Meteorological Office, Bracknell.

Slingo, A 1985b Simulation of the earth's radiation budget with an 11-layer general circulation model. Meteorol. Mag. 114, 121-141.

Slingo, A and Wilderspin, R C 1986 Development of a revised long wave radiation scheme for an atmospheric general circulation model. Quart. J.R. Met. Soc. 112, 371-386.

Walker, J and Rowntree, P R 1977 The effect of soil moisture on circulation and rainfall in a tropical model. Quart. J. R. Met. Soc., 103, 29-46.

Wetherald, R T and Manabe, S 1986 An investigation of cloud cover change in response to thermal forcing'. Climate Change, 8 5-24.

Williams, J, Barry, R G and Washington, W M 1974 Simulation of the Atmospheric Circulation using the NCAR Global Circulation Model with ice age boundary conditions. J. Appl. Meteorology 13, 305-317.

Wilson, C A and Mitchell, J F B 1987 A 2 x CO_2 climate sensitivity experiment with a global climate model including a simple ocean. Met O 20 DCTN 48, Meteorological Office, Bracknell, submitted for publication.

Wilson, M F and Henderson-Sellers, A 1985 A global archive of land cover and soils data for use in general circulation climate models. J. Climatol., 5, 119-143.

Yeh T-C, Wetherald, R T and Manabe, S 1984 The effect of soil moisture on the short term climate and hydrology change - A numerical experiment. Month. Weath. Rev. 112, 474-490.

TABLE 1 Orbital parameters for present and 9000 years before present (9 Kbp)

	Present	9 Kbp
Longitude of Perihelion (relative to the vernal equinox)	102.5°	311.2°
Obliquity	23.44°	24.23°
Eccentricity	0.0167	0.0193

TABLE 2 Comparison of changes found in this paper (MGN) and Kutzbach and Guetter (1986) (KG) between 9Kbp and present day climate over northern hemisphere land, July and January.

	July		January	
	MGN	KG	MGN	KG
ΔSW (top) (Wm^{-2})	35	39	-15	-15
ΔT (sfc) (K)	2.6	1.1	0.0	-0.5
Δ(total cloud) (fract)	.02	.01	.00	.00
ΔP (mm/day)	.58	.71	-.09	-.02

Note: SW is the incoming short wave radiation; T is temperature; P is precipitation.

TABLE 3 Comparison of changes found in this paper (MGN) and Kutzbach and Guetter (1986) (KG) between 9 Kbp and present day climate over land, latitude zone 0-30°N, July and January.

	July		January	
	MGN	KG	MGN	KG
ΔSW (top) (Wm^{-2})	32	31	-24	-26
ΔR (sfc) (Wm^{-2})	7	18	-10	-15
Δ(total cloud) (fract)	.10	.04	.00	.00
ΔP (mm/day)	0.7	1.4	-0.4	0.0
ΔT (sfc) (K)	0.3	1.2	-1.5	-1.8
Δ(δT(L-O)) (K)	0.3	1.3	-1.5	-2.3
Δ(δPMSL(L-O)) (mb)	-2.6	-2.6	1.7	1.4

NOTE: R is the net radiation balance; δT(L-O) is the difference in surface temperature between land and ocean; δPMSL(L-O) is the difference in mean sea level pressure between land and ocean.

TABLE 4 Comparison of changes from present day climate at 9 Kbp with (9I) and without (9C) the Laurentide ice sheet, averaged over northern hemisphere land (July).

	9C	9I
ΔT (sfc) (K)	2.6	2.1
Δ(total cloud) (fract)	.02	.01
ΔP (mm/day)	.58	.32
Δ(P-E) (mm/day)	.07	-.02
ΔPMSL (mb)	-3.9	-2.3

Note: P-E is precipitation minus evaporation.

TABLE 5 Change in date of the northern solstices and equinoxes relative to present (days; a positive entry indicates that an event occurs later in the calendar year in the 9 Kbp experiment).

Summer solstice	0.0
Autumnal equinox	-5.4
Winter solstice	-3.7
Vernal equinox	1.8

Figure Captions

Figure 1a. Precipitation in a 15-year mean control simulation for June, July and August. Contours are at 0, 1, 1, 2, 5, 10, 20 mm/day, stippled above 5 mm/day.

Figure 1b. As Figure 1a but for December, January and February.

Figure 2a. Time vs. latitude diagram of zonally averaged differences in incoming solar radiation at the top of the tmosphere, 9Kbp-0Kbp. Contours are at 10 W/m^2 intervals, negative values stippled.

Figure 2b. Zonally averaged differences in annual mean incoming solar radiation at the top of the atmosphere, 9Kbp-0Kbp.

Figure 3. Time vs. latitude diagram of zonally averaged differences in incoming solar radiation at the surface, 9 Kbp-0 Kbp. Contours are at 10 W/m^2 intervals, negtive values stippled.

Figure 4a. Time vs. latitude diagram of zonally averaged differences in surface temperature over land, 9 Kbp-0 Kbp. Contours are at 1 K intervals, negative values stippled.

Figure 4b. As Figure 4a but over sea and sea-ice.

Figure 5. Monthly mean zonally averaged parameters at 77.5°N.

a. Surface temperature (K) for 0 Kbp (solid line) and 9 Kbp (dashed line).

b. Differences (9 Kbp-0 Kbp) in net surface heating (Wm^{-2}, solid line) and surface temperature (K, dashed line).

c. Ice depth, metres, at 0 Kbp (solid line) and 9 Kbp (dashed line).

Figure 6. Arctic sea-ice extents at 9 Kbp, 0 Kbp, X indicates ice-cover at 0 Kbp and 0 cover at 9 Kbp. Note that the polarmost row remains covered throughout the year.

a. May

b. July

c. September

d. December

Figure 7. Zonally meaned differences over land (9 Kbp-0 Kbp) in monthly averaged parameters at 17.5°N (solid line) and 42.5°N (dashed line).

a. Surface Temperature (K).

b. Net surface solar heating (Wm^{-2}).

c. Planetary albedo (%).

d. Soil moisture (cm).

e. Latent heat flux (Wm^{-2}).

f. Sensible heat flux (Wm^{-2}).

Figure 8. Zonally meaned differences over the ocean (9 Kbp-0 kbp) in monthly averaged parameters at 42.5°N.

a. Surface temperature (K).

b. Net downward solar flux at the surface (solid line, Wm^{-2}) and total cloud cover (dashed line, %).

Figure 9. Sigma (= pressure/surface pressure) vs. latitude diagrams of zonally averaged differences between 9 Kbp and 0 Kbp for the period June to August.

a. Temperature. Contours are at 0.5 K intervals and areas of decrease are stippled.

b. West to east component of wind. Contours every 1 m/s, areas of reduced eastward component are stippled.

c. Total layer cloud. Contours are at 0.01 intervals and negative values are stippled.

Figure 10. Differences between 9 Kbp and present for the period June to August.

a. Surface temperature. Contours at 0, ± 2, ± 4 and ± 8K, areas of decrease are stippled.

b. Mean sea level pressure. Contours are at 0, ± 2, ± 4, ± 8 mb, areas of decrease are stippled.

c. 850 mb divergence (10^{-5} s^{-1}). Areas of divergence greater than 0.04 are stippled lightly, and less than -0.04 are stippled heavily. Also shown are differences in 850 mb. wind, with a scale in the bottom left hand corner. Mountaineous areas where the model topography is higher than 850 mb have been masked in black.

d. 250 mb wind. Isotachs every 5 ms^{-1}, regions in excess of 5 ms^{-1} are stippled.

e. Precipitation. Contours at 0, ±1, ±2 mm/day with areas of decrease stippled.

f. Soil moisture. Contours at 0, ±2, ±5 cm. Stippled where negative; heavily where less than -5 cms.

Figure 11. Sigma (= pressure/surface pressure) vs. latitude cross section of zonally averaged differences in temperature (9 Kbp-present). Contours are at intervals of 0.5 K, negative regions are stippled.

Figure 12. As Figure 10, but for the period December to February.

a. Surface temperature.

b. Mean sea level pressure.

c. Precipitation.

d. Soil moisture.

Figure 13. Surface topography over North America including the Laurentide ice sheet. Contours every 250 m, areas higher than 1000 m stippled.

Figure 14. Change in surface temperature 9 Kbp (including a Laurentide ice sheet) minus present. For the period June to August. Contours at 0, ±2, ±4, ±8 K; negative areas stippled.

Figure 15. As Figure 14, but for December to February.

Figure 16. Time vs. latitude diagram of changes in downward insolation at the top of the atmosphere. (9 Kbp-present) for 'celestial' or 'astronomical' months (see Appendix 1). Contours every 10 Wm^{-2}, areas of decrease are stippled.

Figure 17. Level of statistical significance of changes in surface temperature (June, July and August). Contours at the 90 and 99% level of confidence (see Appendix 2). Area of significant increase stippled heavily, areas of significant decrease stippled lightly.

Figure 18. As Figure 17, but for pressure at mean sea level.

Figure 19. As Figure 17, but for precipitation.

Figure 20. As Figure 17, but for soil moisture.

Figure 21. As Figure 17, but for December, January, February.

Figure 22. As Figure 18, but for December, January, February.

Figure 23. As Figure 19, but for December, January, February.

Figure 24. As Figure 20, but for December, January, February.

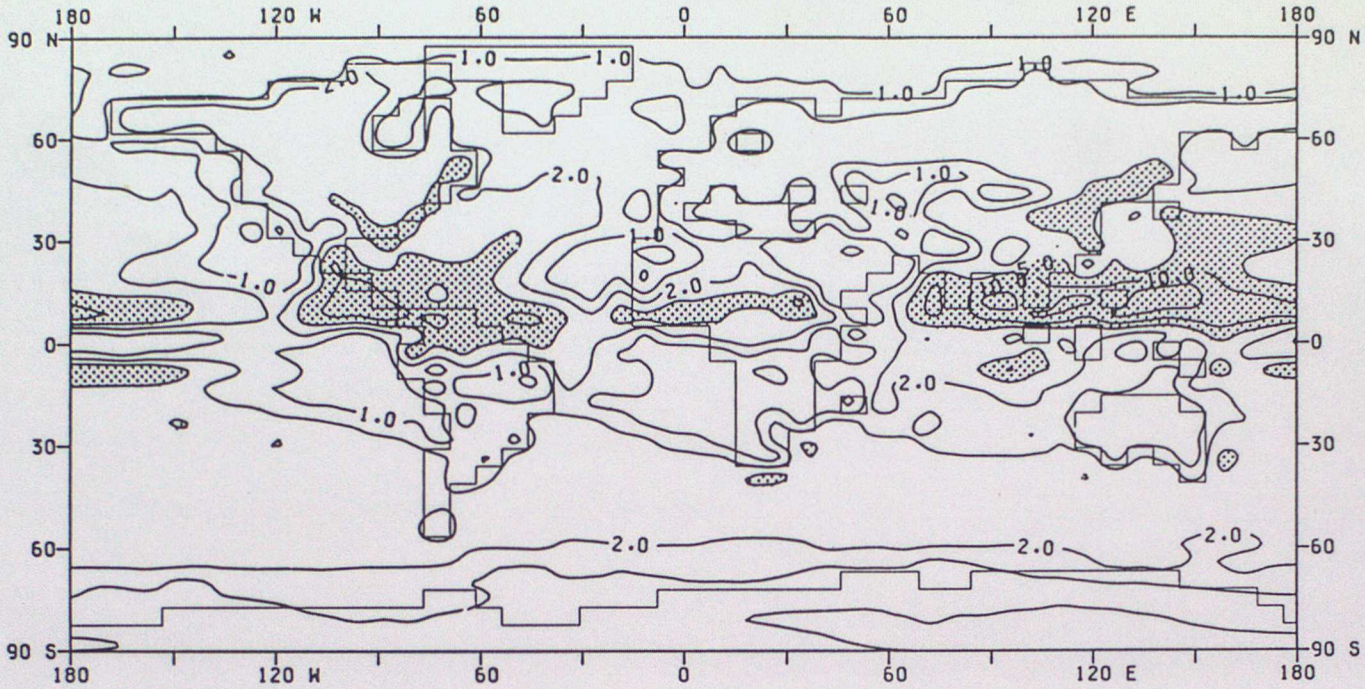

Figure 1 (a)

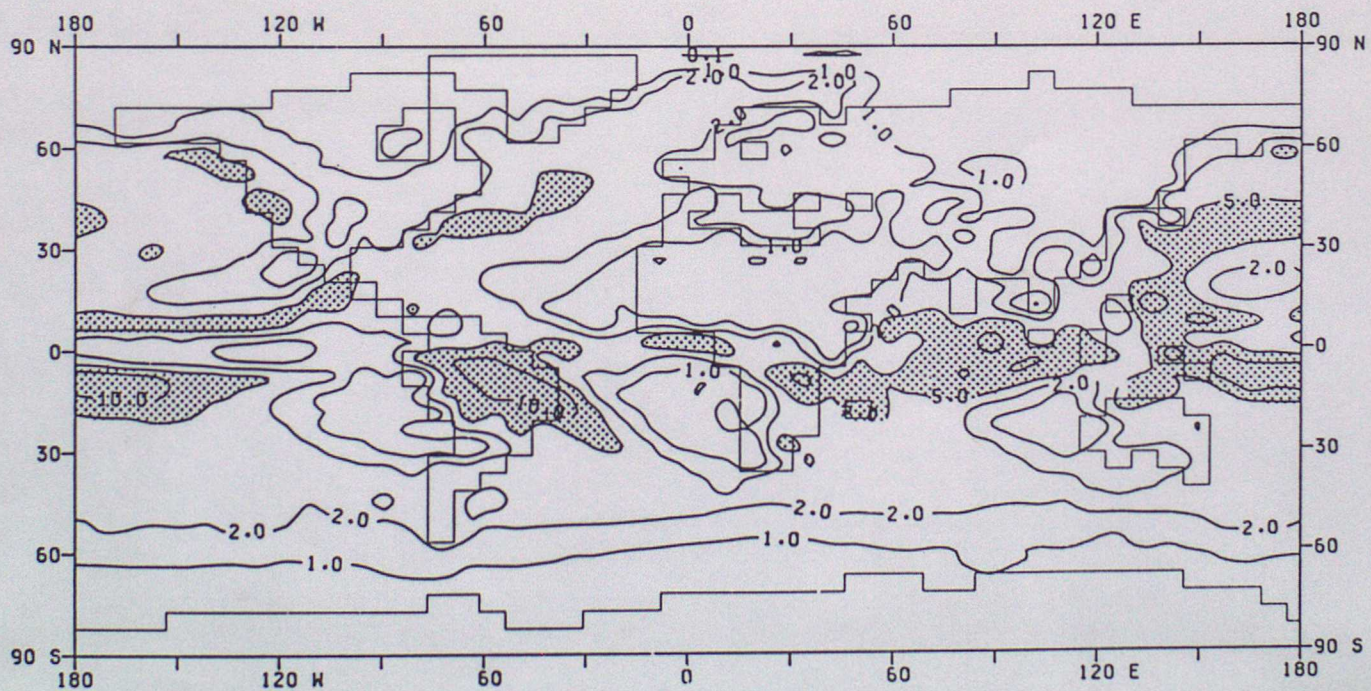

Figure 1 (b

Zonal Mean Differences In Incoming Solar Radiation

At The Top Of The Atmosphere 9Kbp - 0Kbp

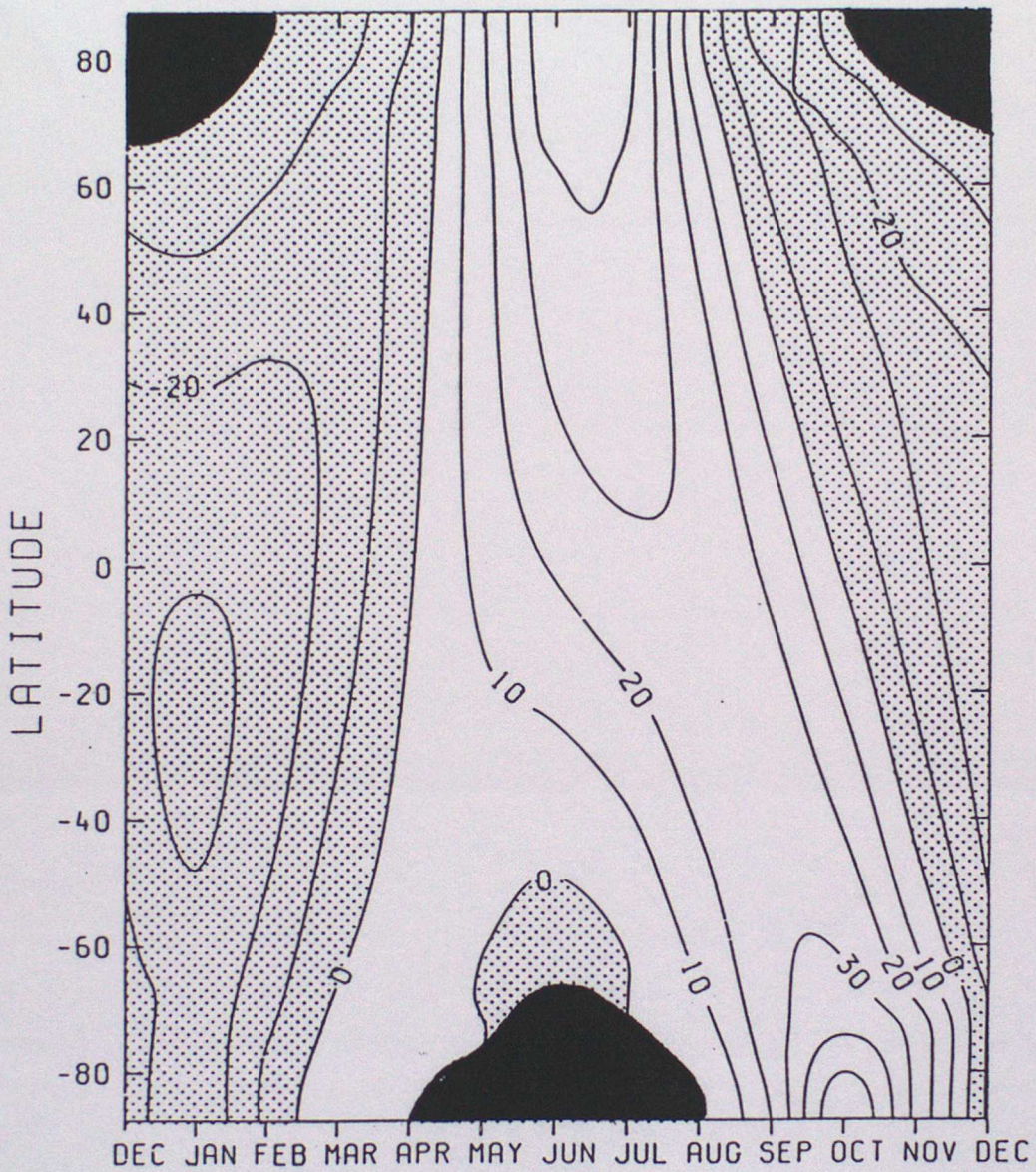

Figure 2(a)

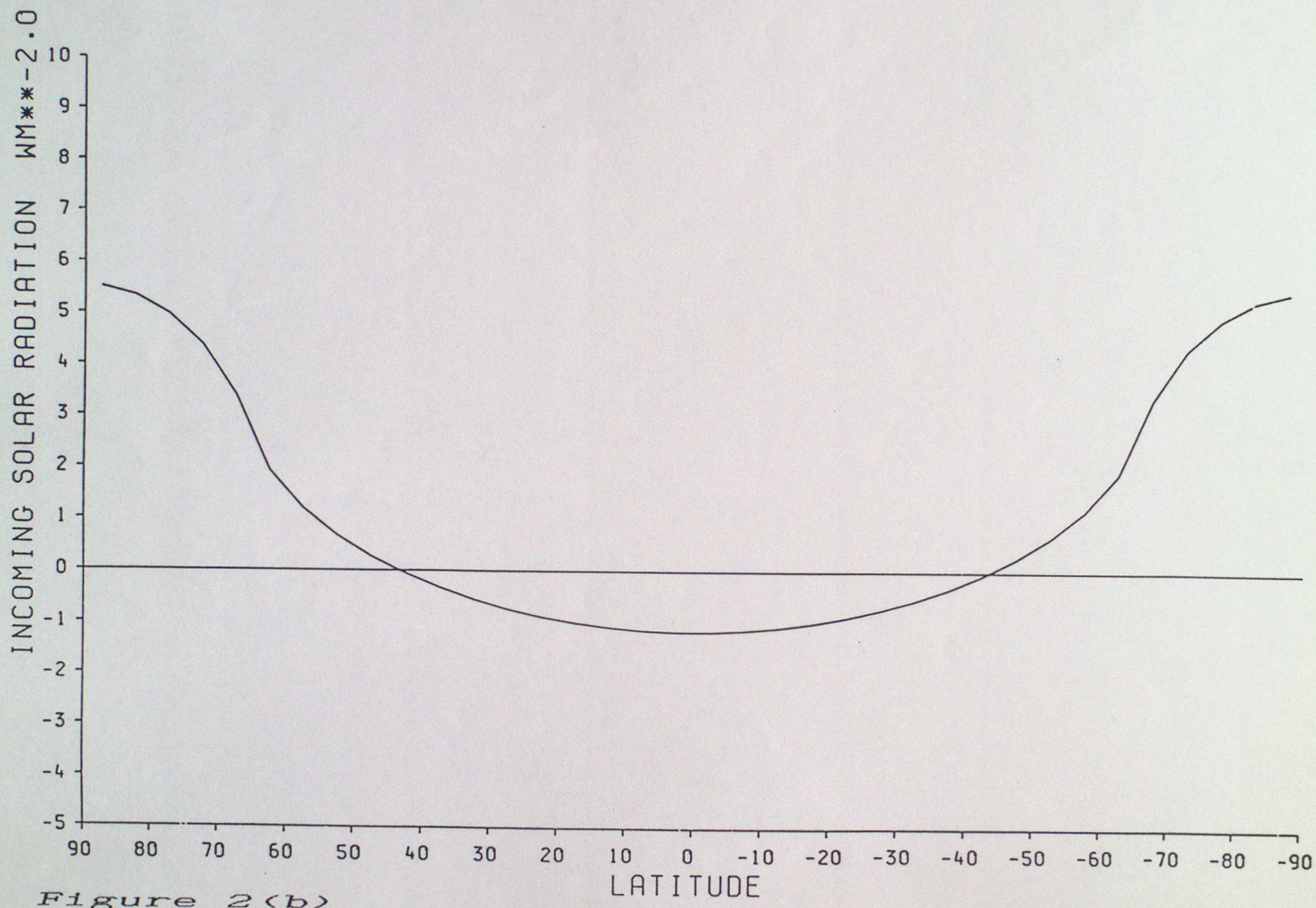
INCOMING SOLAR RADIATION AT TOP OF ATMOSPHERE
ANNUAL MEAN 9000BP - PRESENT
INCOMING SOLAR RADIATION WM**-2.0
10
9
8
7
6
5
4
3
2
1
0
-1
-2
-3
-4
-5
90 80 70 60 50 40 30 20 10 0 -10 -20 -30 -40 -50 -60 -70 -80 -90
LATITUDE

Figure 2(b)

Zonal Mean Differences In Incoming Solar Radiation

At The Surface 9Kbp - .0Kbp

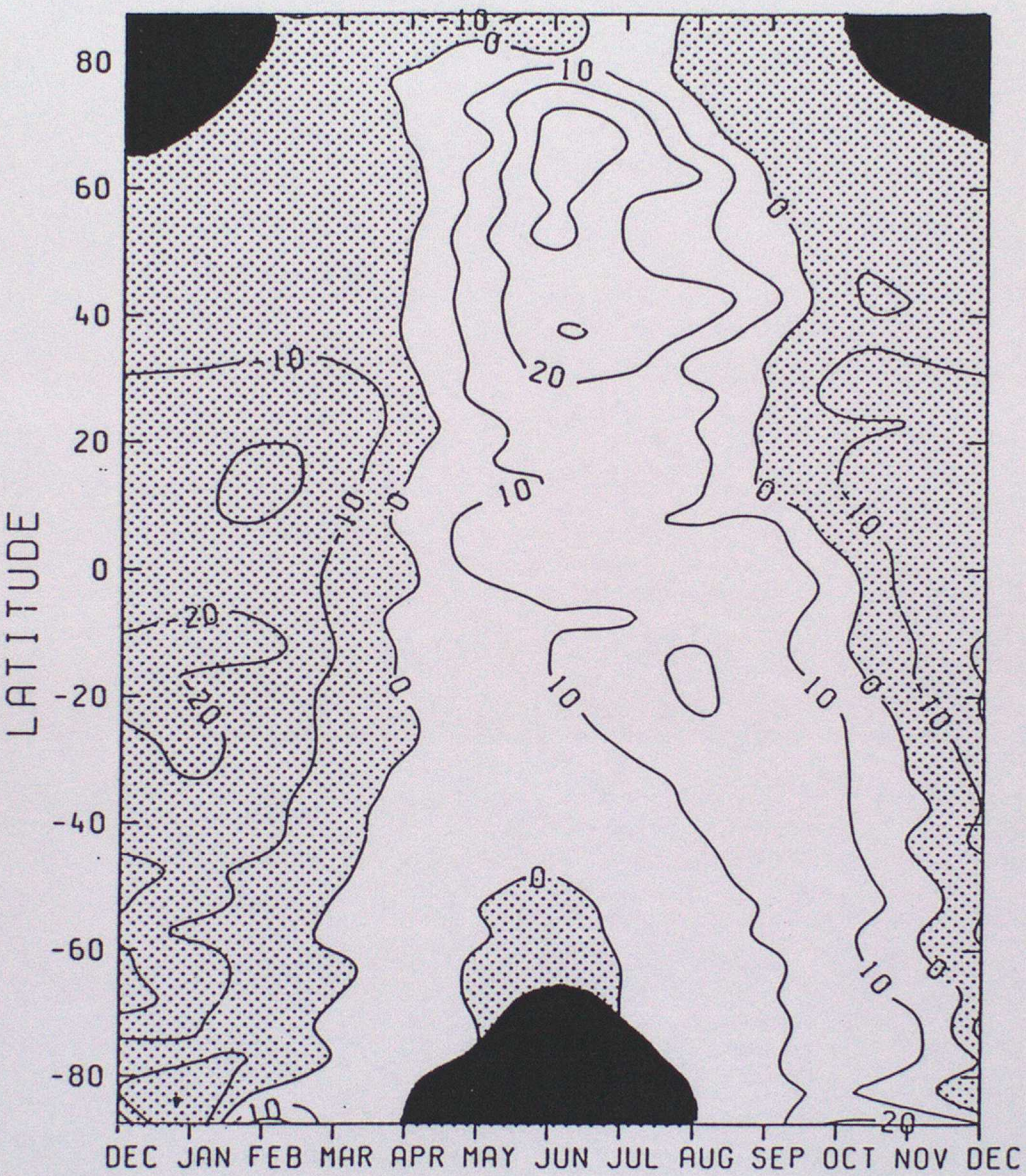

Figure 3

Zonal Mean Differences In Surface Temperature

Over Land Points 9Kbp - 0Kbp

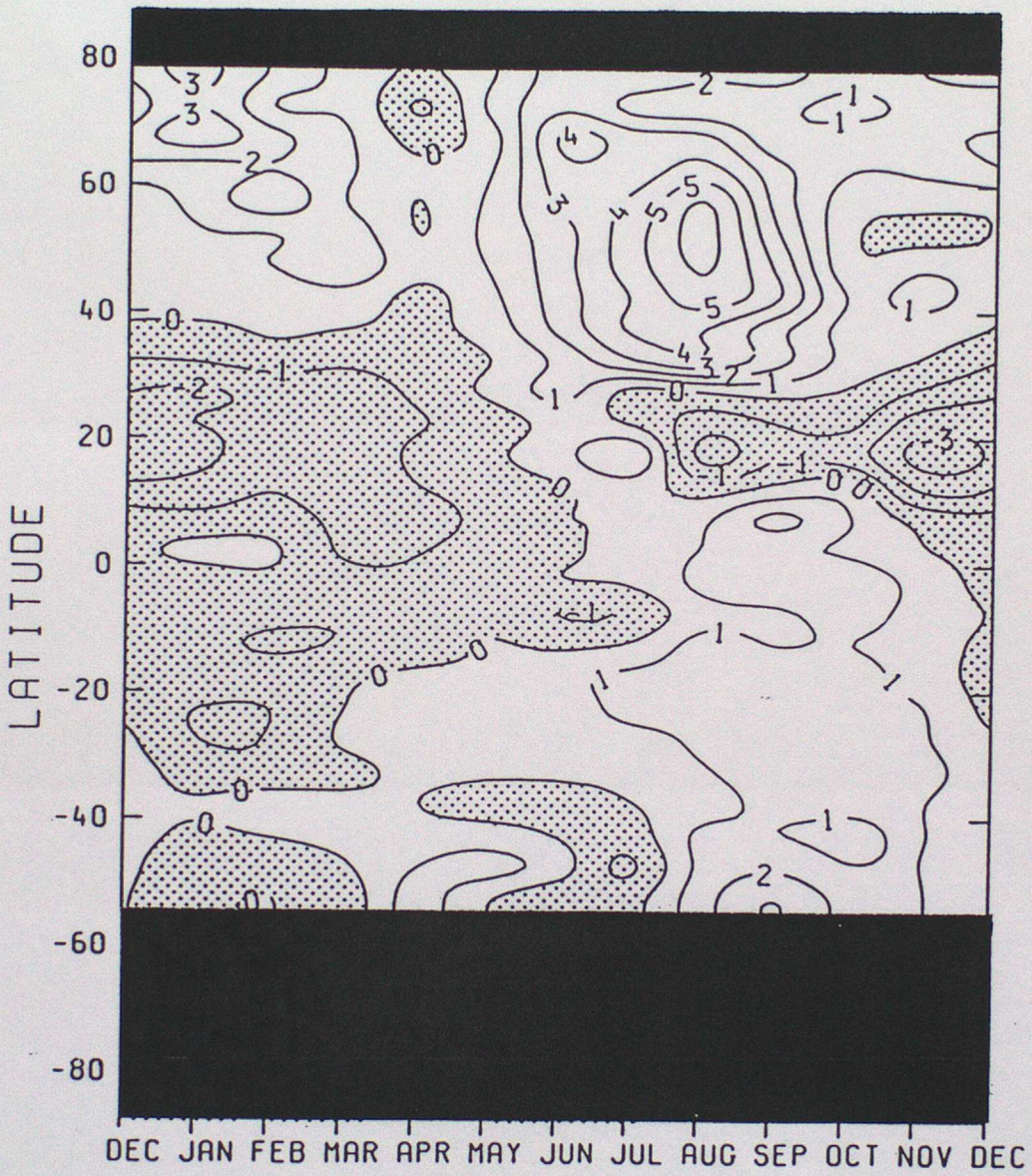

Figure 4(a)

Zonal Mean Differences In Surface Temperature

Over Sea And Sea-ice Points 9Kbp - 0Kbp

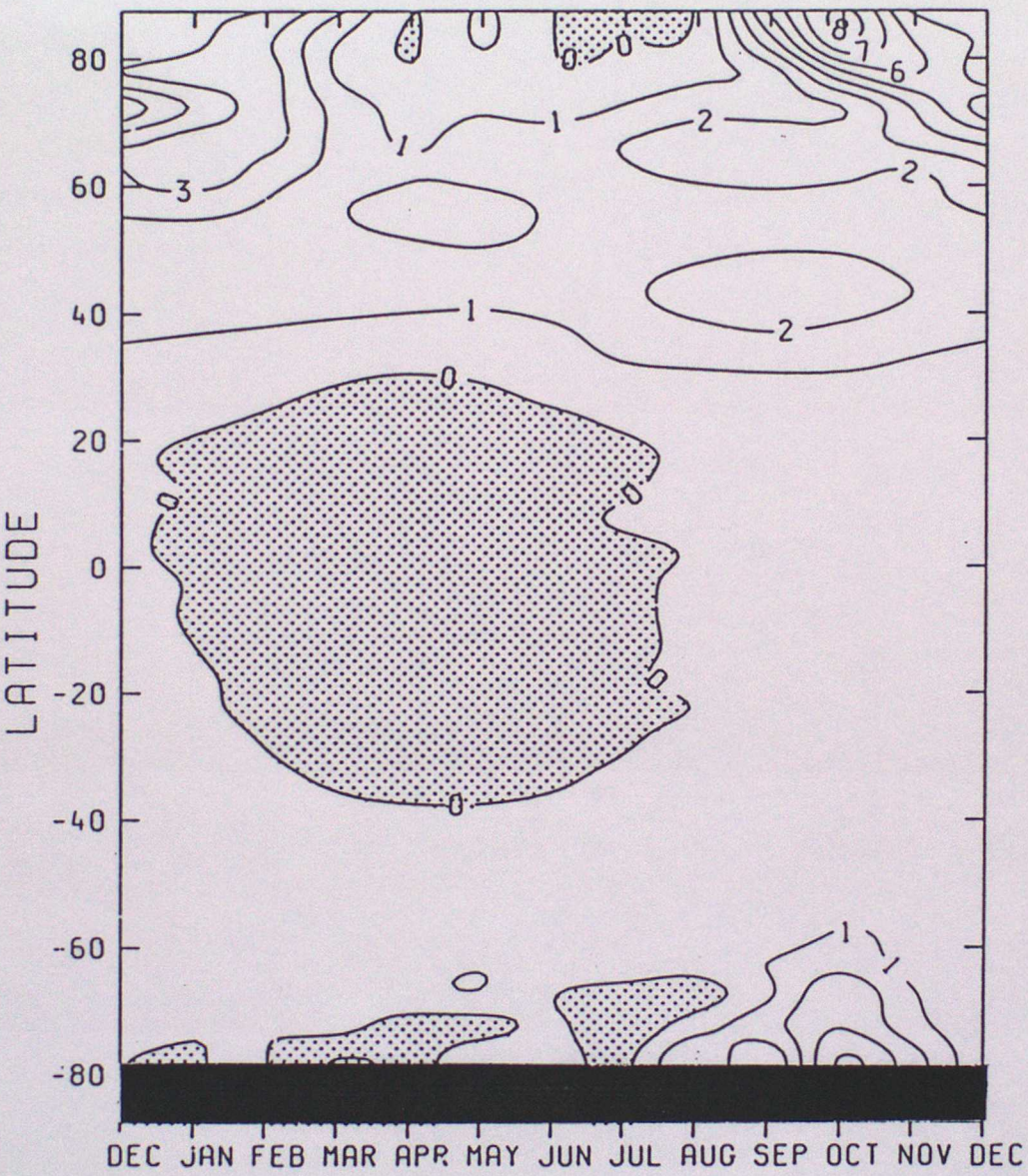

Figure 4(b)

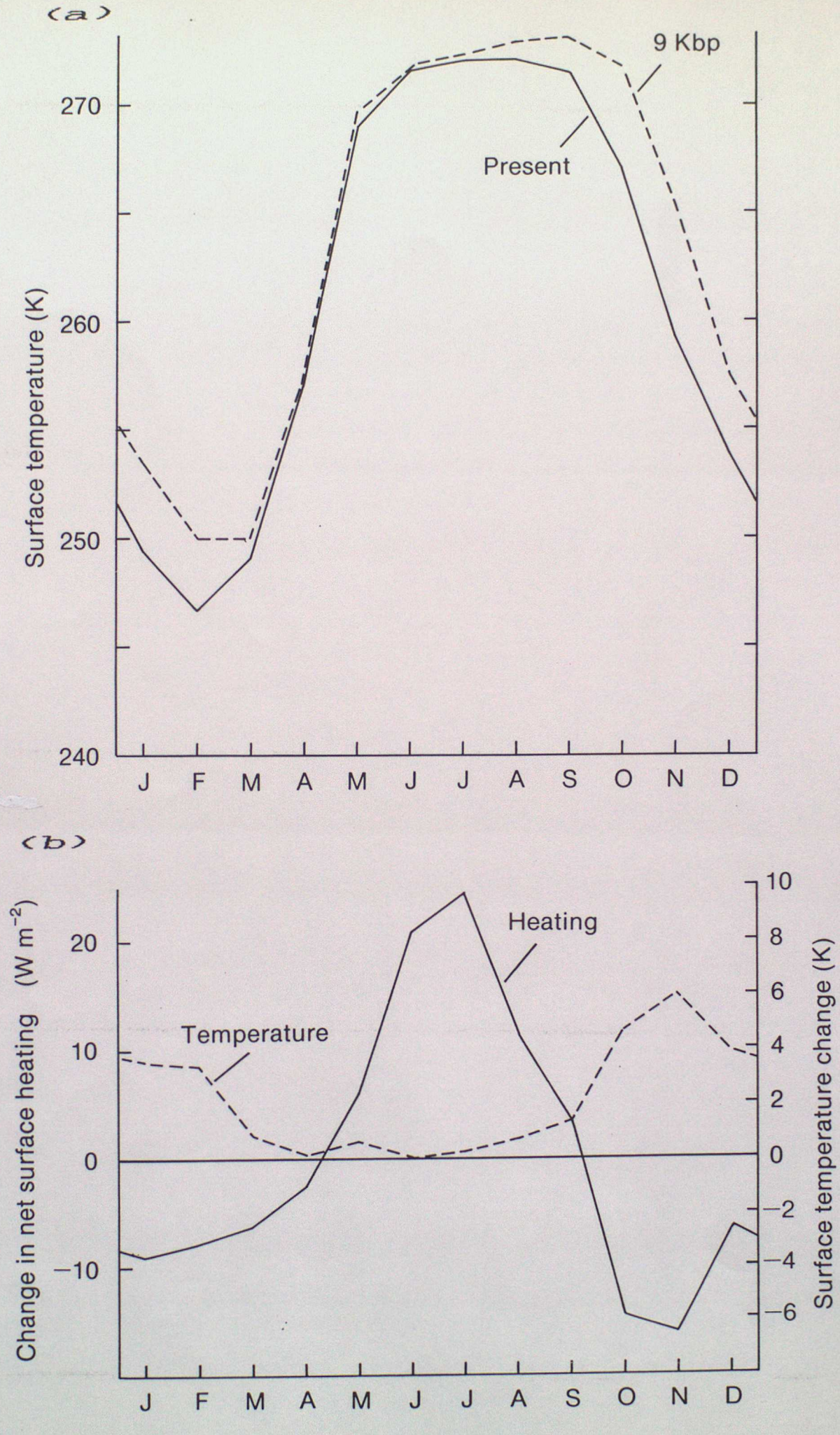
(a)
9 Kbp
Present
270
260
250
240
Surface temperature (K)
J F M A M J J A S O N D
(b)
Heating
Temperature
20
10
0
−10
Change in net surface heating (W m^{-2})
10
8
6
4
2
0
−2
−4
−6
Surface temperature change (K)
J F M A M J J A S O N D

Figure 5

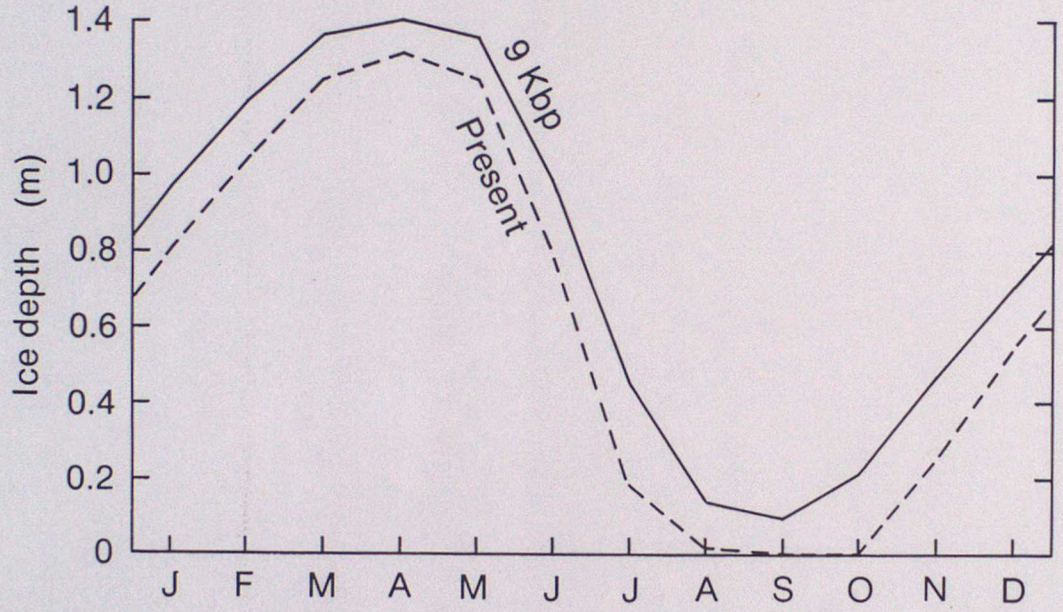

Figure 5(c)

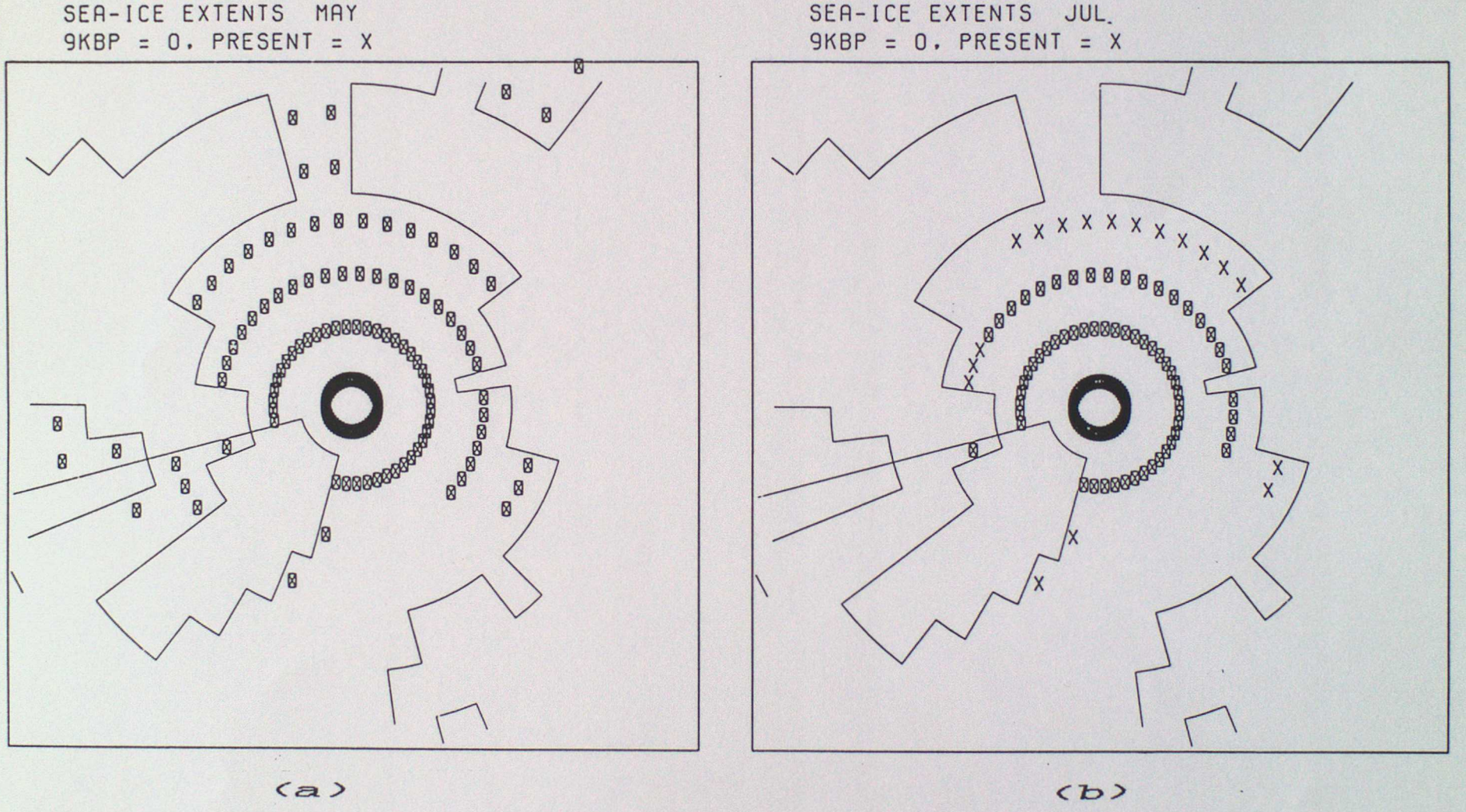
SEA-ICE EXTENTS MAY
9KBP = O, PRESENT = X
SEA-ICE EXTENTS JUL.
9KBP = O, PRESENT = X
(a)
(b)

Figure 6

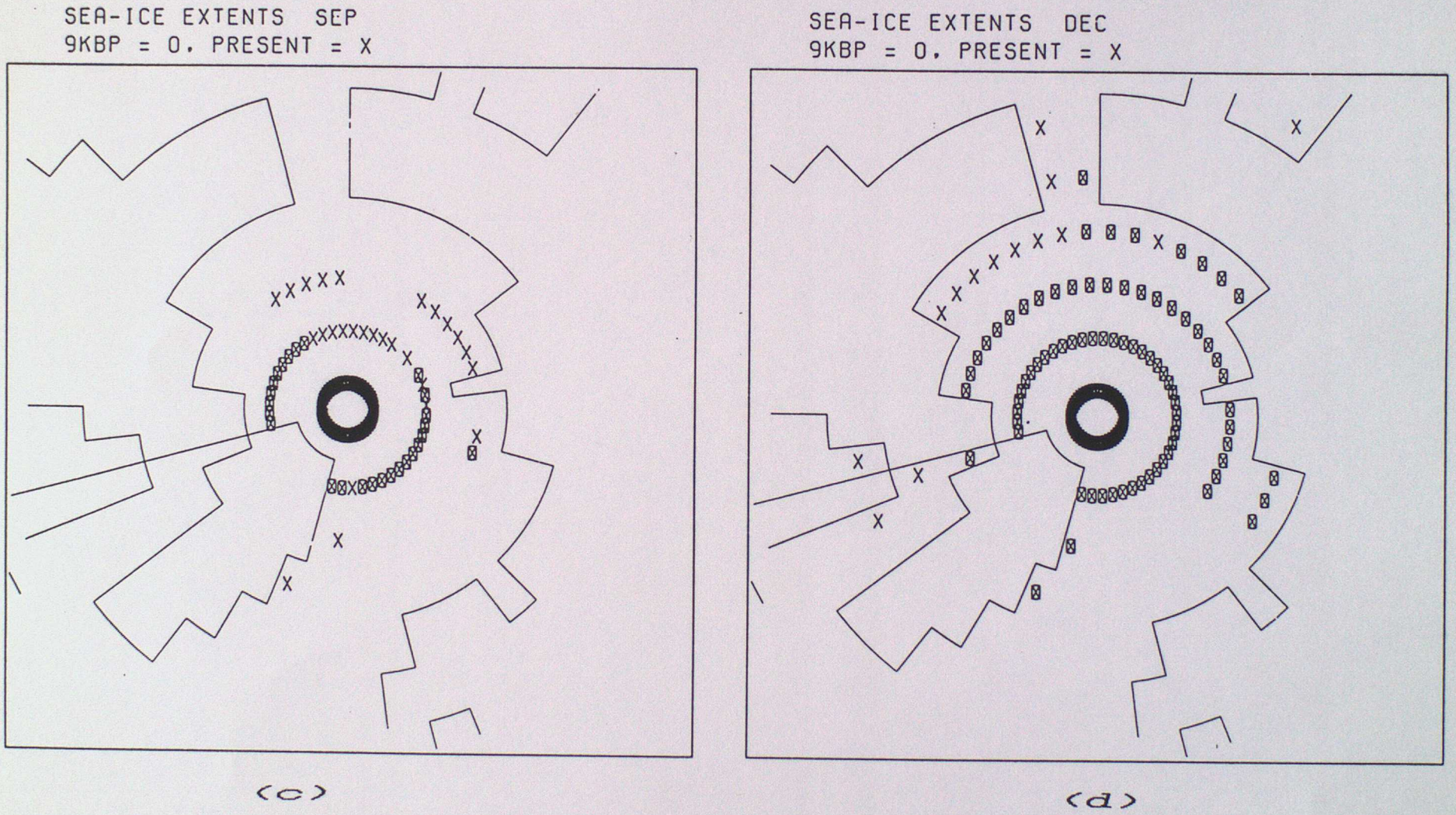
SEA-ICE EXTENTS SEP
9KBP = O. PRESENT = X
SEA-ICE EXTENTS DEC
9KBP = O. PRESENT = X
(c)
(d)

Figure 6

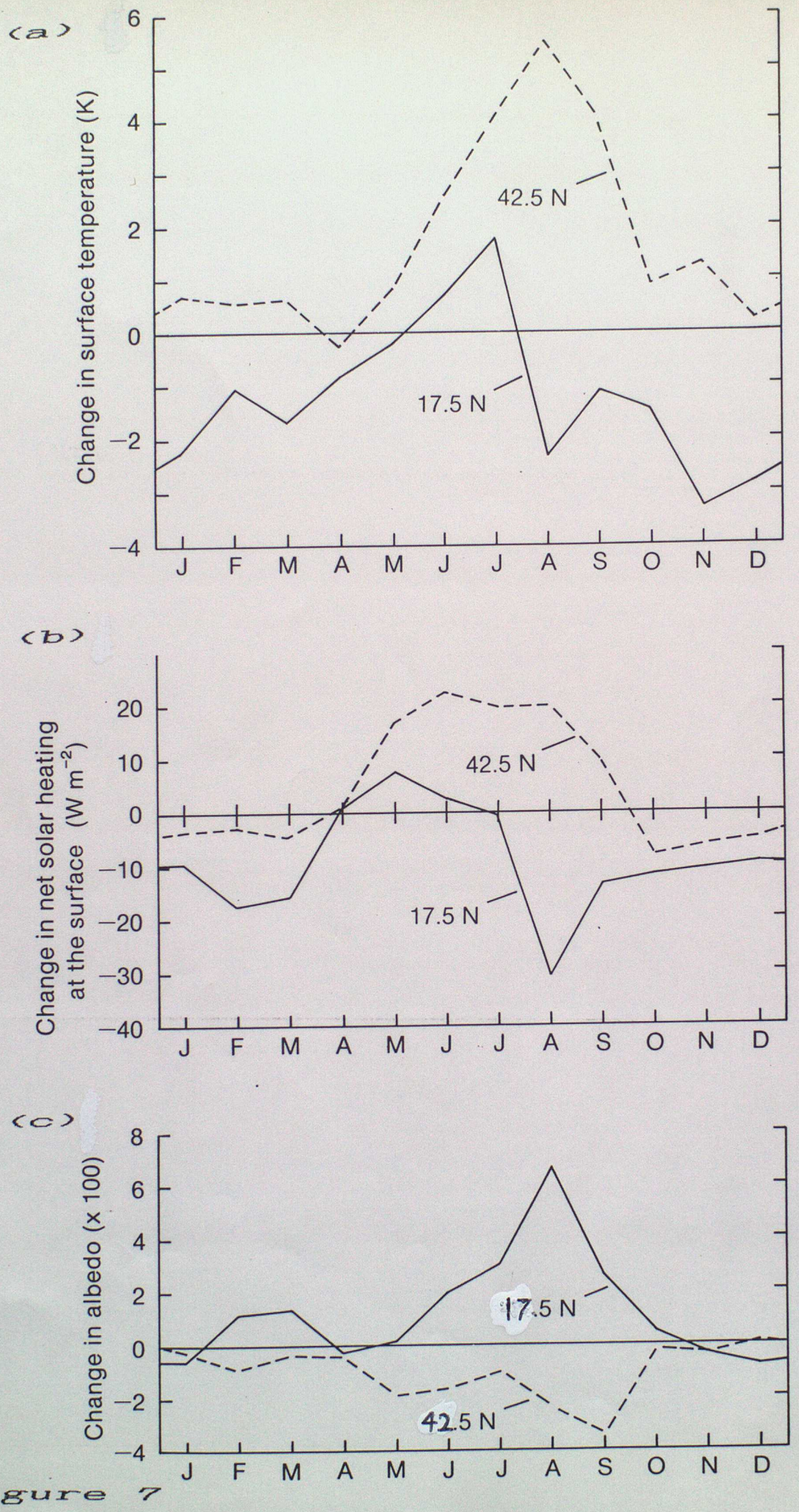
(a)
Change in surface temperature (K)
6
4
2
0
−2
−4
42.5 N
17.5 N
J F M A M J J A S O N D
(b)
Change in net solar heating at the surface (W m^{-2})
20
10
0
−10
−20
−30
−40
42.5 N
17.5 N
J F M A M J J A S O N D
(c)
Change in albedo (x 100)
8
6
4
2
0
−2
−4
17.5 N
42.5 N
J F M A M J J A S O N D

Figure 7

(d)

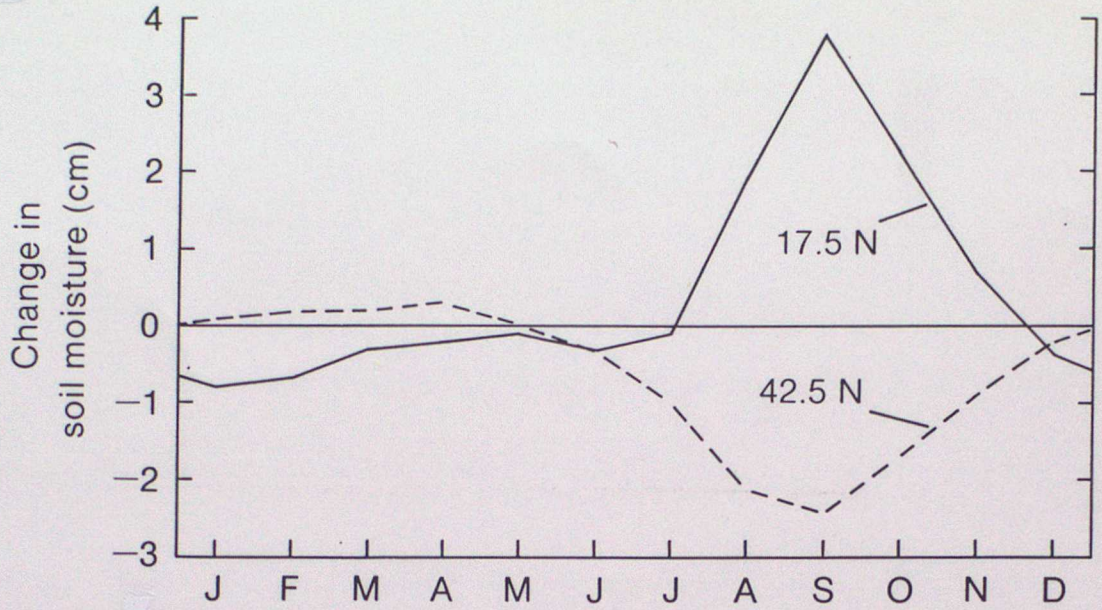
Change in soil moisture (cm)
4
3
2
1
0
−1
−2
−3
17.5 N
42.5 N
J F M A M J J A S O N D

(e)

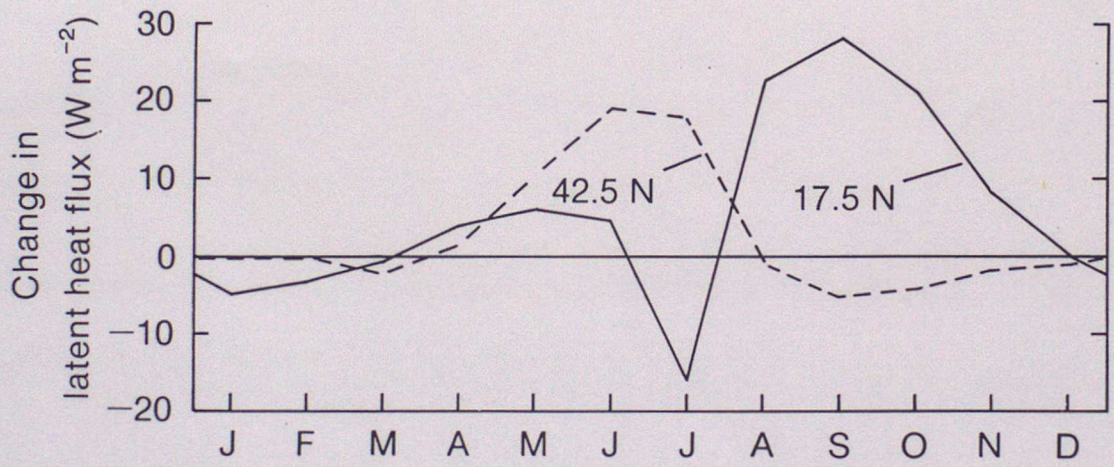
Change in latent heat flux (W m^{-2})
30
20
10
0
−10
−20
42.5 N
17.5 N
J F M A M J J A S O N D

(f)

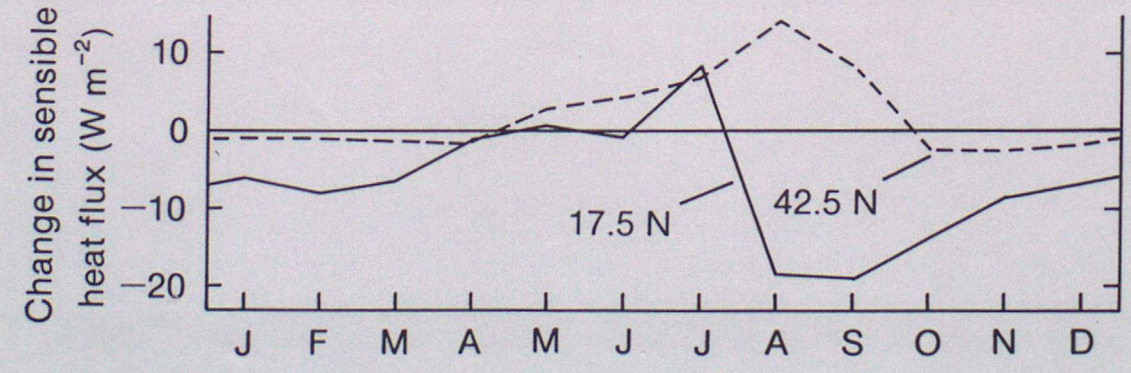
Change in sensible heat flux (W m^{-2})
10
0
−10
−20
17.5 N
42.5 N
J F M A M J J A S O N D

Figure 7

(a)

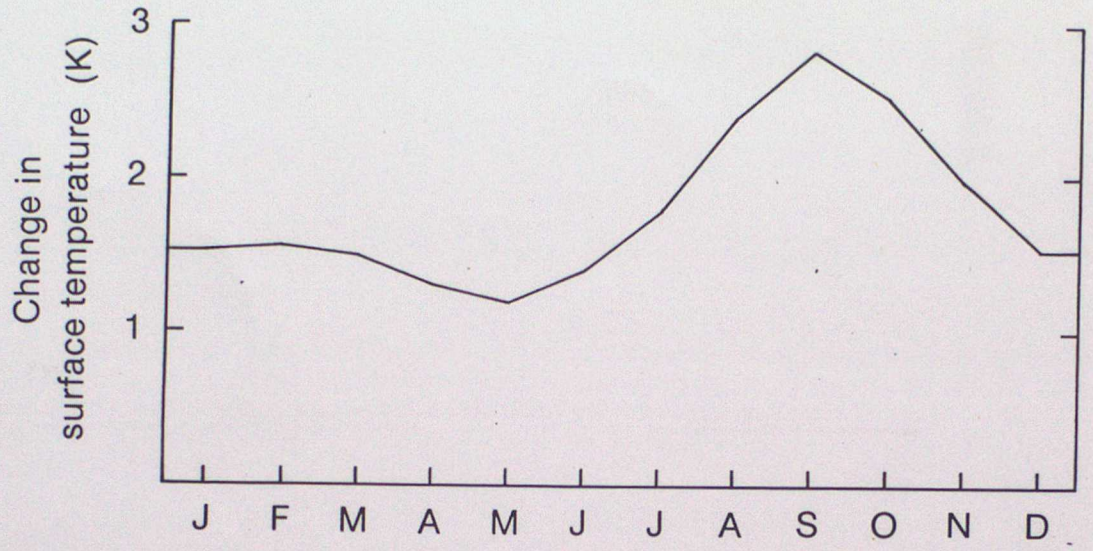
Change in surface temperature (K)
3
2
1
J F M A M J J A S O N D

(b)

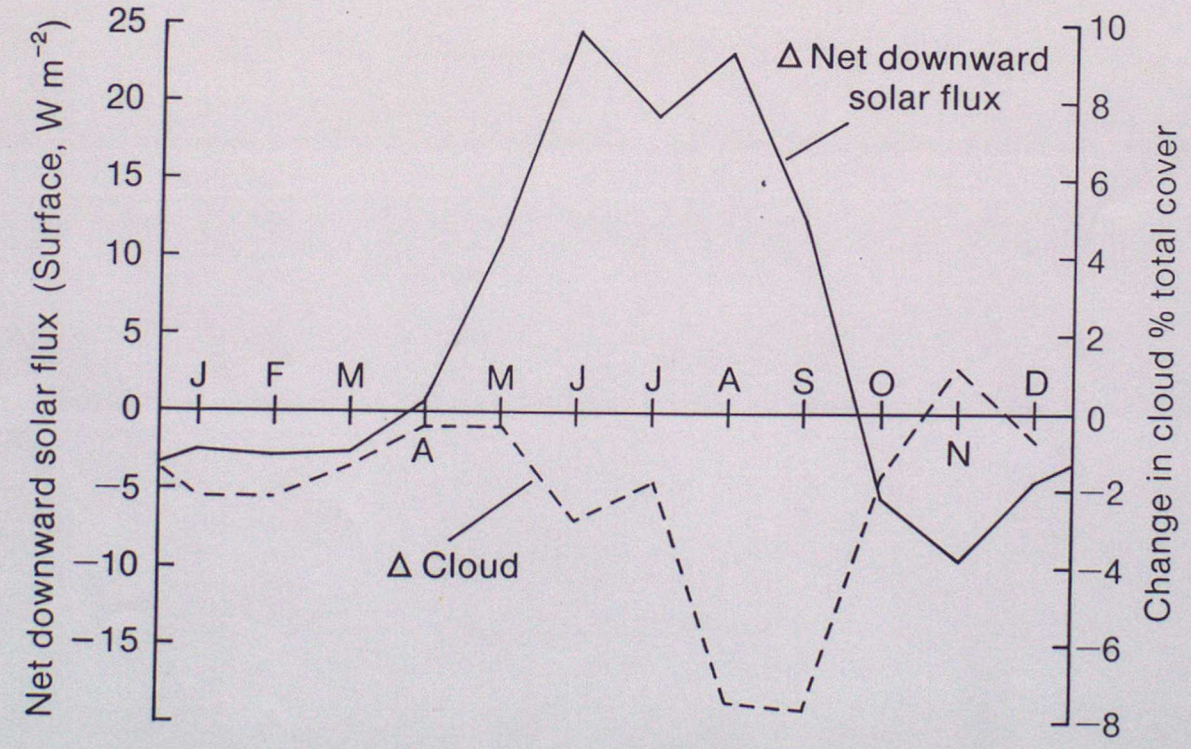
Net downward solar flux (Surface, W m^{-2})
25
20
15
10
5
0
−5
−10
−15
J F M A M J J A S O N D
Δ Net downward solar flux
Δ Cloud
Change in cloud % total cover
10
8
6
4
2
0
−2
−4
−6
−8

Figure 8

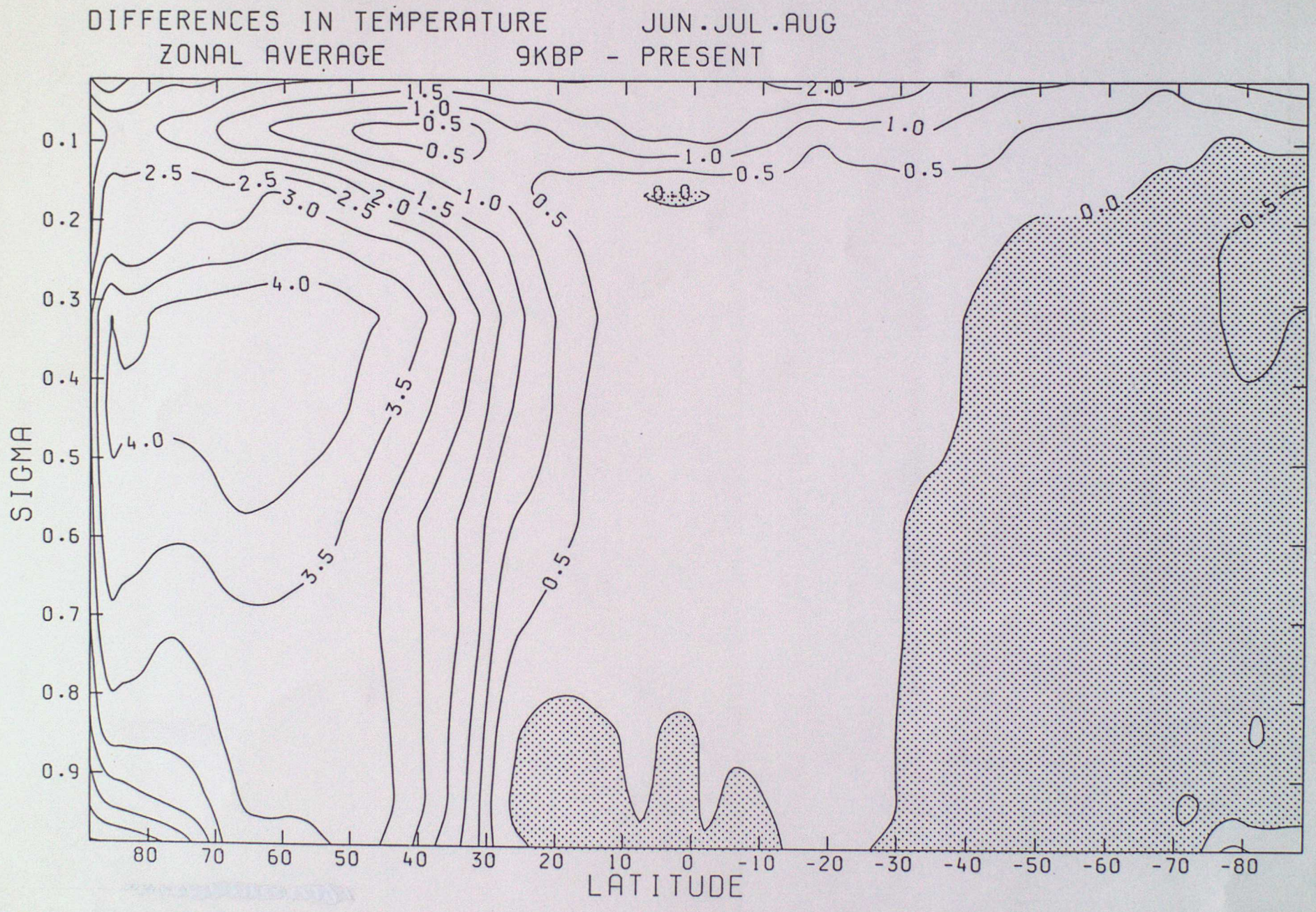
DIFFERENCES IN TEMPERATURE JUN.JUL.AUG
ZONAL AVERAGE 9KBP - PRESENT
SIGMA
0.1
0.2
0.3
0.4
0.5
0.6
0.7
0.8
0.9
1.5
1.0
0.5
0.5
2.0
1.0
0.5
0.5
2.5
2.5
3.0
2.5
2.0
1.5
1.0
0.5
0.0
0.0
0.5
4.0
3.5
4.0
3.5
0.5
80 70 60 50 40 30 20 10 0 -10 -20 -30 -40 -50 -60 -70 -80
LATITUDE

Figure 9(a)

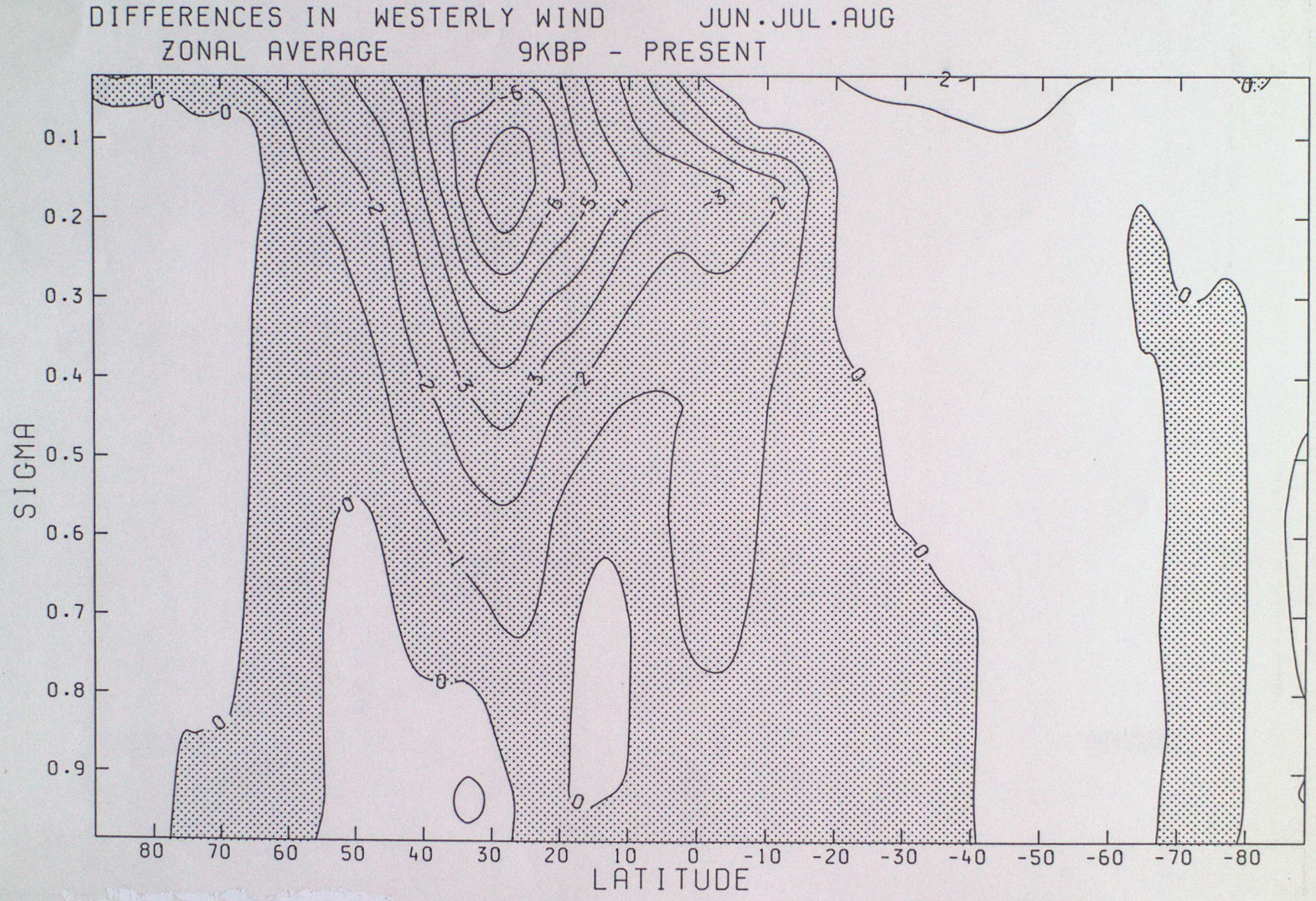
DIFFERENCES IN WESTERLY WIND JUN.JUL.AUG
ZONAL AVERAGE 9KBP - PRESENT
SIGMA
0.1
0.2
0.3
0.4
0.5
0.6
0.7
0.8
0.9
80 70 60 50 40 30 20 10 0 -10 -20 -30 -40 -50 -60 -70 -80
LATITUDE

Figure 9(b)

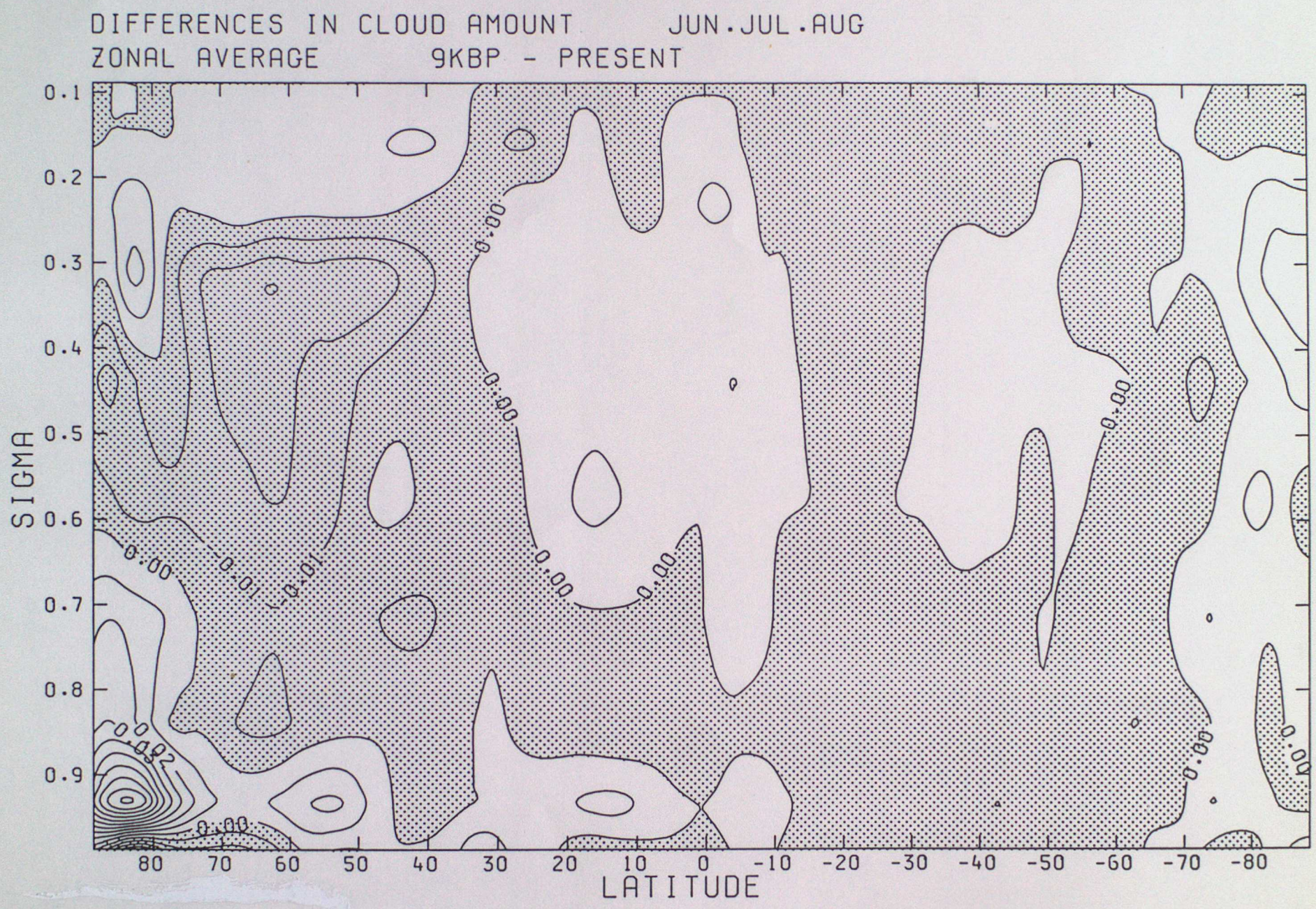
DIFFERENCES IN CLOUD AMOUNT JUN.JUL.AUG
ZONAL AVERAGE 9KBP - PRESENT
SIGMA
0.1
0.2
0.3
0.4
0.5
0.6
0.7
0.8
0.9
0.00
-0.01
-0.01
0.00
0.00
0.00
0.00
0.00
0.00
0.00
0.02
0.03
80 70 60 50 40 30 20 10 0 -10 -20 -30 -40 -50 -60 -70 -80
LATITUDE

Figure 9(c)

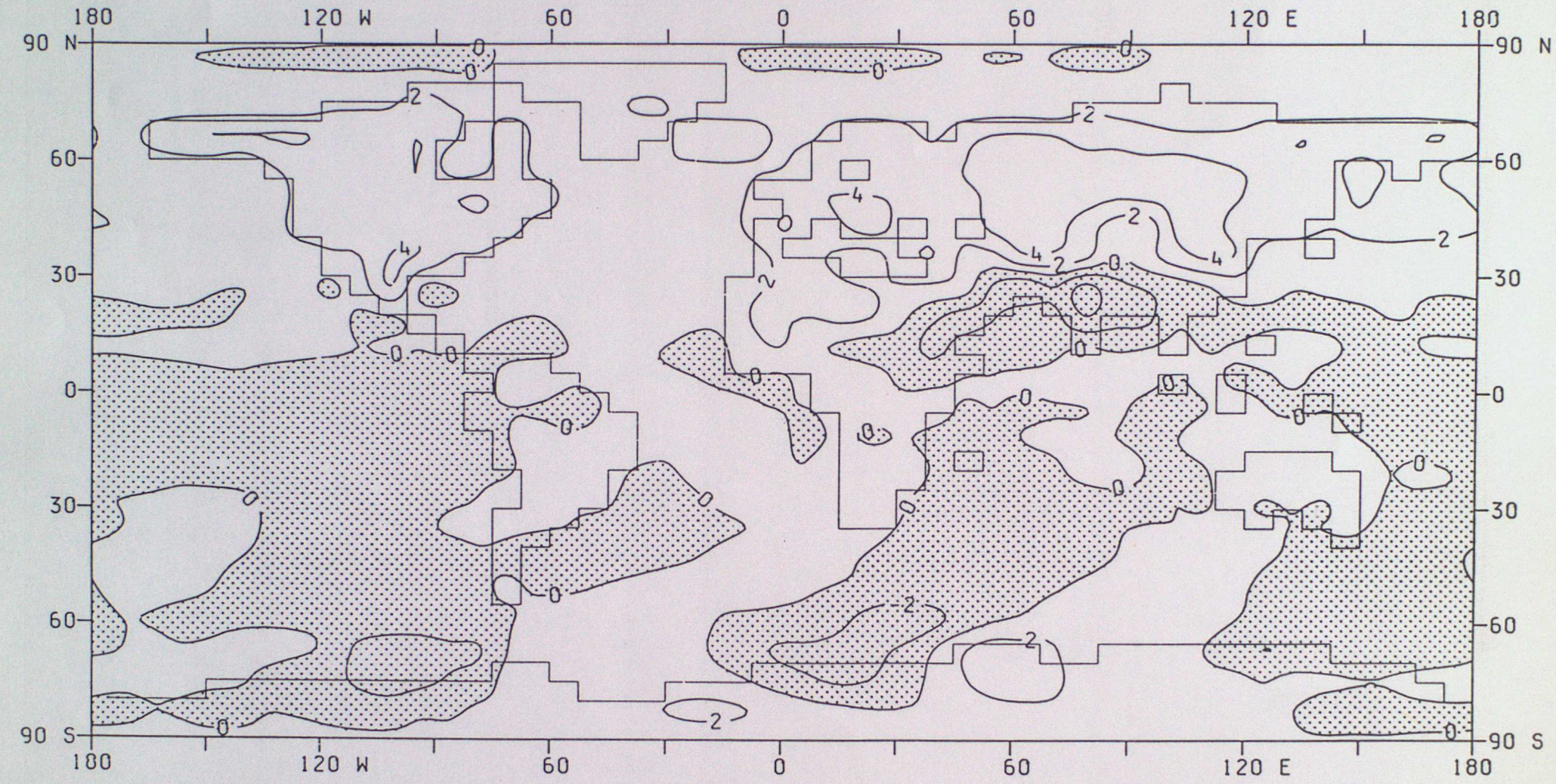

Figure 10(a)

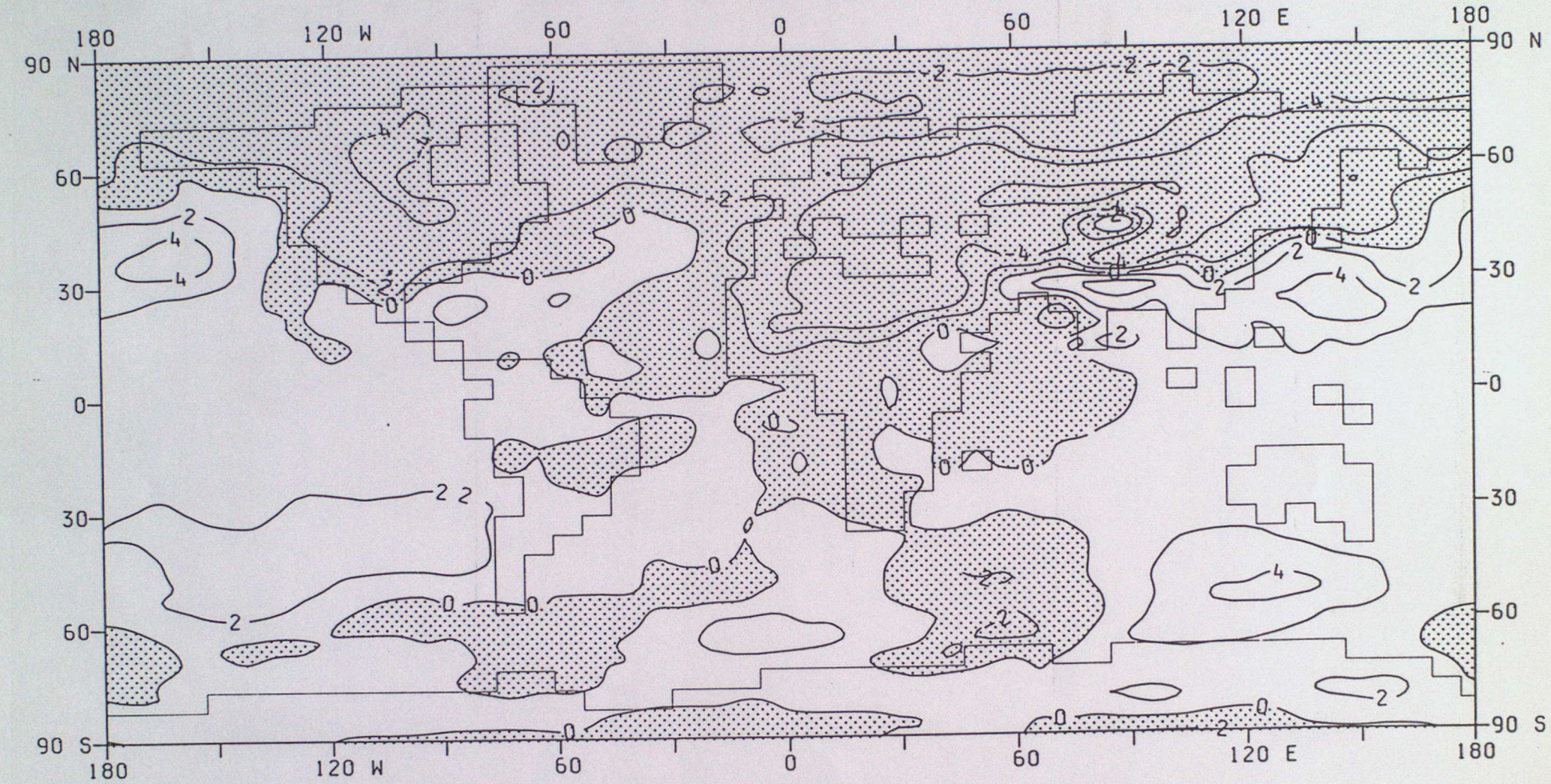
180
120 W
60
0
60
120 E
180
90 N
60
30
0
30
60
90 S
180
120 W
60
0
60
120 E
180
90 N
60
30
0
30
60
90 S

Figure 10(b)

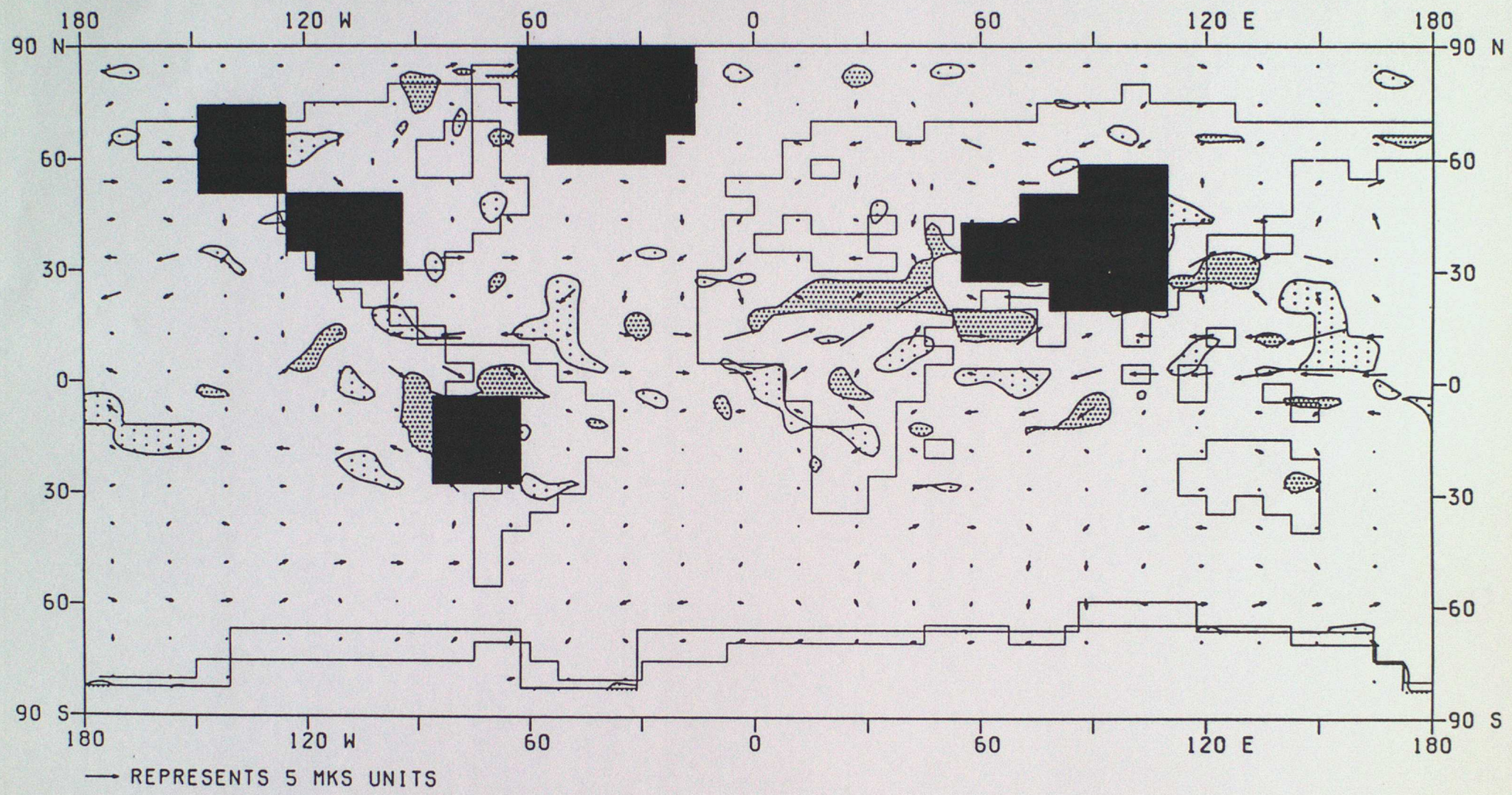
180
120 W
60
0
60
120 E
180
90 N
60
30
0
30
60
90 S
REPRESENTS 5 MKS UNITS

Figure 10(c)

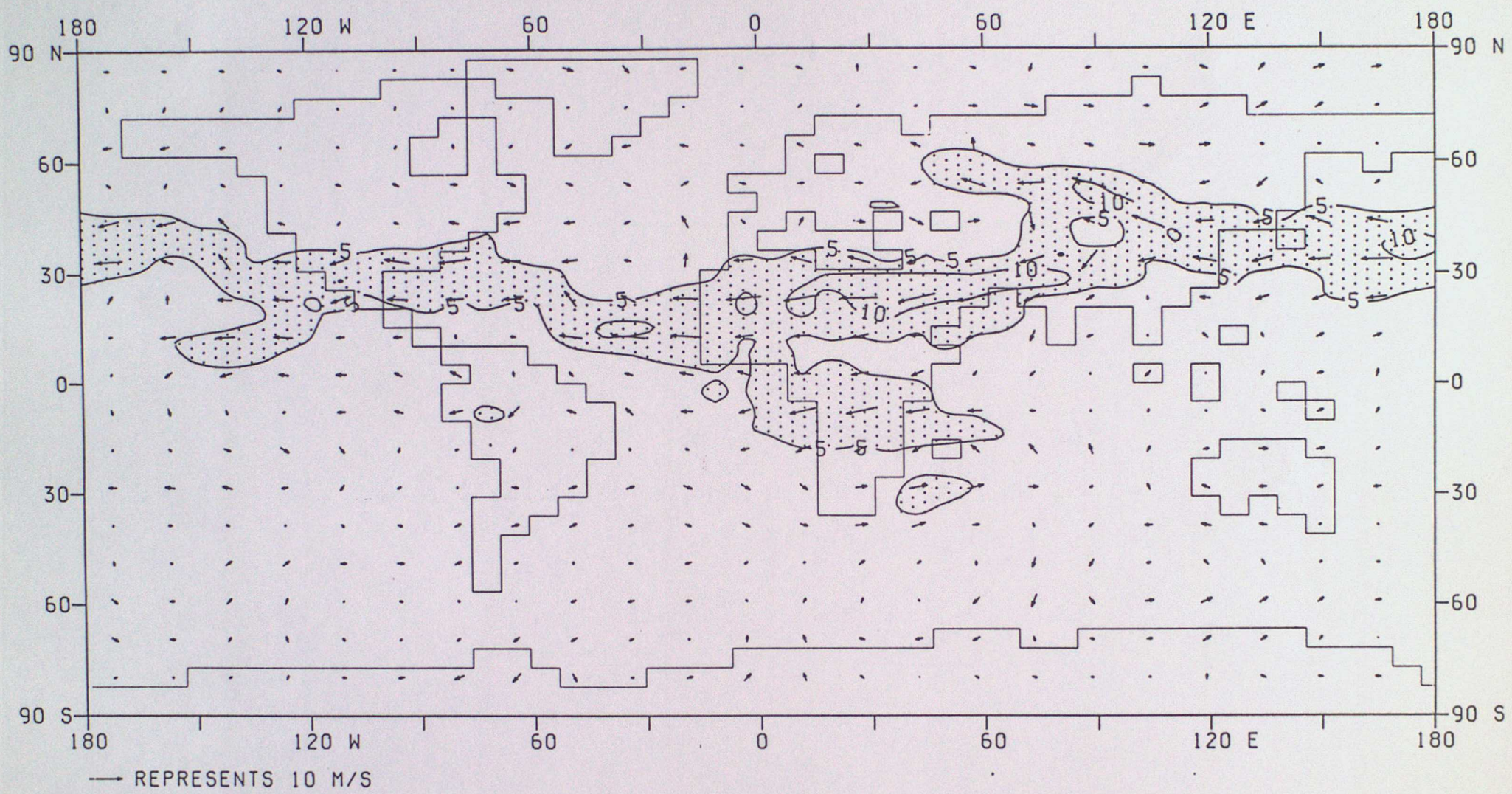
180
120 W
60
0
60
120 E
180
90 N
60
30
0
30
60
90 S
5
10
REPRESENTS 10 M/S

Figure 10(d)

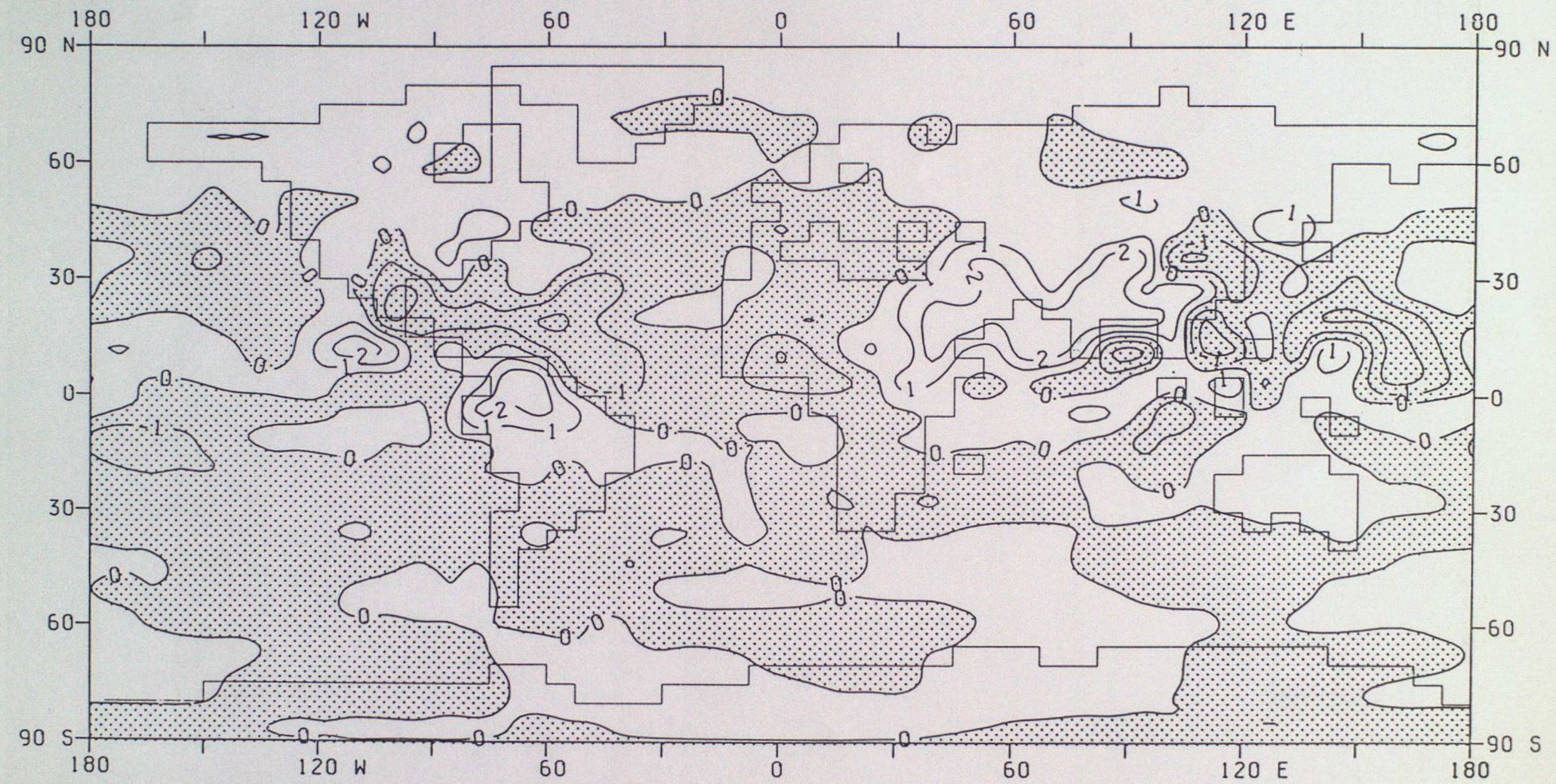

Figure 10(e)

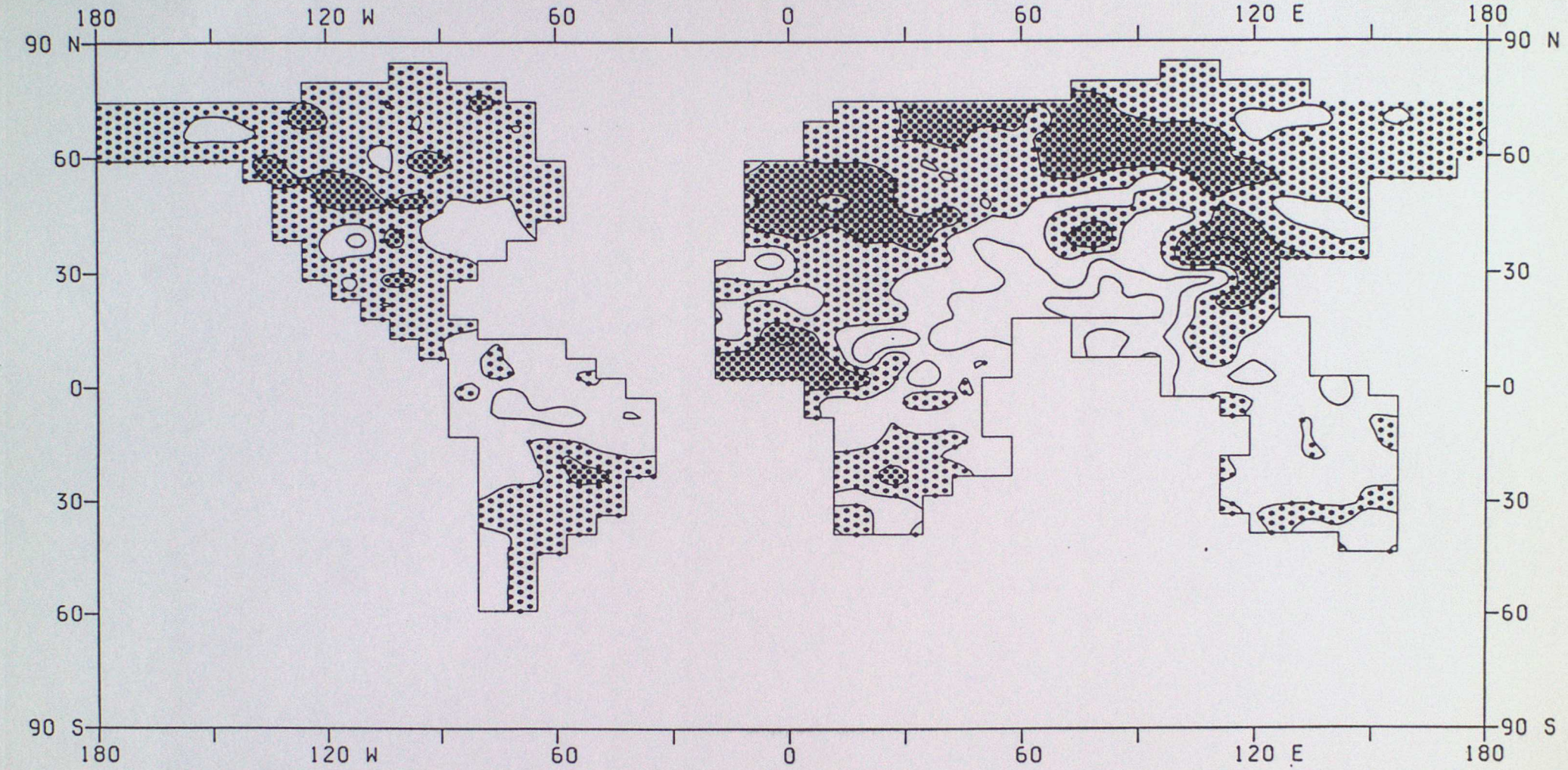

Figure 10(f)

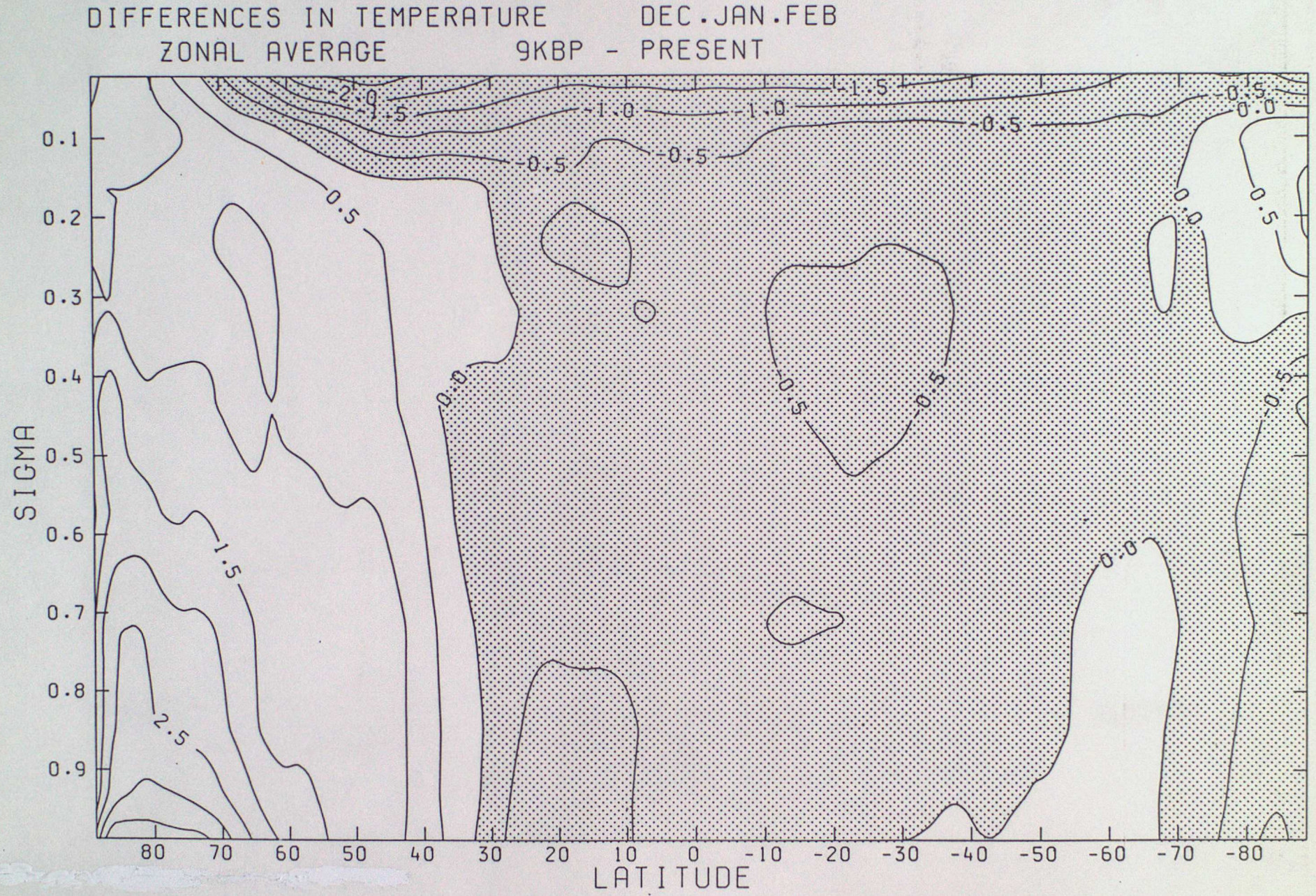
DIFFERENCES IN TEMPERATURE DEC.JAN.FEB
ZONAL AVERAGE 9KBP - PRESENT
SIGMA
0.1
0.2
0.3
0.4
0.5
0.6
0.7
0.8
0.9
-2.0
-1.5
-1.0
-0.5
0.0
0.5
1.5
2.5
80 70 60 50 40 30 20 10 0 -10 -20 -30 -40 -50 -60 -70 -80
LATITUDE

Figure 11

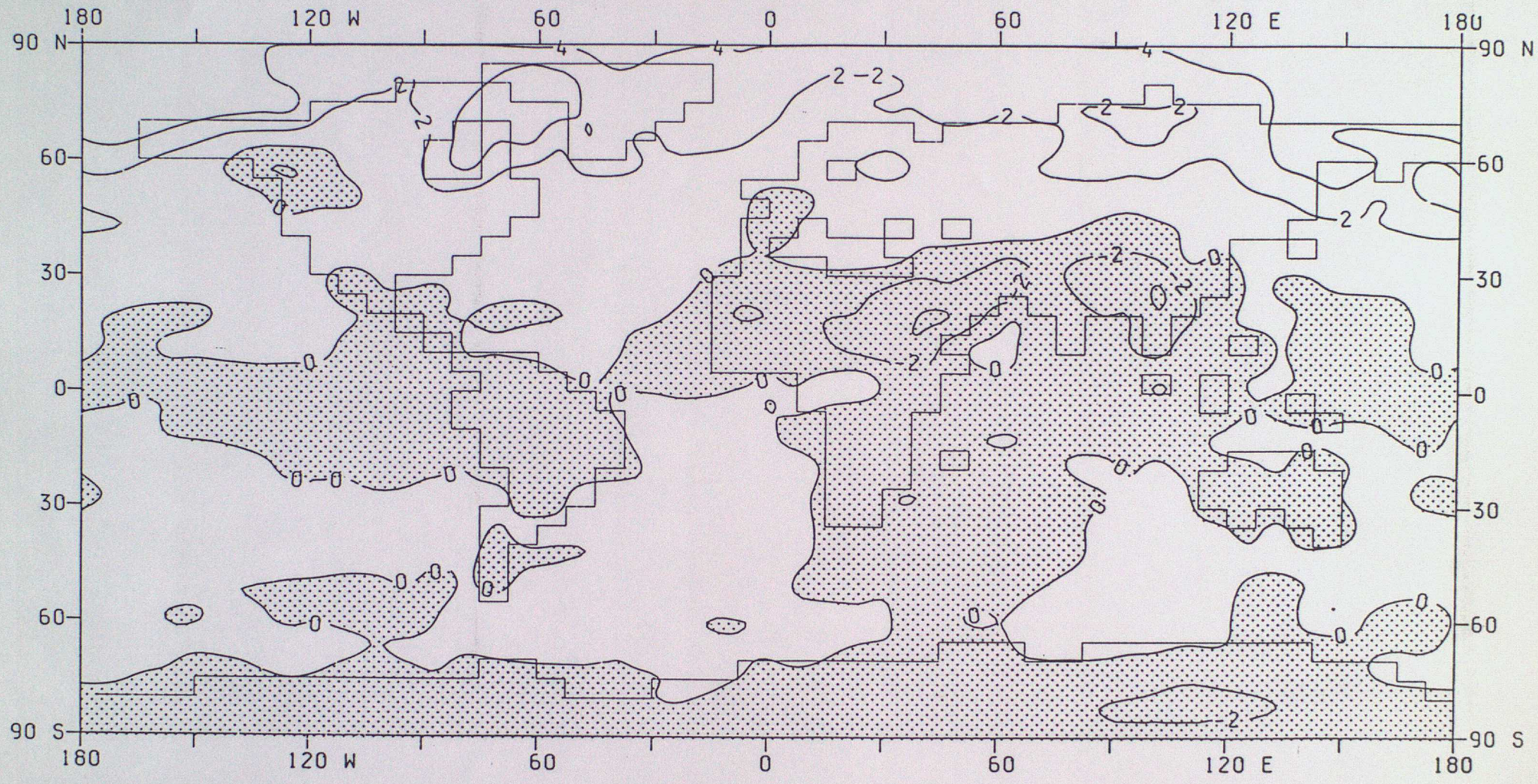

Figure 12(a)

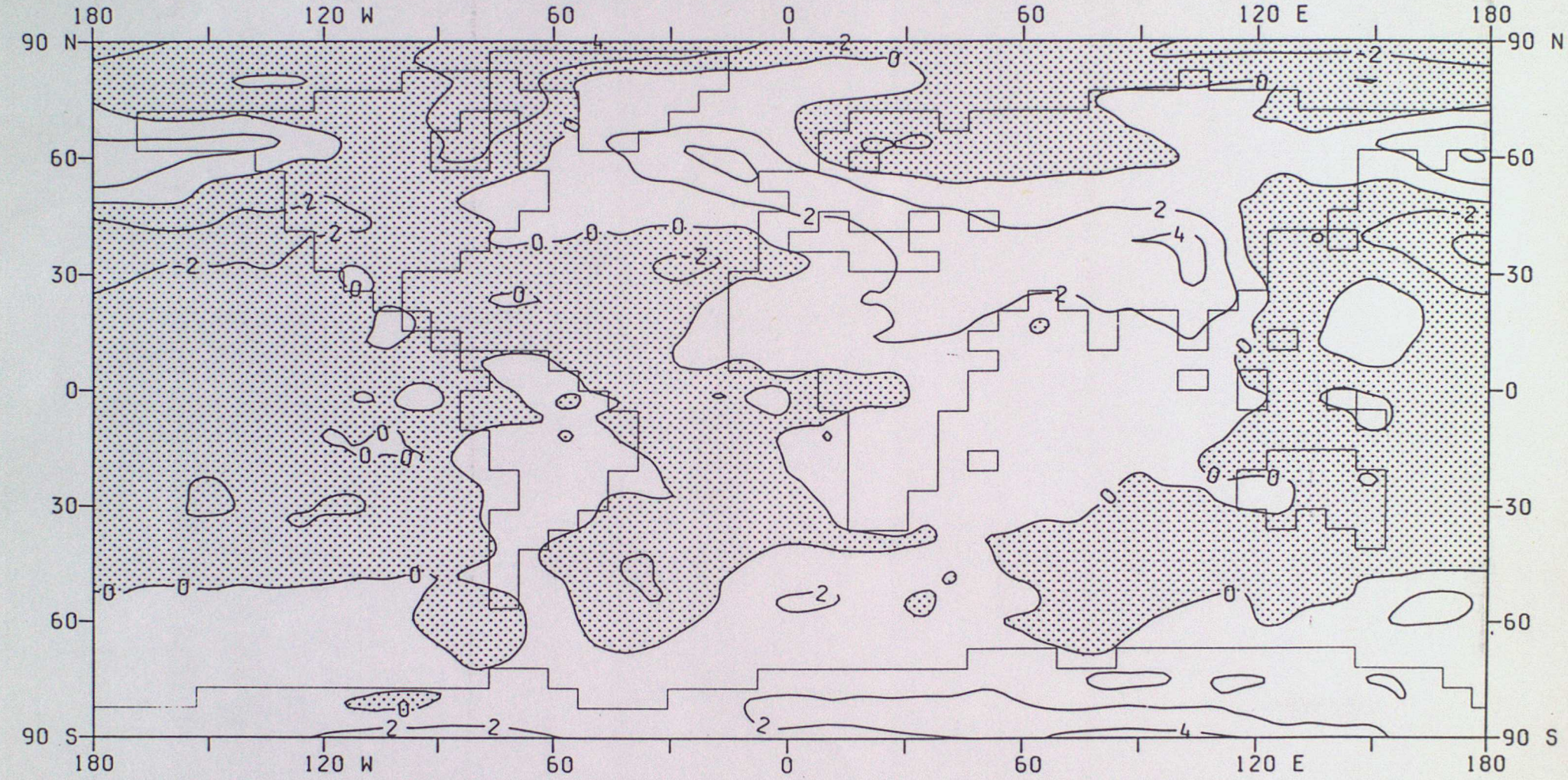

Figure 12(b)

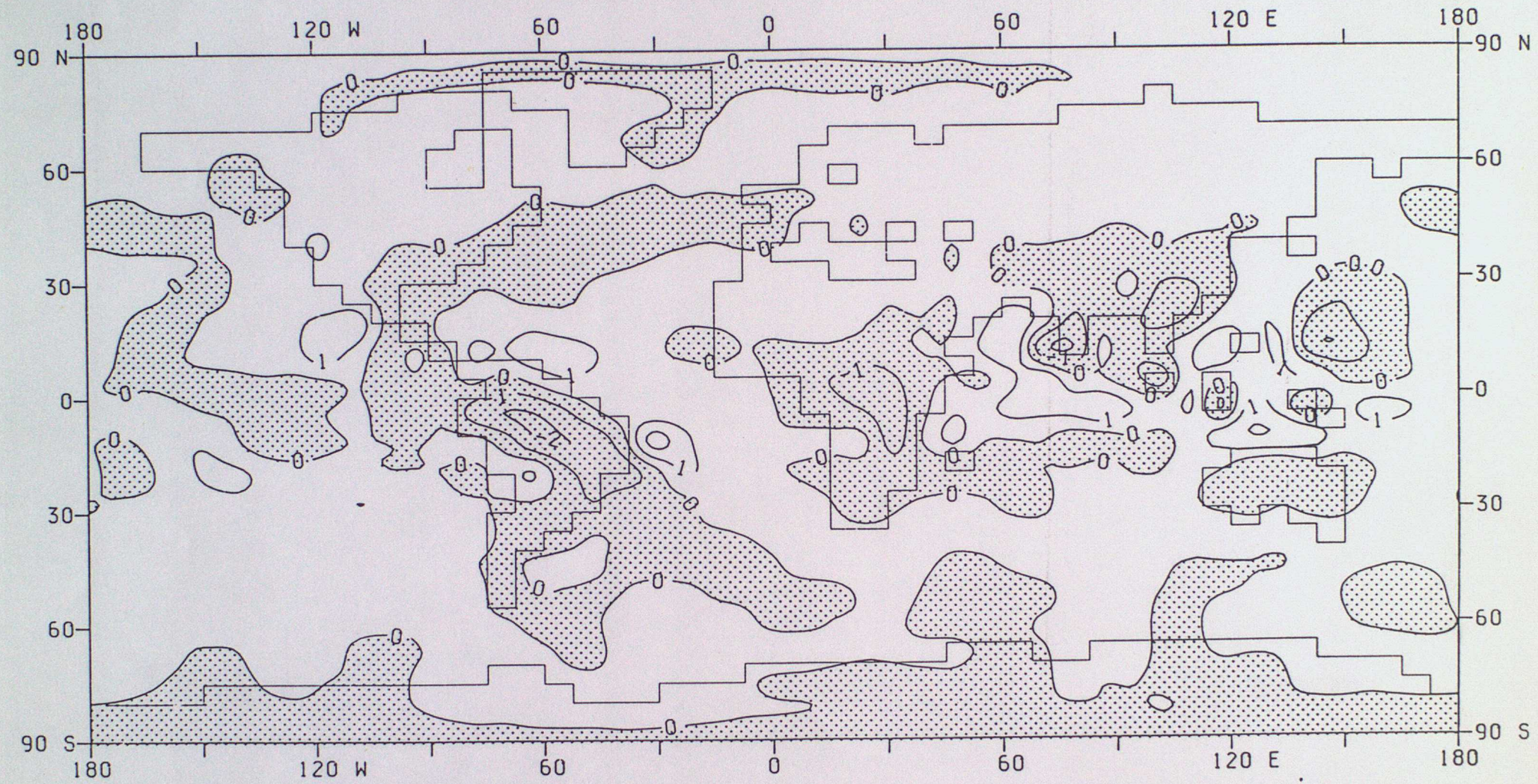
180
120 W
60
0
60
120 E
180
90 N
60
30
0
30
60
90 S
180
120 W
60
0
60
120 E
180
90 N
60
30
0
30
60
90 S

Figure 12(c)

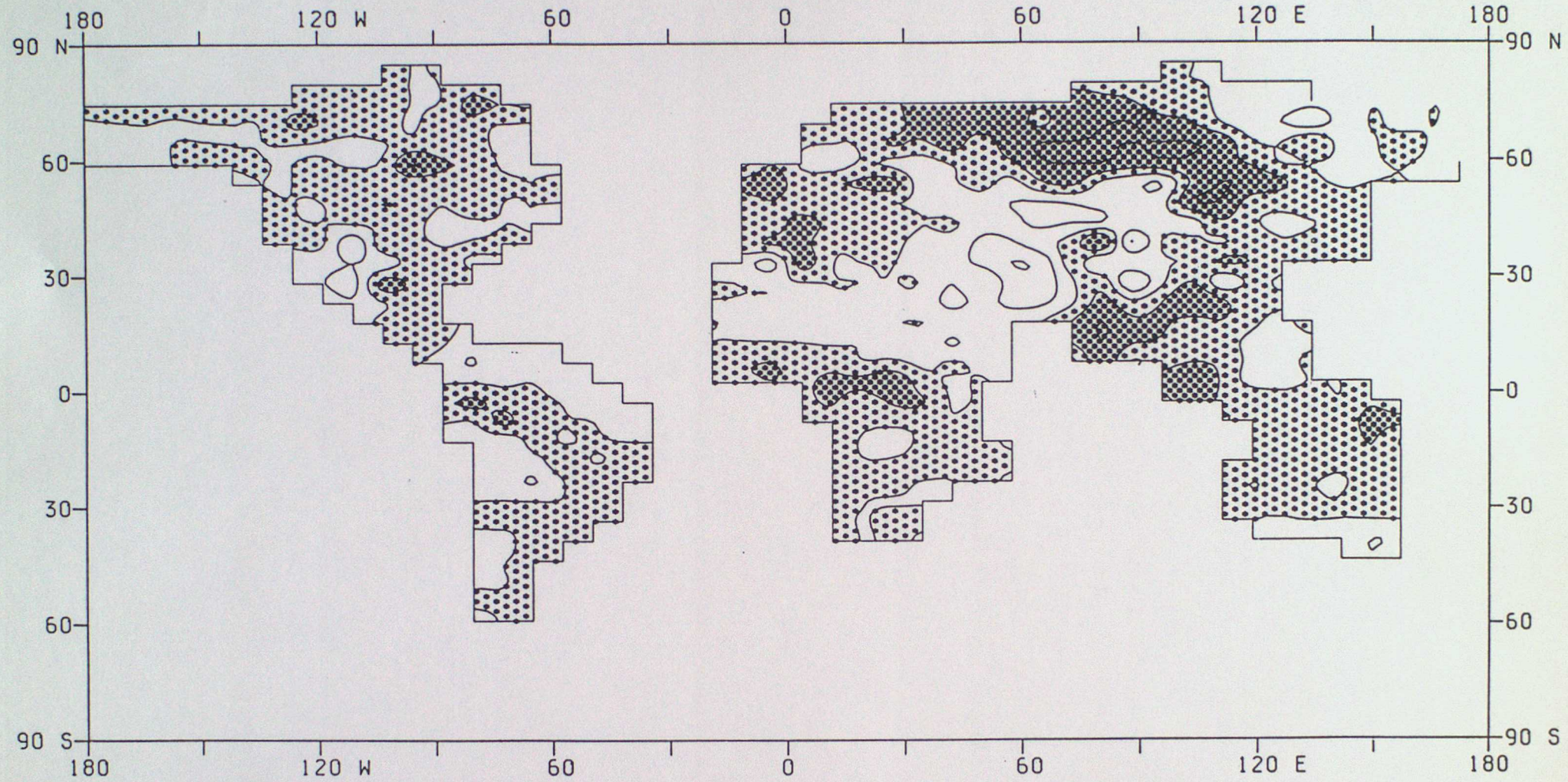

Figure 12(d)

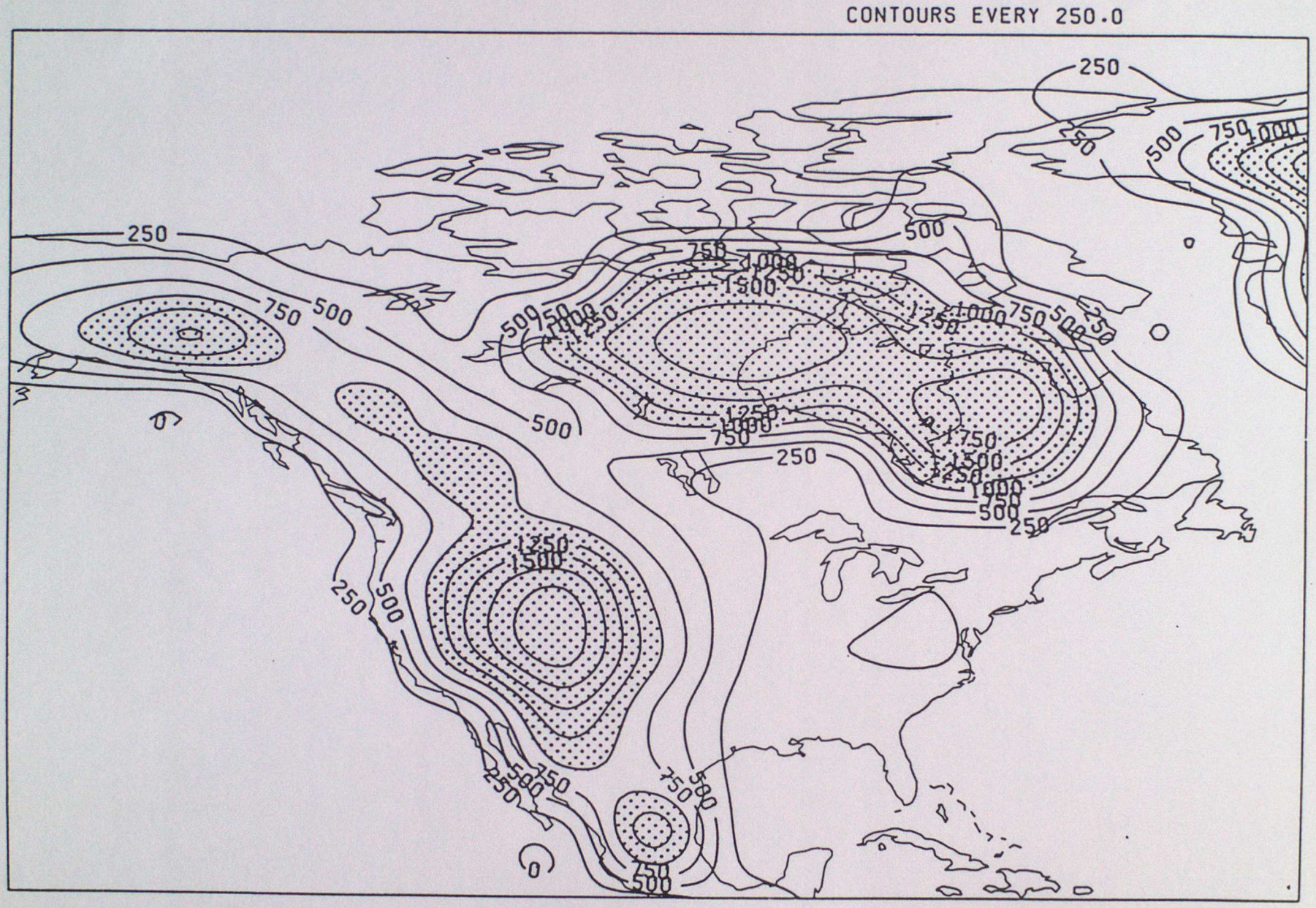

Figure 13

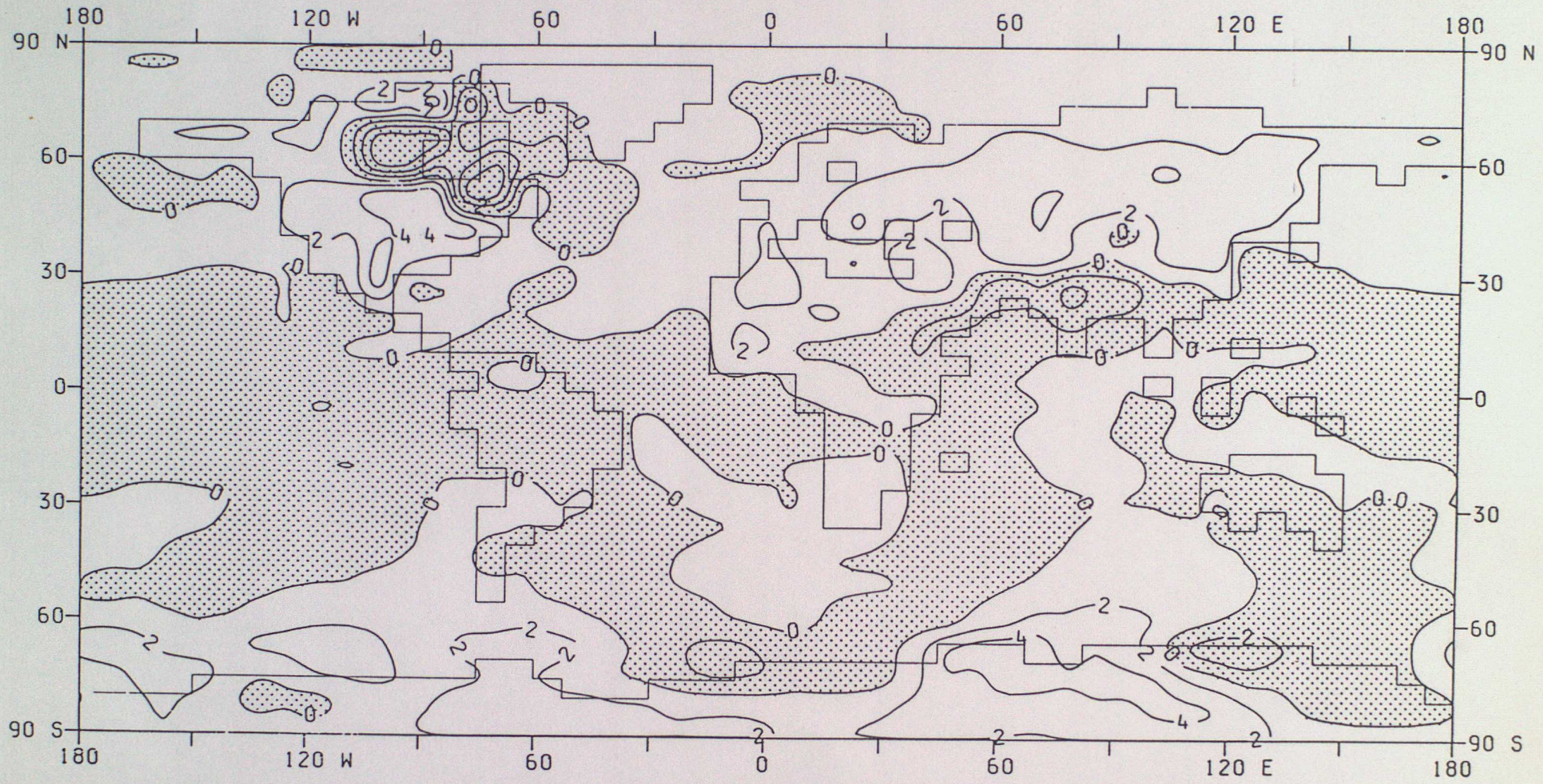

Figure 14

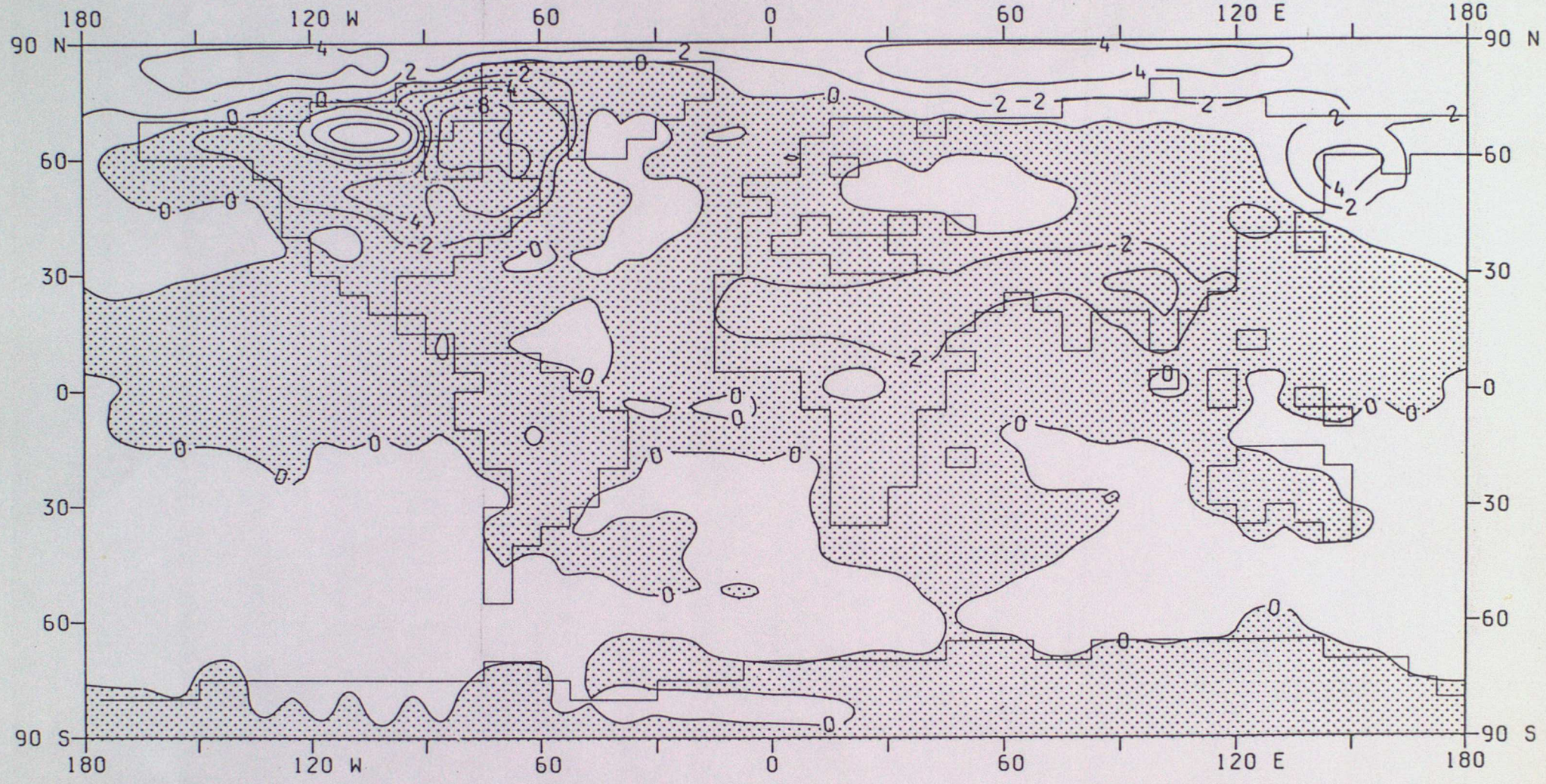

Figure 15

Zonal Mean Differences In Downward Insolation

At The Top Of The Atomsphere 9Kbp - 0Kbp

Using Astronomical Months

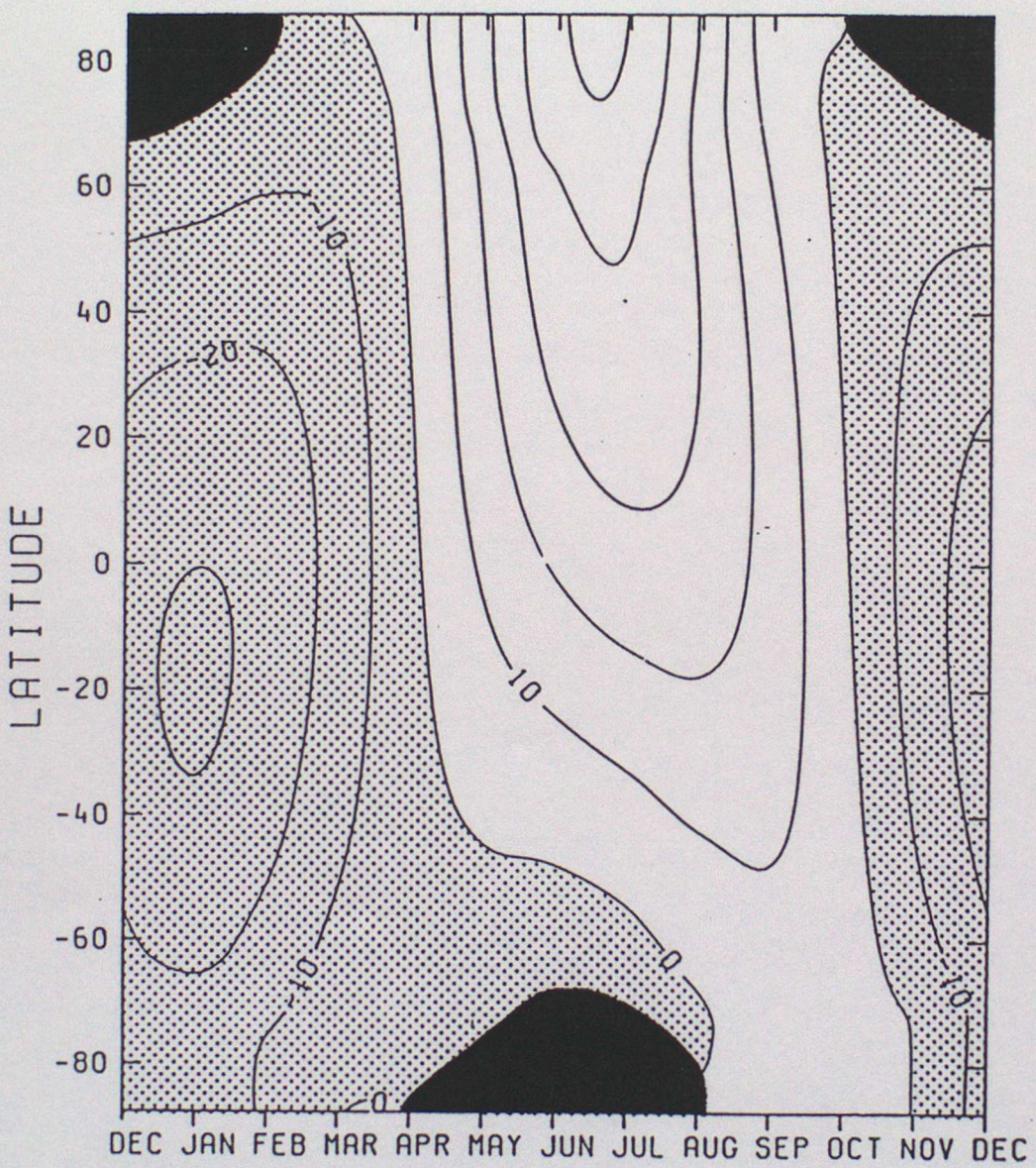

Figure 16

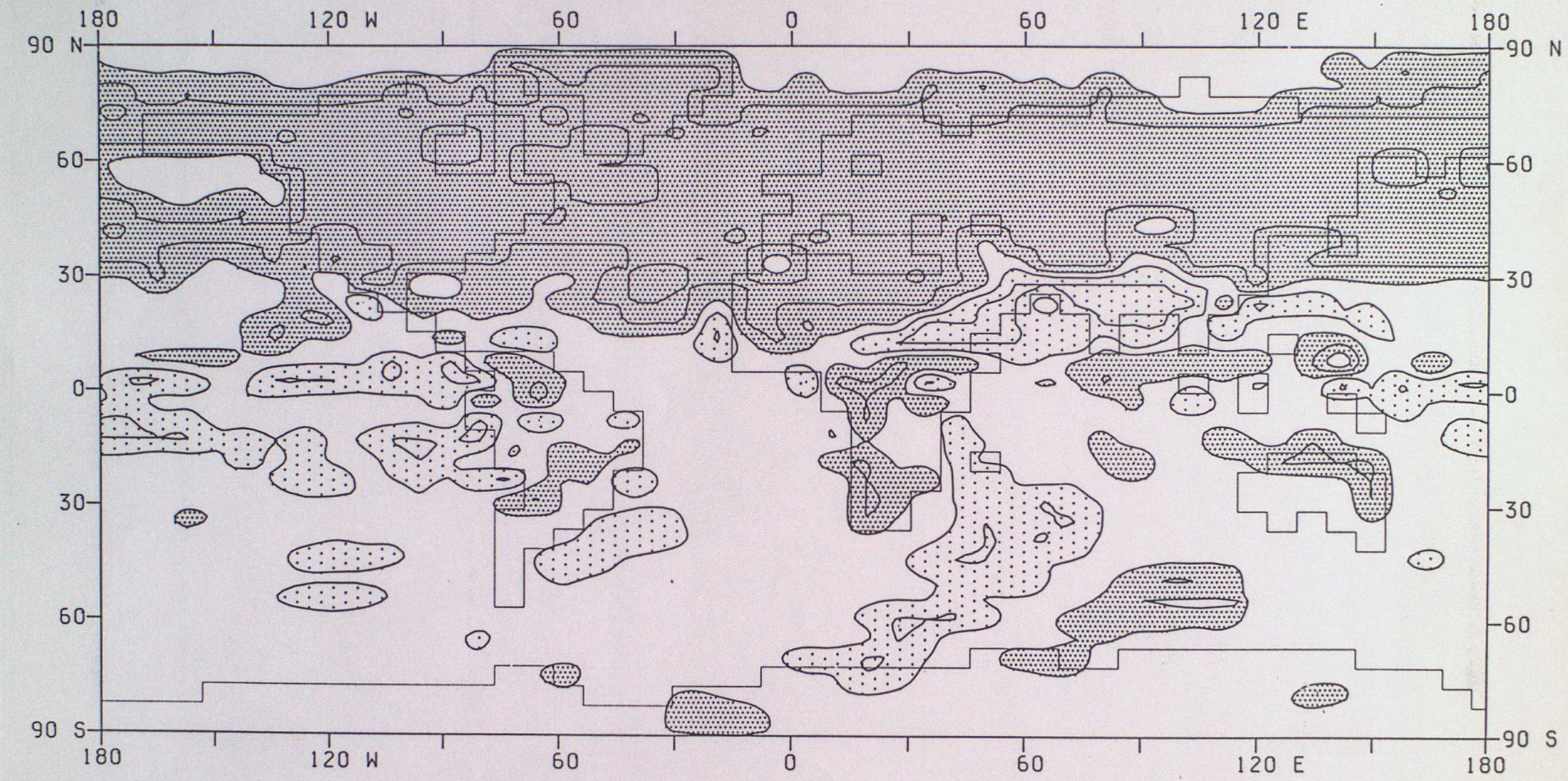

Figure 17

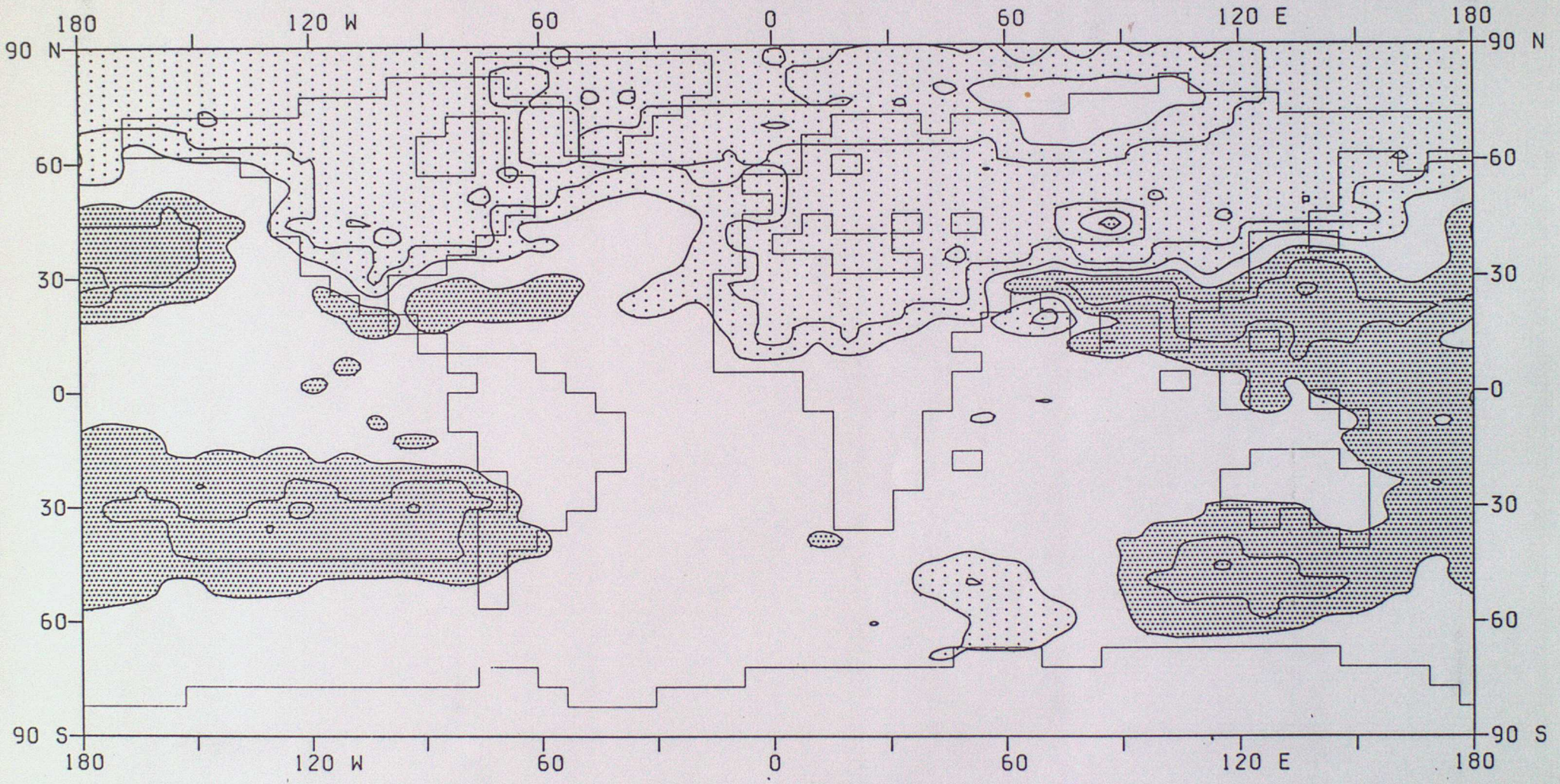

Figure 18

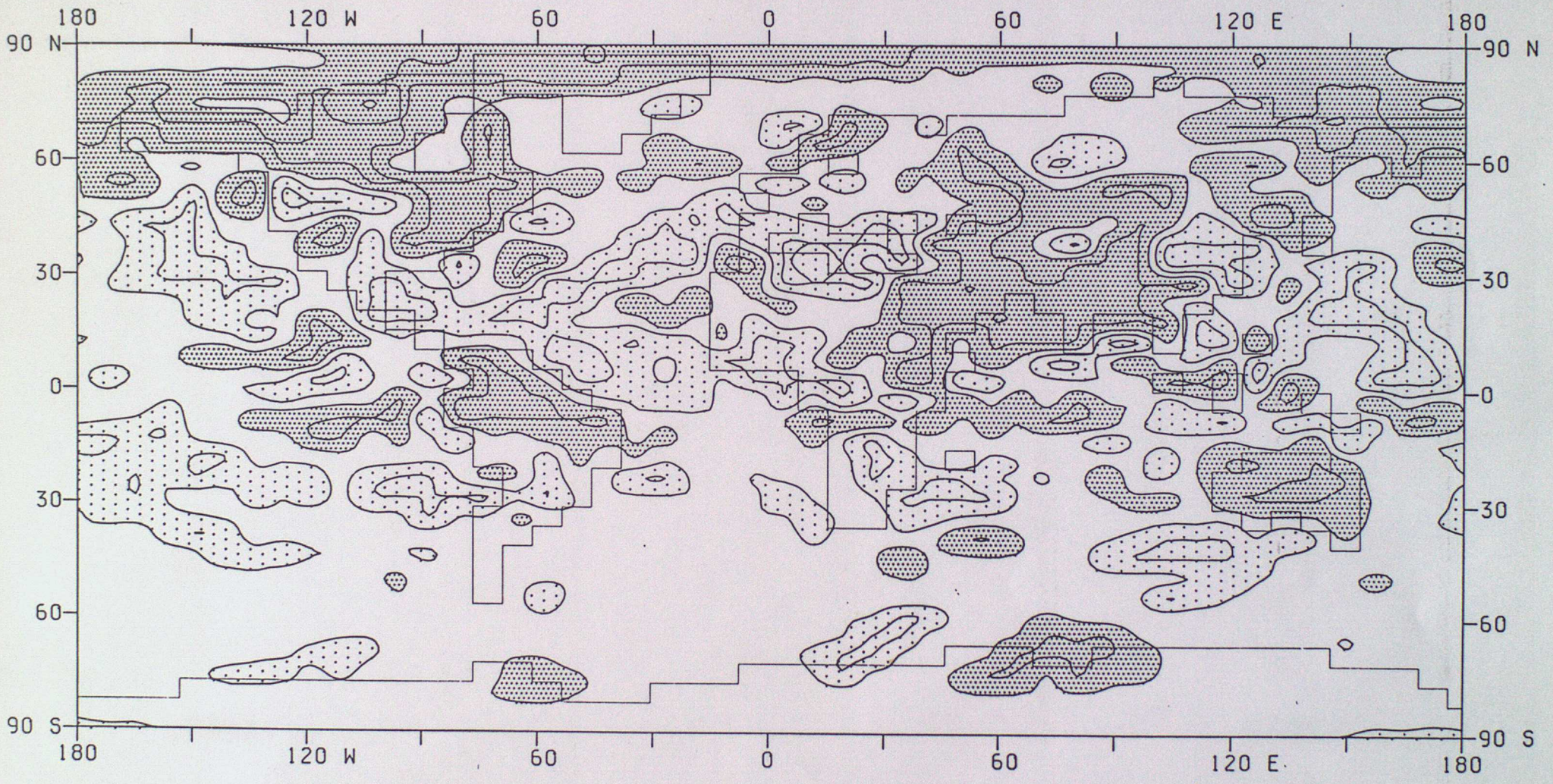

Figure 19

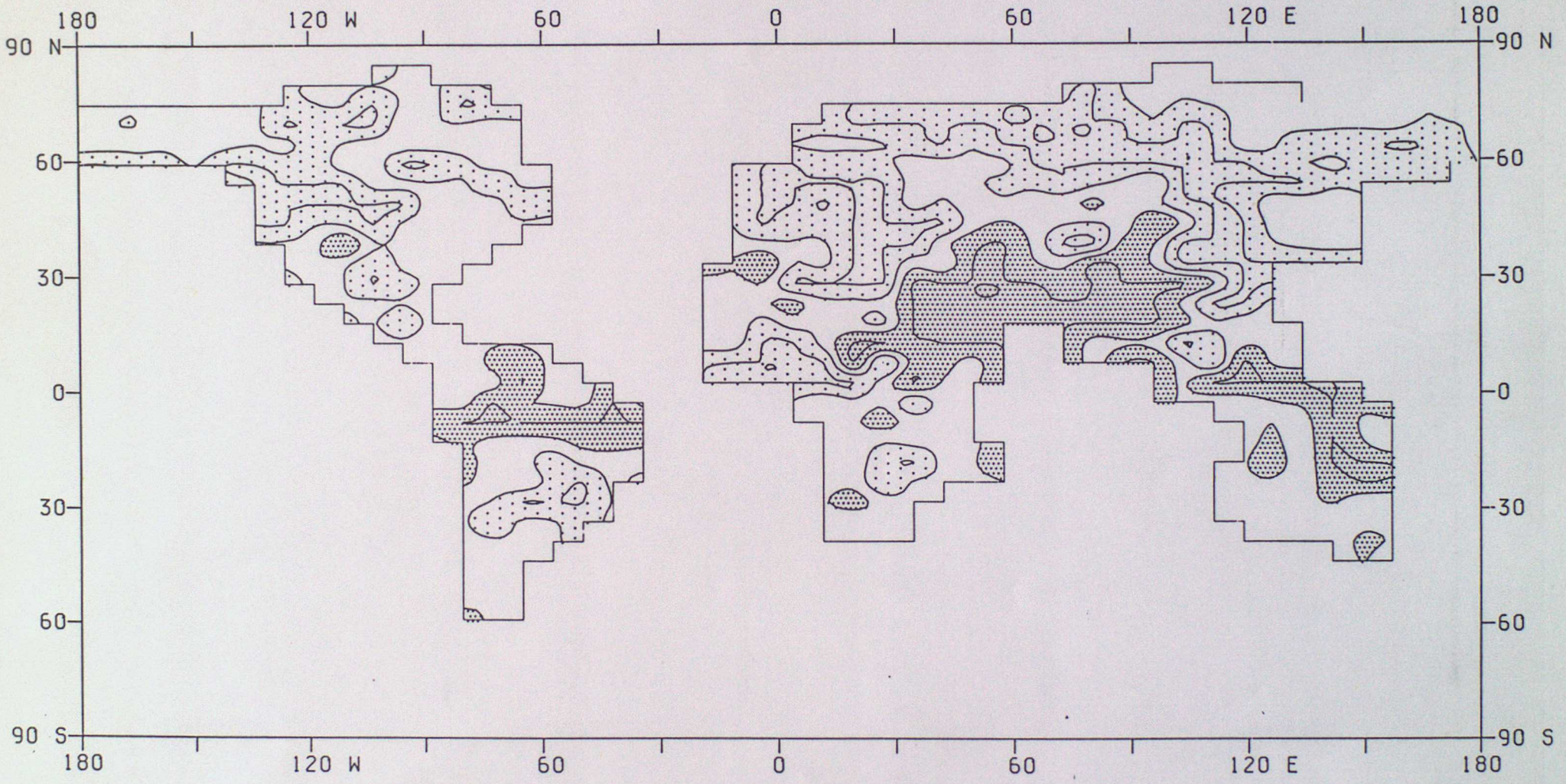

Figure 20

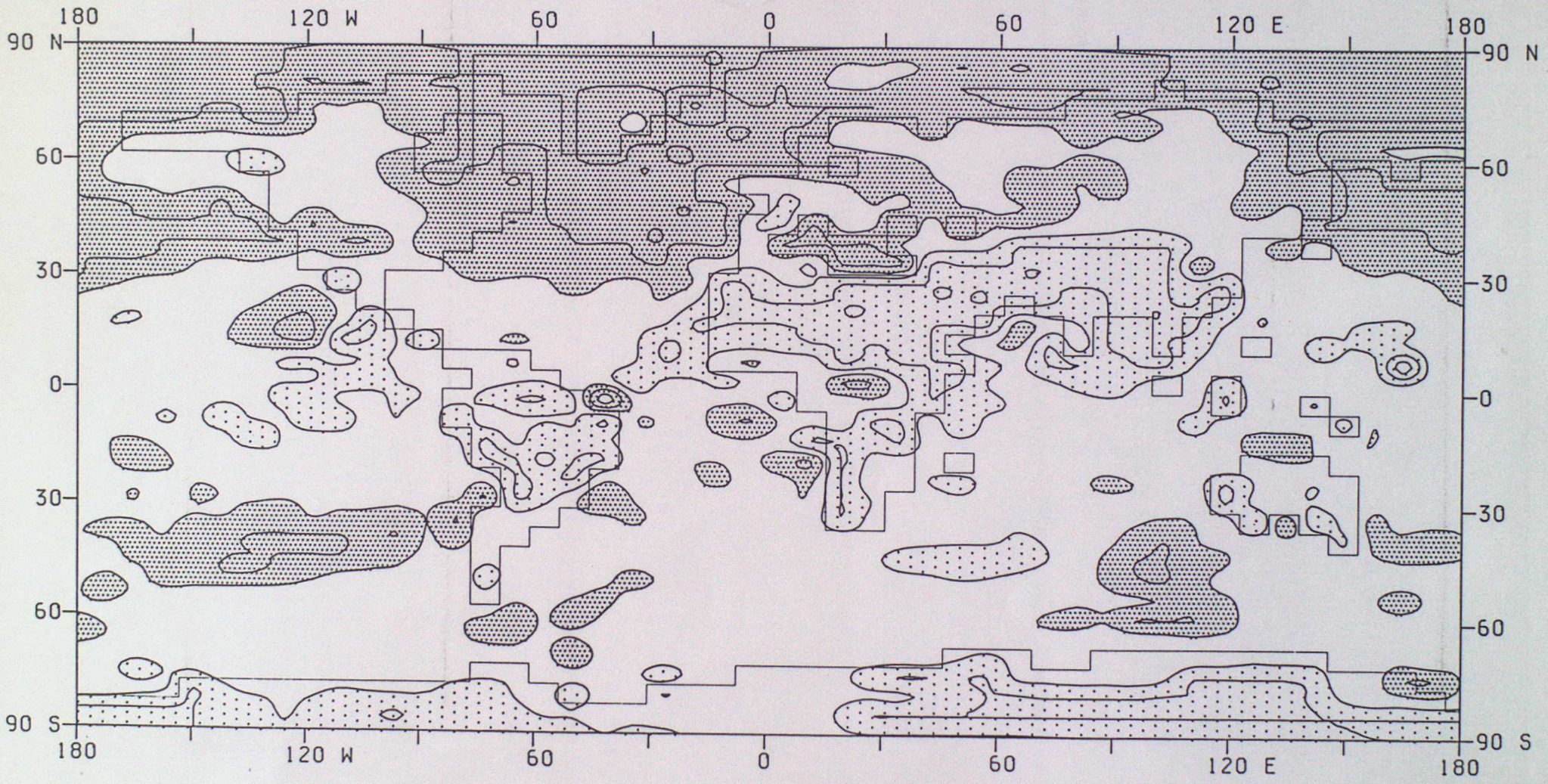

Figure 21

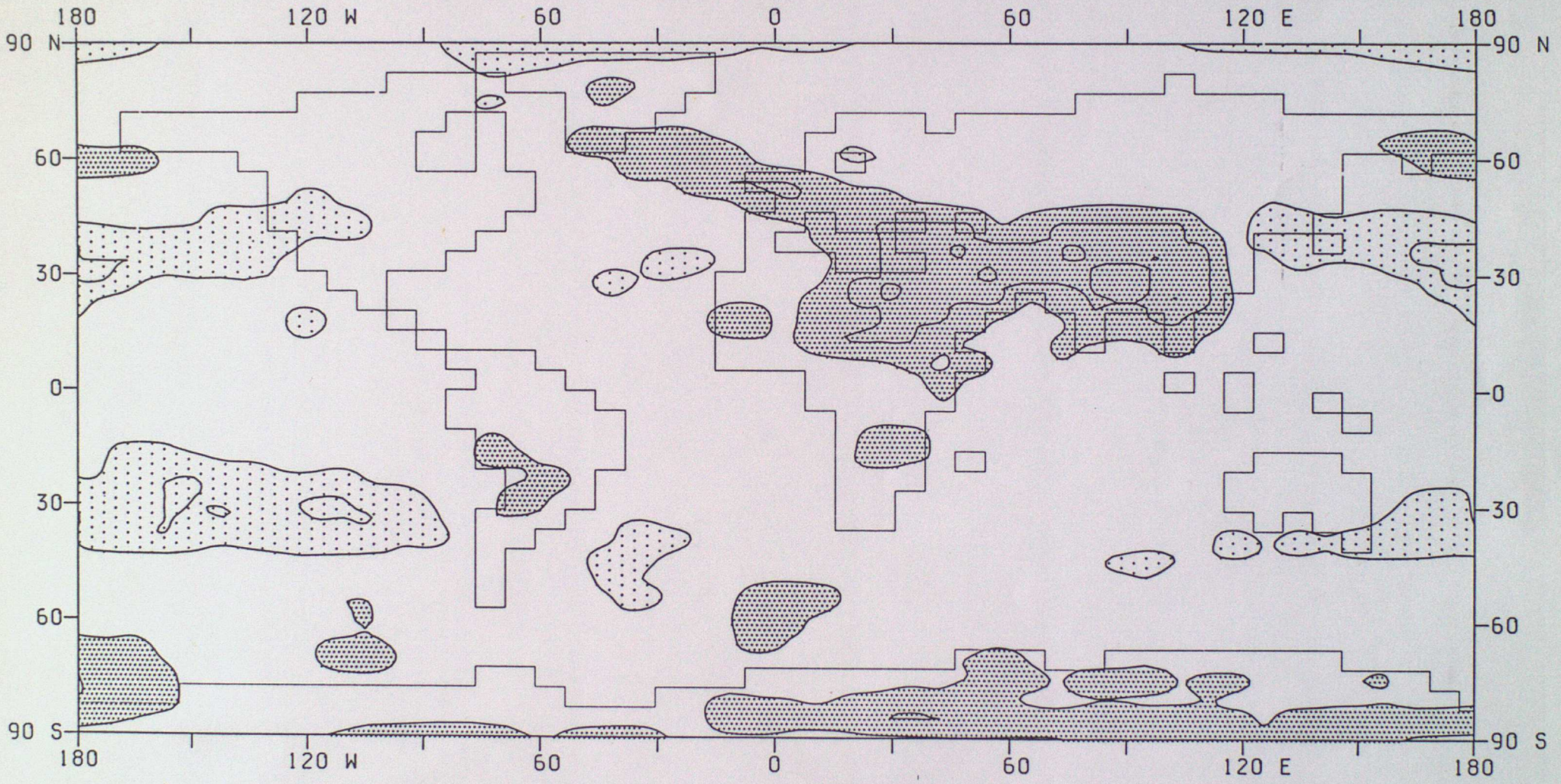
180
120 W
60
0
60
120 E
180
90 N
60
30
0
30
60
90 S
180
120 W
60
0
60
120 E
180
90 N
60
30
0
30
60
90 S

Figure 22

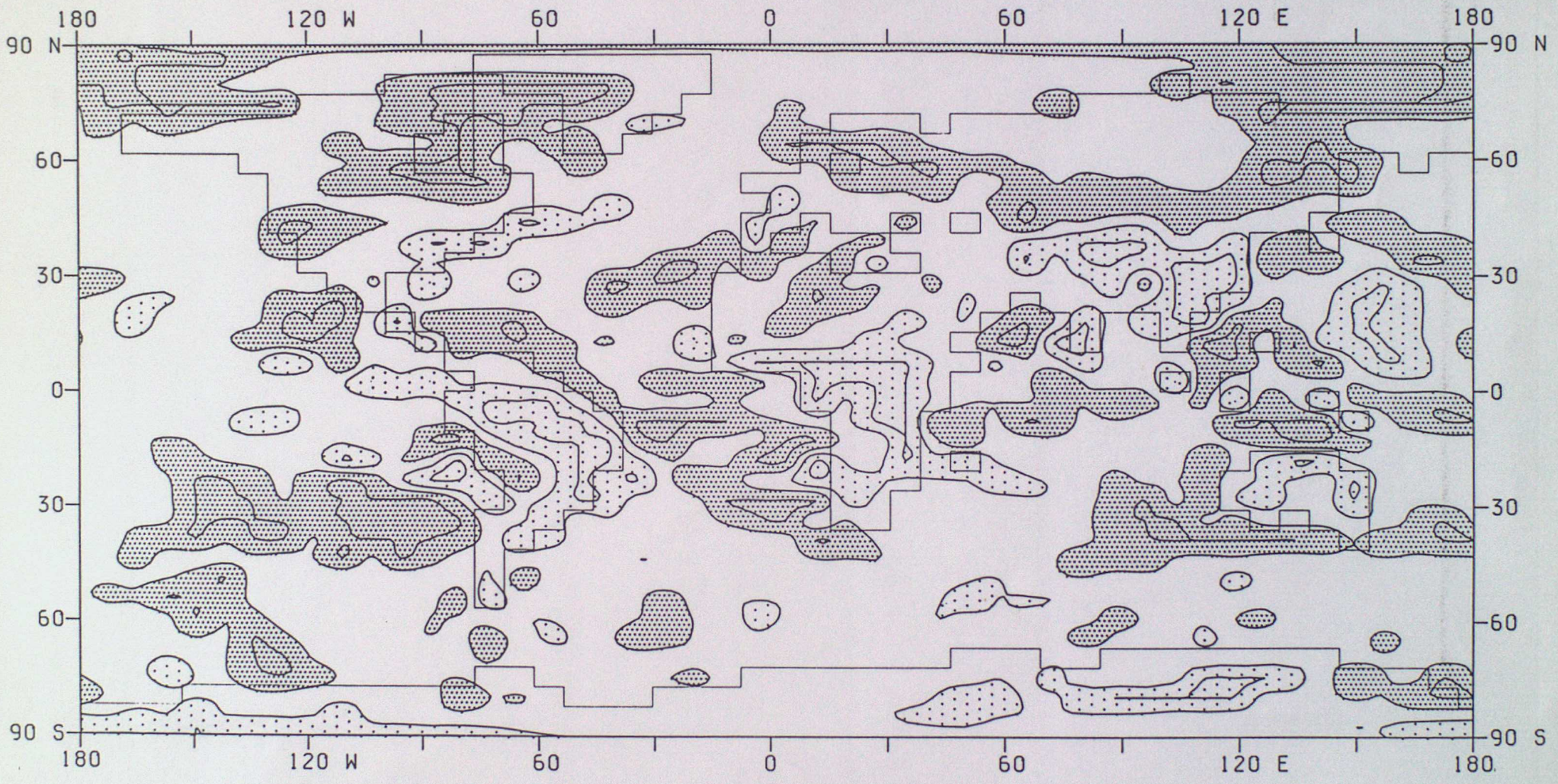

Figure 23

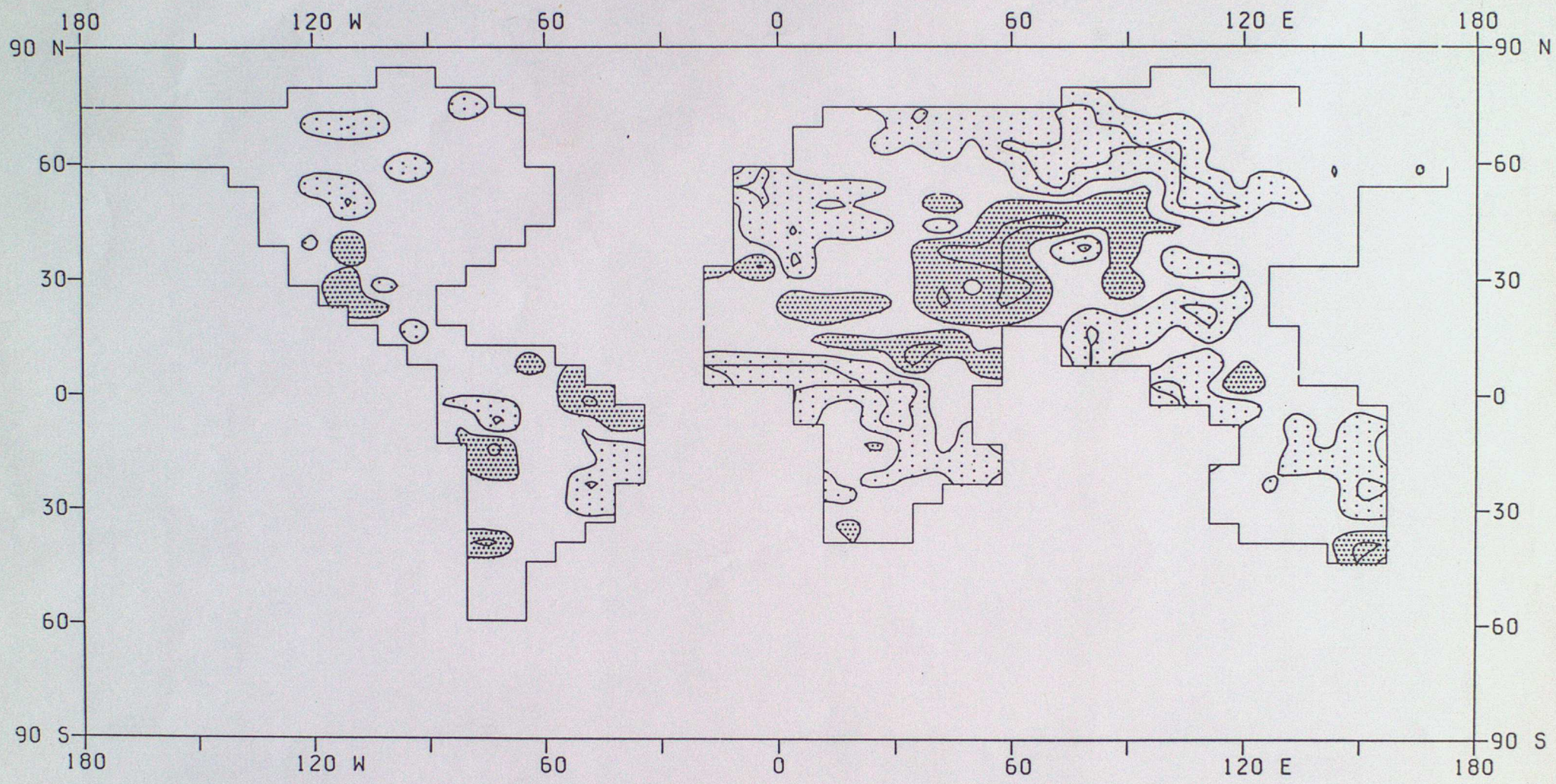

Figure 24

DYNAMICAL CLIMATOLOGY TECHNICAL NOTES

DCTN 1	June 1984	A scheme for incorporating the thermodynamic sea-ice model into a coupled ocean-atmosphere model. C Gordon and M Bottomley
DCTN 2	Sept 1984	The parametrization of the upper ocean mixed layer in coupled ocean/atmosphere models. C Gordon and M Bottomley
DCTN 3	Sept 1984	The response of a simple thermodynamic sea-ice model to GCM forcing appropriate for perennial sea-ice. M Bottomley
DCTN 4	Sept 1984	Potential vorticity in the stratosphere derived using data from satellites. S A Clough, N S Grahame and A O'Neill
DCTN 5	Sept 1984	Simulation of the seasonal cycle of SST using globally specified climatological data to force simple ocean models. N S Grahame
DCTN 6	Sept 1984	Development of an improved GCM radiation scheme. A Slingo and R C Wilderspin
DCTN 7	Sept 1984	On the specification of surface fluxes in coupled atmosphere/ocean general circulation models. J F B Mitchell, C A Wilson and C M Price
DCTN 8	Sept 1984	A survey of possible repercussions of the Soviet river reversal programme on Arctic sea-ice. H Cattle
DCTN 9	Oct 1984	A study of a strong stratospheric warming during January 1982 T D A Fairlie
DCTN 10	Nov 1984	An intercomparison of the Met O 11 M45 model and the Met O 20 11-level model on the Cyber 205 J F Dyson
DCTN 11	Nov 1984	Simulation of observed time series of temperature and precipitation over eastern England. D N Reed
DCTN 12	Nov 1984	Forecasts and analyses of the onset of the Southwest monsoon. R Kershaw
DCTN 13	Nov 1984	On modelling the effects of CO_2 on climate. J F B Mitchell
DCTN 14	Dec 1984	Development of a revised longwave radiation scheme for an atmospheric general circulation model. A Slingo and R C Wilderspin
DCTN 15	Jan 1985	Rossby wavetrains in the stratosphere forced by localised disturbances in the troposphere. C J Marks (Oxford), A O'Neill and V D Pope

DYNAMICAL CLIMATOLOGY TECHNICAL NOTES

DCTN 16	Jan 1985	Observing system experiments using the Meteorological Office's 15-level model. R A Bromley
DCTN 17	Feb 1985	Atmospheric general circulation simulation of the climate of the Mediterranean region. H Cattle
DCTN 18	Feb 1985	Diurnal variation and cloud in a general circulation model. C A Wilson and J F B Mitchell
DCTN 19	Feb 1985	The sensitivity of the Saharan region in a general circulation model. W M Cunnington and P R Rowntree
DCTN 20	Mar 1985	The impact of aircraft observations on analyses and forecasts from the operational 15-level model. B R Barwell
DCTN 21	Mar 1985	Non-linear effects on heat-induced circulation of the tropical atmosphere. A E Gill and P J Phlips
DCTN 22	Apr 1985	Simulation of cloudiness with the U.K. Meteorological Office 11-layer AGCM. A Slingo and R C Wilderspin
DCTN 23	Apr 1985	An integrated approach to the representation of cloud processes. R N B Smith
DCTN 24	May 1985	Nuclear Winter: Calculations of the shortwave radiative effects of soot aerosols. A Slingo and P Goldsmith
DCTN 25	Jul 1985	Sea ice and the Antarctic winter circulation: a numerical experiment. J F B Mitchell and T S Hills
DCTN 26	Jul 1985	A Budyko-Sellers model for study of ocean-atmosphere interaction. W J Ingram
DCTN 27	Aug 1985	The effect of a shoaling thermocline on equatorially-trapped Kelvin waves. A E Gill and B A King
DCTN 28	Sept 1985	CO_2 climate sensitivity and model dependence of results. J F B Mitchell, C A Wilson and W M Cunnington
DCTN 29	Sept 1985	Handbook of the Meteorological Office 11-layer atmospheric general circulation model. Volume 1 : Model Description Edited by A Slingo
DCTN 30	Sept 1985	Impact of land surface variations on African rainfall in general circulation models. P R Rowntree, M F Wilson and A B Sangster

DCTN 31 Nov 1985 The annual cycle of sea level in the eastern tropical Pacific.
G R Bigg and A E Gill

DCTN 32 Nov 1985 An analytic model of the heat-induced tropical circulation in the presence of a mean wind.
P J Phlips and A E Gill

DCTN 33 Nov 1985 The effect of resolution and diffusion on the simulated climate.
J F Dyson

DCTN 34 Jan 1986 Rossby adjustment over a step.
M K Davey, A E Gill, E R Johnson and P F Linden

DCTN 35 Jan 1986 Issues concerning the evaluation of effective surface roughness of heterogeneous terrain.
D J Carson

DCTN 36 Mar 1986 Climate sensitivity and past climates : evidence from numerical studies
J F B Mitchell

DCTN 37 Mar 1986 Parametrizations of land-surface processes in Meteorological Office numerical weather prediction and climate models
D J Carson

DCTN 38 Apr 1986 Modelling of land-surface processes and their influence on European Climate
D A Warrilow, A B Sangster and A Slingo

DCTN 39 Apr 1986 Simulation of climatic change due to increased CO_2
J F B Mitchell

DCTN 40 May 1986 On the interpretation of the Eliassen-Palm flux divergence.
Part I : Theory
D G Andrews

DCTN 41 June 1986 Experiments on tropical circulation with a simple moist model.
M K Davey and A E Gill

DCTN 42 Jun 1986 Parameter regimes for studying isolated eddies.
P D Killworth and M K Davey

DCTN 43 Jun 1986 A comparison of the impact of an envelope orography and of a parametrization of orographic gravity-wave drag on model simulations.
A Slingo and D W Pearson

DCTN 44 Jul 1986 The effect of a sea-surface temperature anomaly on a prediction of the onset of the south-west monsoon over India.
R Kershaw

DCTN 45 Jul 1986 An introduction to the parametrization of land-surface processes.
D J Carson

DYNAMICAL CLIMATOLOGY TECHNICAL NOTES

DCTN 46 Sept 1986 Lateral boundaries and the heat-induced flow in the tropical atmosphere.
P J Phlips and A E Gill

DCTN 47 Nov 1986 Simulation of the diurnal cycle of outgoing longwave radiation with an atmospheric GCM.
A Slingo, R C Wilderspin and S J Brentnall

DCTN 48 Feb 1987 A 2 x CO_2 climate sensitivity experiment with a global climate model including a simple ocean
C A Wilson and J F B Mitchell

DCTN 49 Feb 1987 Sensitivity of the Met O 20 11-layer model to increased land surface roughness length
C C Heasman

DCTN 50 Feb 1987 The influence of atmospheric waves on the general circulation of the middle atmosphere
D G Andrews

DCTN 51 Feb 1987 Transport mechanisms in the middle atmosphere: an introductory survey
D G Andrews

DCTN 52 Mar 1987 The Met O 20 stratosphere-mesosphere model
M Fisher

DCTN 53 Apr 1987 Simulations of linear and nonlinear disturbances in the stratosphere
A O'Neill and V D Pope

DCTN 54 Apr 1987 Aspects of dynamics of the middle atmosphere inferred using data from a satellite and from a numerical model
T D A Fairlie and A O'Neill

DCTN 55 Apr 1987 The seasonal evolution of the stratosphere in the northern hemisphere
A O'Neill and V D Pope

DCTN 56 Apr 1987 The adjustment of numerical weather prediction models to local perturbations
B R Barwell and R A Bromley

DCTN 57 Jun 1987 Climate simulations for 9000 years before present: Seasonal variations and the effect of the Laurentide ice sheet
J F B Mitchell, N S Grahame and K J Needham